REGULATION OF MCM HELICASE LOADING DURING EARLY DIFFERENTIATION AND CELL CYCLE RE-ENTRY

Jacob Peter Matson

A dissertation submitted to the faculty at the University of North Carolina at Chapel Hill in partial fulfillment of the requirements for the degree of Doctor of Philosophy in the Department of Biochemistry and Biophysics.

Chapel Hill
2019

Approved by:

Jeanette G. Cook

Dale A. Ramsden

Henrik G. Dohlman

Robert J. Duronio

Michael Ben Major

Jeremy E. Purvis

ABSTRACT

Jacob Peter Matson: Regulation of MCM helicase loading during early differentiation and cell cycle re-entry
(Under the direction of Jeanette G. Cook)

Cells initiate DNA replication at thousands of DNA replication origins every cell cycle. Minichromosome maintenance complexes (MCM) unwind DNA to initiate replication in S phase. MCM loading onto DNA, called “origin licensing”, occurs in G1 phase. Multiple mechanisms restrict origin licensing to G1 phase to prevent aberrant MCM loading and genotoxic re-replication in S phase. For this reason, cells load 5-10 fold excess MCM in G1 as dormant origins to protect against replication stress in S phase. The origin licensing checkpoint ensures sufficient MCM loading before S phase entry. MCM loading occurs in G1, yet cells have a variety of G1 lengths. Stem cells have short G1s while differentiated cells have long G1 phases. Additionally, cells may exit the cell cycle to quiescence, a state without division. Cells re-entering the cell cycle from quiescence have longer G1s than actively proliferating cells. How cells accomplish the same MCM loading under these different G1 lengths is poorly understood.

We used quantitative single cell flow cytometry and live cell imaging to measure MCM loading across varying G1 lengths. We found that stem cells with short G1s load MCM significantly faster than differentiated cells with long G1s. MCM loading rate decreases and G1 length increases during stem cell differentiation to all germ layers. The rapid licensing is due to increased Cdt1 protein in stem cells. Rapid origin licensing is intrinsic to pluripotency, as slowing MCM loading in stem cells promotes their differentiation. Cells re-entering into long G1 phases from quiescence are underlicensed with less loaded MCM at S phase entry than proliferating cells. The underlicensing causes replication stress sensitivity in S phase, and

repeated rounds of quiescence and re-entry increase the replication stress sensitivity. A defective origin licensing checkpoint combined with a slow MCM loading rate causes the underlicensing during cell cycle re-entry, and extending the first G1 phase rescues the underlicensing. Thus, cell cycle re-entry is a higher risk cell cycle than active proliferation. Proper regulation of the rate and amount of MCM loading is critical across different G1 types to control differentiation, proliferation and genome stability.

ACKNOWLEDGEMENTS

Thank you to my mentor Dr. Jean Cook. I have learned quite a lot about being a scientist from you, including experimental design, writing, and thinking a few steps ahead. Your career advice has been valuable, as has your scientific expertise and guidance, particularly allowing me to try new things and supporting scientific collaborations. I enjoyed our animated discussions about science and the push to make new discoveries. Thank you to my thesis committee, Dr. Dale A Ramsden, Dr. Henrik G Dohlman, Dr. Robert J. Duronio, Dr. Michael Ben Major, and Dr. Jeremy E. Purvis for your insightful advice and suggestions over the years.

Thank you to all the current and past Cook lab members that I have worked with over my graduate career. In particular, thank you to my rotation mentor Dr. Kate Coleman for teaching me many experimental techniques and for the good advice. Thank you Dr. Pedro Pozo for talking about the struggles of grad school and always being excited about MCM. Thank you Huaitong Wu for your dedicated help with my experiments. Thank you Juanita Limas for being a character and rooting for Megan. Thank you to the collaborators over my graduate career, Dr. Kathleen Mulvaney and the Major Lab, Dr. James Shellhammer and the Dohlman lab, Dr. Ryan Baxley and the Bielinsky lab at Univ. of Minnesota, and Phil Coryell and the Purvis lab.

Thank you to my parents Jon and Jaci and twin brother James for your support. You always believed in me and supported my dream of becoming a scientist. You gave me the foundation and determination to be a successful independent adult. Sorry I moved so far away, at least you get interesting east coast vacations now! I love you all. Lastly, thank you to my successful and gorgeous future wife Megan Seston. I'm grateful for your support, consistent cheerleading and for putting up with my late nights and weekends in lab, and overall busyness. I love you.

TABLE OF CONTENTS

LIST OF FIGURES

LIST OF ABBREVIATIONS

APC – Anaphase promoting complex

BSA – Bovine serum albumin

CDC6 – Cell division cycle 6

CDK – Cyclin dependent kinase

CDT1 - Cdc10 dependent transcript 1

CDX2 - Caudal Type Homeobox 2

CMG – Cdc45 MCM GINS

CSK – cytoskeleton buffer

DDK – Dbf4-dependent kianse

DMEM - Dubecco's modified Eagle's medum

DNA – Deoxyribonucleic acid

DOX - doxycycline

EDU - 5-ethynyl-2'-deoxyuridine

FBS- Fetal bovine serum

FUCCI – Fluorescent ubiquitin cell cycle indicator

HBO1 – Histone acetyltransferase binding to ORC1

hESC – human embryonic stem cell

HRP – Horseradish peroxidase

iPSC – induced pluripotent stem cell

KO - knockout

MCM – Minichromosome maintenance complex

MEM – Minimum eagle's medium

NPC – Neural progenitor cells

ORC – Origin recognition complex

ORCA – Origin recognition complex associated protein

PBS- Phosphate buffered saline

PCNA – Proliferating cell nuclear antigen

PCR – Polymerase chain reaction

PP2A – Protein phosphatase 2A

RB – Retinoblastoma protein

RNA – Ribonucleic acid

RPE – Retinal pigmented epithelial cells

siRNA – Silencing ribonucleic acid

TBST – Tris buffered saline tween-20

UV – ultraviolet radiation

CHAPTER 1: INTRODUCTION

Cell cycle structures

The eukaryotic cell cycle consists of four phases: G1, S, G2, and M phase. However, all cells do not have the exact same cell cycle structure, with some cells having large variations in G1 lengths. Additionally, some cell cycles are missing phases altogether such as endoreduplication cycles which lack M phase (Edgar and Orr-Weaver, 2001). My research has focused on events in G1 and S phase. My overall goal is to understand how cells with different cell cycle structures progress through the same molecular pathways in G1 phase and enter into S phase. G1 length varies between cell cycles during development, where stem cells have rapid cell cycles with short G1 lengths and differentiated cells have slow cell cycles with long G1 lengths (VanOudenhove et al., 2016). I compared these two cell cycles to understand how a change in G1 length changes regulation of G1 events and regulates development. Cells in G1 phase may leave the cell cycle and exit to quiescence, a state outside the cell cycle without cell division. Quiescent cells can re-enter the cell cycle in G1 phase to begin dividing again. I compared cells transitioning from quiescence back into G1 phase and actively proliferating cells to understand how active cell cycle regulation differs from cell cycle re-entry from quiescence. I found that G1 regulation is critical for maintaining pluripotency in stem cells and that abnormal G1 regulation during cell cycle re-entry makes the first cell cycle a high risk cycle compared to proliferating cell cycles. Thus, understanding unique cell cycle structures will provide insight into how their structure influences cell fate decisions and the lifecycle of a cell.

Stem cells have an abbreviated G1 phase to maintain their pluripotency. Stem cell pluripotency is the ability of a stem cell to differentiate into multiple specialized cell types comprising all three germ layers, endoderm, ectoderm, and mesoderm (Soufi and Dalton,

2016). The cell cycle is linked to the probability of a stem cell to become a differentiated cell. Studies show that stem cells treated with a differentiation stimulus tend to differentiate asynchronously, suggesting that stem cells only respond to a stimulus at certain times. Pauklin and Vallier showed that pluripotent cells respond to differentiation cues only in G1 phase and that cells in early G1 phase respond to endoderm and mesoderm cues and cells in late G1 phase respond to ectoderm cues (Pauklin and Vallier, 2013). Further studies revealed that key cell cycle regulators in S, G2, and M phase including Checkpoint kinase 2 and Cyclin B are refractory to differentiation cues, restricting the stem cell responses to differentiation cues to G1 phase (Gonzales et al., 2015). Taken together, these studies demonstrate the reason stem cells differentiate asynchronously is because their cell cycles are asynchronous and some cells must progress through the cycle into G1 before responding to a stimulus. Thus, a short G1 phase balances self-renewal and differentiation by limiting the time for differentiation.

Pluripotent stem cells maintain their short G1 phase by overriding several of the normal G1 regulatory mechanisms that increase G1 length. (For a detailed discussion on G1 regulation and cell cycle commitment see Chapter 2). Differentiated cells have a period of low Cyclin Dependent Kinase (CDK) activity in early G1 phase that gradually increases as cells move through G1. Eventually CDK2 activity hyperphosphorylates the Retinoblastoma protein (Rb) and other substrates to promote S phase entry. Pluripotent stem cells eliminate much of early G1 by maintaining near constitutive high CDK2 activity (Neganova et al., 2009). The high CDK2 activity results in a shortened G1 phase that is molecularly similar to the time when Rb is hyperphosphorylated in G1 phase of differentiated cells. Stem cells also have low levels of the CDK2 inhibitor proteins p27 and p21, which promotes high CDK2 activity (Neganova and Lako, 2008; Soufi and Dalton, 2016). Another major regulator of early G1 phase is the Anaphase Promoting Complex (APC), which regulates key proteins that drive S phase entry by targeting them for destruction in early G1 phase (Siddiqui et al., 2013). Inactivation of APC^{Cdh1} in mid to late G1 phase allows S phase entry and is proposed to mark the point of no return for

commitment to S phase (Cappell et al., 2016). APC^{Cdh1} activity is attenuated and almost completely inactive in pluripotent stem cells due to inhibitory phosphorylation by CDK2, high levels of the APC inhibitor Emi1, and high levels of Skp2 (which targets APC subunits for degradation) (Ballabeni et al., 2011; Bar-On et al., 2010). All of these deregulations of G1 control in pluripotent stem cells drive an abbreviated G1 phase of only 2-3 hours. Once stem cells begin differentiation, they regain a long G1 phase by increasing CDK inhibitor proteins, increasing APC activity, and decreasing CDK2 activity (VanOudenhove et al., 2016; Boward et al., 2016). Thus, pluripotent cells maintain a short G1 phase by deregulation of G1 cell cycle control and gain a longer G1 phase upon differentiation.

Another instance of a unique cell cycle structure are quiescent cells re-entering the cell cycle with a longer G1 phase than actively proliferating cells. Quiescence is a state outside the cell cycle where cells do not divide (quiescence is also known as G0). However, it is distinct from a G1 arrest, and characterized by repression of cell cycle genes and activation of genes to maintain the quiescent state including upregulation of anti-differentiation, anti-apoptotic and anti-senescent genes (Sang et al., 2008; Legesse-Miller et al., 2012; Imai et al., 2014; Coller et al., 2006). Quiescence is a broad category that encompasses several kinds of cell cycle exit, all unified as a reversible cell cycle exit instead of a permanent cell cycle exit. Multiple signals induce exit to quiescence, including mitogen withdrawal, contact inhibition and loss of adhesion, and each signal invokes unique changes in gene expression as well as a core expression program common to all forms of quiescence (Coller et al., 2006). Additionally, quiescence varies by the length of time a cell is quiescent. Longer term quiescence is associated with greater gene repression and chromatin compaction than short term quiescence (Coller et al., 2006; Evertts et al., 2013). The longer a cell remains in quiescence, the longer it takes to re-enter the cell cycle (Kwon et al., 2017). Thus, quiescence exists as a spectrum of states with different inputs and degrees of quiescence, yet all are unified by the ability to re-enter the cell cycle into a long G1 phase.

Quiescent cells re-entering the cell cycle into G1 phase must first reset all the restrictive regulations that maintain quiescence and prevent proliferation. One key hurdle to re-enter the cycle is Rb hyperphosphorylation, which activates E2F transcription as part of the restriction point. The deeper the quiescence, the longer it takes to activate E2F gene expression, making the first G1 phase during cell cycle re-entry longer than G1 of proliferating cells (Kwon et al., 2017). Cells must alter regulatory pathways upstream and downstream of Rb to fully re-enter G1 phase. In proliferating cells, Rb is monophosphorylated in G1 phase, but in quiescent cells Rb is unphosphorylated requiring the extra step of CDK4/Cyclin D phosphorylation of Rb during cell cycle re-entry (Narasimha et al., 2014). Next, CDK2 would hyperphosphorylate Rb to activate E2F gene expression but that also has additional steps. CDK2 is cytoplasmic in quiescent cells and must translocate to the nucleus (Dietrich et al., 1997; Nevis et al., 2009). Additionally, the CDK2 inhibitor p27 is upregulated in quiescence and must be degraded by specialized ubiquitin ligases during the transition from G0 to G1 (Kamura et al., 2004; Susaki et al., 2007). The program of cell cycle gene repression in G0 is mediated by the DREAM complex, which includes the Rb related protein p130 and requires the Dyrk1a kinase activity for DREAM complex assembly (Litovchick et al., 2007, 2011). To re-enter the cell cycle, G0 cells must disassemble the DREAM complex and decrease Dyrk1a kinase activity, presumably through protein degradation (Liu et al., 2016; Chen et al., 2013; Bhattacharya et al., 2003). Taken together, all of these hurdles cause G1 during cell cycle re-entry to be longer than G1 in proliferating cells.

Minichromosome Maintenance Complexes and origin licensing

A major purpose of G1 phase is to prepare cells for DNA replication in S phase. In S phase, helicases begin DNA replication by unwinding DNA at DNA replication origins. A DNA replication origin is a region of the genome where DNA replication first begins. The central component of the replicative helicase is the Minichromosome maintenance complex (MCM) (Deegan and Diffley, 2016). Cells load MCMs onto DNA replication origins in G1 phase, and the

MCM loading is also referred to as “origin licensing” (DePamphilis et al., 2006). Once cells enter S phase, replication origins “fire” when MCM (along with other proteins) unwinds DNA to begin replication (Remus and Diffley, 2009). MCM travels with replication forks to unwind DNA ahead of the DNA polymerase that replicates DNA. MCMs are unloaded off DNA once replication forks terminate (Moreno et al., 2014; Maric et al., 2014). Thus, MCM regulation is divided into two phases – origin licensing occurs in G1 phase and origin firing occurs in S phase.

Origin licensing begins as early as the telophase preceding G1 in some cell types, or in G1 phase (Dimitrova et al., 2002). The exact timing of when MCMs load onto DNA is not clear, but it certainly happens over time as cells progress through G1 (that is, all MCMs are not loaded onto origins simultaneously). An origin is licensed for replication once it has two DNA loaded MCM hexamers loaded head to head (called double hexamers). However, MCMs cannot load onto DNA on their own; other proteins facilitate MCM loading onto DNA. First, the Origin Recognition Complex (ORC) binds to origin DNA. ORC recruits Cell Division Cycle 6 (CDC6) and CDC6 binds ORC directly. CDC6 is required to recruit MCMs to origins, and has an ATPase function with the additional role of quality control, ejecting incorrectly bound MCMs. Next, Cdc10 dependent transcript 1 (CDT1) binds to MCM to facilitate loading onto DNA. MCM is a hexameric ring with a gate between MCM2 and MCM5 that opens and closes to encircle DNA (Samel et al., 2014). CDT1 alters MCM conformation to hold the gate open and allow loading onto DNA (Frigola et al., 2017). The CDT1-MCM complex interacts with ORC-CDC6 to induce conformational changes that facilitate MCM loading onto DNA and MCM ring closing (Sun et al., 2013). The MCM loading reaction occurs twice to result in two head to head MCMs forming a double hexamer on DNA (Evrin et al., 2009; Remus et al., 2009). It is currently controversial if one ORC loads both MCM hexamers or two adjacent ORCs each load one MCM, but the end result is that CDT1, CDC6 and ORC all dissociate, leaving behind the DNA loaded MCM double hexamer, a fully licensed origin (Ticau et al., 2015; Coster and Diffley, 2017).

DNA Replication Origins

Origin licensing occurs at discrete genomic loci, in the context of other DNA based processes including transcription, chromatin, and DNA sequence.

Budding yeast have origin consensus sequences to specify origin locations, but higher eukaryotes do not have an origin consensus sequence (Leonard and Méchali, 2013). Instead, metazoan origins are associated with euchromatin, G-quadraplexes, promoters and termination sites (Prioleau and Macalpine, 2016). Loaded MCM double hexamers can slide along DNA, pushed by RNA polymerase to locations other than the origin where MCM was first loaded (Gros et al., 2015). Therefore, actively transcribed genes may sweep MCM out of the transcribed region, localizing MCM to the beginning or end of transcribed genes (Powell et al., 2015; Chen et al., 2019). This repositioning of MCM is important, as intragenic origins in actively transcribed genes cause transcription-replication conflict in S phase (Macheret and Halazonetis, 2018). Thus, locations of origins in higher eukaryotic are influenced by many factors.

Chromatin environment shapes origin location and may require additional proteins facilitate MCM loading. The ORC associated protein (ORCA) localizes to heterochromatin and recruits ORC to DNA during G1 phase. Cells without ORCA cannot recruit ORC to heterochromatin (Shen et al., 2010). ORCA also recruits histone modifying enzymes to heterochromatic regions to promote their replication in late S phase (Giri et al., 2015). CDT1 recruits the H4-histone acetyltransferase HBO1 (Human acetylase binding to ORC1) to origins to acetylate nearby histones, which is required for MCM loading (Miotto and Struhl, 2008, 2010). Finally, the lysine methyltransferase Set8 monomethylates histone H4K20 to promote origin licensing (Tardat et al., 2010). The monomethyl is converted to dimethyl and is present on about 80% of histones across the genome (Kuo et al., 2012). ORC1 contains a bromo adjacent homology domain that binds to H4K20me2 (which requires H4k20me1 first) and promotes recruitment of ORC to origins, thus promoting MCM loading (Kuo et al., 2012). These data

suggest that origin licensing depends on the chromatin environment, and that origins at genomic loci with different chromatin structure may require specialized MCM loading reactions.

MCMs in S phase

Licensed origins require several co-factors to convert the loaded MCM double hexamer to active helicases in S phase. The fully active helicase is called CMG and consists of Cdc45, MCM2-7 and GINS (Psf1, Psf2, Psf3 and Sld5) (Costa et al., 2011). S phase kinase activity of CDK2 and the Dbf4-dependent kinase (DDK) phosphorylate various components of CMG to activate them and fire the origin (Labib, 2010). DDK exclusively phosphorylates double hexamers and not free MCM by binding MCM2 and MCM4 across both hexamers, one from each adjacent MCM in the double hexamer (Sun et al., 2014). Origins fire throughout S phase in a generalized order called the replication timing program (Aparicio, 2013). Origins are classified as early or late depending on when they fire in S phase and is regulated by many factors including chromatin modifications, higher order nuclear structure and stress such as a DNA damage response (Fragkos et al., 2015). New origin licensing is strictly prohibited in S phase by mechanisms targeting all the MCM loading proteins. CDC6 is phosphorylated by CDK2/Cyclin A and exported to the cytoplasm (Yim et al., 2013; Petersen et al., 1999a). ORC1 is phosphorylated by CDK2/Cyclin A and targeted for destruction by the E3 ubiquitin ligase SCF^{Skp2} (DePamphilis, 2003; Méndez et al., 2002). CDT1 is targeted for degradation by $CRL4^{Cdt2}$ and SCF^{Skp2} as well as directly inhibited by Geminin protein binding and CDK1/Cyclin A phosphorylation (Arias and Walter, 2005; Sugimoto et al., 2004; Nishitani et al., 2004; McGarry and Kirschner, 1998; Zhou et al., 2018). The methyltransferase Set8 is also degraded by $CRL4^{Cdt2}$ to prevent re-replication (Tardat et al., 2010). If any licensing occurs in S phase, cells may re-replicate their DNA, causing double strand breaks, aneuploidy and genome instability (Truong and Wu, 2011; Neelsen et al., 2013). Therefore, MCM loading and firing must be strictly segregated to ensure proper genome replication.

Cells must load all the MCM required for replication in the preceding G1 phase, but in times of replication stress cells need more MCM to ensure complete replication. For that reason, cells typically load 5-10 times extra MCM than normally required to complete S phase as "dormant origins" (Woodward et al., 2006; Ge et al., 2007; Ibarra et al., 2008). When a replication fork encounters replication stress it will stall and stop replicating. Cells then fire a nearby dormant origin to start a new replication fork and rescue the stalled fork (Yekezare et al., 2013). Cells may continue to proliferate with decreased origin licensing, but fewer dormant origins makes them hypersensitive to replication stress. Mice with diminished dormant origins have defects in proliferative tissues such as the hematopoietic system, increased genome stability, and cancer (Pruitt et al., 2007; Kunnev et al., 2010; Shima et al., 2007). Ensuring sufficient loaded MCM at S phase entry is critical to maintain genome stability.

The Origin Licensing Checkpoint

Cells ensure sufficient loaded MCM through the origin licensing checkpoint. The licensing checkpoint is p53-dependent pathway that decreases CDK2 activity to block S phase entry until there is a sufficient amount of loaded MCM (Nevis et al., 2009; McIntosh and Blow, 2012). The licensing checkpoint seems to inhibit CDK2 by multiple mechanisms, but the exact pathway is unknown. CDK2 requires phosphorylation of T160 for kinase activity, this phosphorylation is decreased when MCM loading is decreased, suggesting the origin licensing checkpoint regulates CDK2 T160 phosphorylation (Nevis et al., 2009). Another licensing checkpoint target upstream of CDK2 is Cyclin D expression, which is diminished during decreased origin licensing (Liu et al., 2009). Cancer cells tend to have lost p53 and Rb pathway expression or function, and subsequently they also have a defective origin licensing checkpoint (Nevis et al., 2009). The lack of a licensing checkpoint makes cells sensitive to treatments that decrease origin licensing. Cancer cell lines, but not untransformed cells, prematurely enter S phase with few dormant origins during treatments that reduce origin licensing (Shreeram et al., 2002; Nevis et al., 2009; Zimmerman et al., 2013). These cells that lack the origin licensing

checkpoint and enter S phase prematurely are hypersensitive to replication stress and treatment with replication inhibitors causes apoptosis (Feng et al., 2003; Shreeram et al., 2002; Zimmerman et al., 2013). The specific sensitivity of cancer cells but not normal cells to decreased MCM loading makes origin licensing a potential target in cancer therapy, and preliminary drug screens for licensing inhibitors shows promise targeting cancer cells (Gardner et al., 2017).

How does CDK activity affect MCM loading?

The cell cycle is broadly divided into a period of low CDK activity in G1 phase and a period of high CDK activity in S/G2/M phases. MCM loading and DNA replication are restricted to G1 and S phase, respectively. Presumably low CDK activity is permissive for origin licensing and high Cdk activity is inhibitory for origin licensing and permissive for origin firing (Siddiqui et al., 2013). One group claims that CDK2/Cyclin E activity inhibits MCM loading, while another that it is CDK2/Cyclin A activity that inhibits MCM loading (Ekholm-Reed et al., 2004; Wheeler et al., 2008). However, CDK2/Cyclin E is also required to stabilize Cdc6 for MCM loading (Mailand and Diffley, 2005). How can Cdk2 activity both be activating and inhibiting MCM loading at the same time? Is there a clear role for CDK2 in MCM loading? I address this question in Chapter 3 by overproducing Cyclin E and measuring MCM loading rate, finding that Cyclin E does not inhibit MCM loading, rather it only shortens G1 so cells have less time to load MCM.

What are the MCM loading dynamics in G1?

We know that MCM complexes are loaded onto DNA in G1 phase, but the exact details of when in G1 or how fast MCM are loaded are unknown. It could be that MCM load onto DNA at a linear rate, a certain amount per minute. Then G1 length would be the major contributor to the total amount of loaded MCM with longer G1 phases resulting in more loaded MCM. It is unclear when MCM loading begins in G1, and it could be determined by the availability of Cdc6, which is degraded in early G1 by APC^{Cdh1} (Mailand and Diffley, 2005; Petersen et al., 2000). If MCM loading is linear and starts in late G1, then cells with different G1 lengths could still load

the same amount of MCM, because most G1 variation occurs in the early G1 phase (Foster et al., 2010). Another model is that MCM loading increases exponentially as cells move through G1 phase. In this case, no matter if MCM loading begins in early G1 or late G1, the bulk of MCM loading would be in late G1. Some data support a model where most MCM loading occurs in late G1. Symeonidou et al. used Fluorescence Recovery After Photobleaching to measure the immobile (DNA-loaded) fraction of MCM in G1 phase. They found a transient association between MCM in DNA in telophase and early G1 phase, and then a gradual increase in the stable (loaded) fraction throughout G1. However, about 50% of MCM total immobile fraction became immobile in the very late G1 phase, suggesting some factor rapidly promoted loading in late G1. Perhaps there is enough MCM loaded to relieve the licensing checkpoint, increasing Cdk2 activity to stabilize Cdc6? Then Cdc6 could help load more MCM, further increasing Cdk2 activity, which would start a positive feedback loop by stabilizing even more Cdc6. Whichever type of loading is correct, linear or exponential, the length of G1 will also be a factor in the amount of loaded MCM at the start of S phase.

How do cells with different G1 lengths load MCM onto DNA? Do they load at the same rate so cells with short G1s enter S phase with less MCM loaded? Or can the MCM loading rate change between cell types? MCM loading rate has not been measured in cells, however. The only measurements of MCM loading rate were done with *in vitro* reactions using purified yeast proteins to load MCM complexes onto plasmids (Remus et al., 2009; Evrin et al., 2009). It is plausible the MCM complex loading rate could be different between cells because cell express different amounts of licensing proteins (Lau et al., 2007). Cells with high levels of licensing proteins would load faster than cells with low levels of licensing proteins, regardless of the G1 length. This manipulation of MCM loading rate could be important for cancer cells, which overexpress licensing proteins and also likely lack the licensing checkpoint. The cancers cells would need a rapid MCM loading rate to ensure sufficient MCM loading because they would be unable to extend G1 phase as they have a defective licensing checkpoint (Lau et al., 2007). I

address this question in Chapter 3 by measuring average loading rate in stem cells and differentiated cells with short and long G1 lengths. I found that high amounts of Cdt1 promotes a fast MCM loading rate in stem cells with a short G1 phase. However, in Chapter 4 I find that the long G1 during cell cycle re-entry is underlicensed due to slow MCM loading and a defective origin licensing checkpoint.

CHAPTER 2: CELL CYCLE PROLIFERATION DECISIONS: THE IMPACT OF SINGLE CELL ANALYSES[1]

Introduction

The cell cycle is a series of tightly-regulated molecular events controlling DNA replication and mitosis, producing two new daughter cells from a single parent cell. Every cell cycle, individual metazoan cells have the opportunity to adopt one of two mutually-exclusive proliferation-related fates: continued cell cycle progression or cell cycle exit. Cell cycle exit encompasses multiple distinct states including permanent arrests associated with terminal differentiation or senescence and reversible arrest known as quiescence (G0). Settings where the importance of cell cycle entry is particularly apparent include hematopoiesis, replenishing the epithelial lining of the digestive tract, replacing shed skin cells, activation of adaptive immune responses, and wound healing. Tight control over cell cycle entry and exit is also critical for tumor prevention since most transformed cells do not appropriately respond to cues that trigger quiescence. It is thus important to understand the processes that determine cell cycle entry, cell cycle progression, and exit to quiescence. In this review, we highlight advances in understanding such proliferation decisions in mammalian cells and particularly the impact of recent improvements in single cell analysis methods.

Much of our understanding of the molecular determinants of cell cycle progression comes from analyses of cell populations. There are well-documented substantial changes in gene expression, protein abundance, protein post-translational modifications, and DNA synthesis as a population of cells moves from one cell cycle phase to the next, or when a

[1]Modified from: Matson, J. P. and Cook, J. G. (2017) 'Cell cycle proliferation decisions: the impact of single cell analyses', FEBS Journal, 284(3), pp. 362–375. doi: 10.1111/febs.13898.

population becomes quiescent. Commonly-used methods to monitor these changes include immunoblotting and quantitative real-time PCR for individual proteins or messenger RNAs or proteomics and transcriptomics for global analyses. The limits of detection for these methods have, until very recently, required pooled material from many thousands or millions of cells. A culture of genetically identical cells grown together are presumed to behave very similar to one another in the interpretation of such ensemble techniques though this assumption is not necessarily valid.

Even when two cells begin a cell cycle phase at the same time - such as immediately after cytokinesis - marked variation among individual cells and heterogeneous responses to external and internal cell cycle cues lead to different rates of cell cycle progression (Chiorino et al., 2001). Cell cycle heterogeneity arises from intrinsic and extrinsic variability in gene expression resulting in heterogeneity in mRNA and protein levels among individual cells (Snijder and Pelkmans, 2011; Raj and van Oudenaarden, 2008; McAdams and Arkin, 1997). Additional cell cycle variation could be a consequence of cell division itself. Although DNA is actively distributed equally into daughter cells, RNA, proteins, metabolites, and organelles may be randomly and unequally distributed at every cell division (Dueck et al., 2015; Darzynkiewicz et al., 1982). For example, Czerniak *et al.* used antibody staining to examine the distribution of several individual proto-oncoproteins with the potential to profoundly impact cell cycle progression, including the Ras GTPase and the c-Myc transcription factor. These authors found intercellular variability particularly in G1 phase cells, and most notably, differences in antigen concentrations in newly-born sister cells (Czerniak et al., 1992). Once a cell acquires higher or lower concentrations of a key protein, the difference from the population average can remain for two or more cell cycles (Sigal et al., 2006). There may also be coexisting and interconverting subpopulations of cells with different molecular states that influence proliferative fate (Overton et al., 2014; Spencer et al., 2013; Sakaue-Sawano et al., 2008).

Each individual cell “decides” to proliferate or exit the cycle separately from the whole population, integrating numerous signals to time the transition from one phase of the cycle to the next (Spiller et al., 2010). The intercellular heterogeneity and generally asynchronous growth of proliferating cells creates challenges for precisely tracking their behavior. A popular method to overcome heterogeneity is artificially synchronizing cells with inhibitors in one cell cycle phase, releasing them from the block, and monitoring molecular markers over time. Although cell cycle synchronization creates generally homogenous populations, the further each time point is removed from the initial synchronizing block, the more heterogeneous the population becomes (Illustrated in Figure 2.1). Furthermore, the arrests themselves can induce unique stress signaling pathways that aren’t normally engaged (or are engaged at much lower intensity) in normal cell cycles (Murray et al., 2004; Lanni and Jacks, 1998; Kurose et al., 2006). For example, nocodazole synchronization in mitosis can create genome instability after mitotic exit (Minn et al., 1996).

Moreover, a population of cells may harbor consistent or transiently interconverting distinct subpopulations with different proliferation dynamics. Methods that measure the aggregate concentration or activity in a population may mask subpopulations containing different levels of individual protein abundance or activity (Balazsi et al., 2011). If a culture contains two very distinct populations in significant numbers (such as a mixture of proliferating cells and quiescent or senescent cells, ensemble molecular detection methods will report an intermediate level of activity that may not be a true reflection of either state (Figure 2.1B). Only experiments measuring cell cycle parameters from single cells can identify distinct subpopulations that are hidden by methods that average the whole population.

Methods to assess proliferation in individual cells.

Single cell analysis is not itself new in the cell proliferation field. Counting the individual mitotic cells per field in a biopsy tissue sample has been a long-standing practice in clinical settings as one prognostic cancer indicator. Similarly, for decades patient samples have been

routinely probed with antibodies to proteins that are only expressed in proliferating cells, and the expression intensity and number of expressing cells provide valuable diagnostic information (Walker, 1954; Champy, 1922; Gerdes et al., 1983; Yu et al., 1992). With respect to understanding fundamental cell cycle regulation, early studies assessed DNA synthesis (using radioactive nucleotides or nucleotide analogs), protein abundance, localization, post-translational modifications, and cell division in single cells grown under a variety of culture conditions. In this way, the eukaryotic cell cycle was divided into discrete phases (Taylor, 1960; Lajtha et al., 1954; Howard and Pelc, 1953).

The development of microfluidic flow cytometry that measures the intensity of fluorescent DNA or antibody stains revolutionized the cell cycle field. One of the many advantages over the earlier methods is the routine and rapid quantification of thousands of cells per sample and the relatively unbiased comparisons among different samples (Darzynkiewicz et al., 2004). Moreover, multiple molecular parameters can be assessed simultaneously, and the number of distinct measurements is limited only by the spectral properties of the reagents and the fluorescence detectors. Since large numbers of cells are analyzed by flow cytometry simultaneously, researchers have opportunities to derive rates of cell cycle phase transitions and identify minor subpopulations of cells (Kafri et al., 2013; Roy et al., 2013). The opportunities for multiplex measurements have expanded significantly with the recent development of mass cytometry (Bendall et al., 2011).

The advent of genetically-encoded fluorescent proteins expanded the capabilities of single cell analysis in many fields, including the cell cycle. An important recent contribution by Sakaue-Sawano *et al.* took advantage of existing knowledge about specific ubiquitin-mediated protein degradation events to create a pair of cell cycle biosensors they named FUCCI for “fluorescent ubiquitination-based cell cycle indicator.” (Sakaue-Sawano et al., 2008). They generated and co-expressed red and green fluorescent protein fusions that are degraded in S phase or G1 phase respectively. Using flow cytometry, fixed cell microscopy and time-lapse live

Figure 2.1

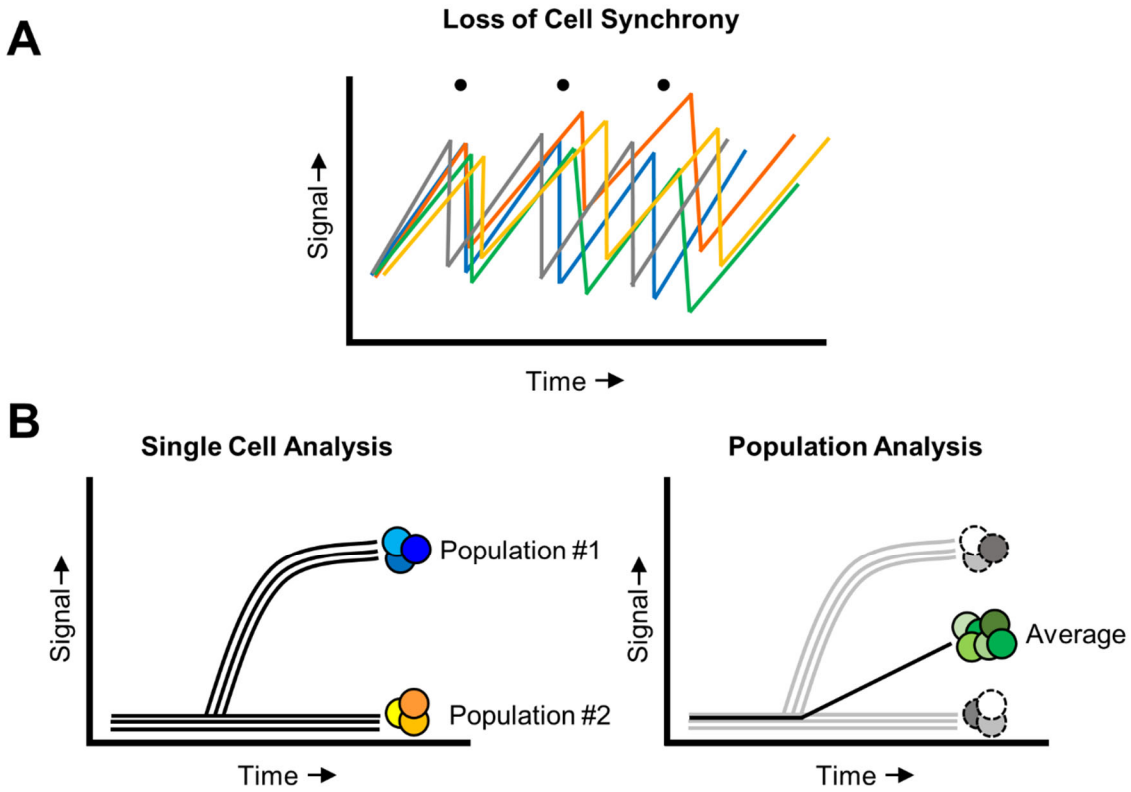

Figure 2.1. Advantages of single cell analysis
(A) Hypothetical molecular signal in individual cells of an artificially-synchronized population. Black dots represent cell divisions. Cells are synchronized in the first cell cycle, but within two to three cell cycles the population is completely asynchronous. (B, Left) Single cell analysis identifies and tracks a representative molecular signal in coexisting cell populations where different subpopulations take different cell cycle fates. (B, Right) Ensemble analysis of the same coexisting populations reports only the average signal that may not represent either subpopulation's cell cycle fate.

cell imaging, these biosensors were utilized initially by Sakaue-Sawano and subsequently by many others in a variety of physiological, developmental, and pathological settings to visualize cell cycle phases (Zielke et al., 2014; Coronado et al., 2013; Sugiyama et al., 2009). New genome editing tools to efficiently incorporate fluorescent tags at endogenous genes will expand the proliferation reporters beyond the original FUCCI pair (Stewart-Ornstein and Lahav, 2016).

The high time resolution of fluorescent live cell imaging using fluorescent reporters is particularly powerful for determining the relationships among two or more events, even when they are closely-spaced in time (Welch et al., 2011; Spiller et al., 2010). Live cell microscopy reveals when a stereotypical order of events characterizes a given cell cycle phase (Muzzey and van Oudenaarden, 2009). For example, live imaging studies in both budding yeast and human cells identified sequences of protein degradation events that characterize passage through the individual subphases of mitosis or at the onset of S phase (Lu et al., 2014; Izawa and Pines, 2011; Coleman et al., 2015). Furthermore, automated cell identification and tracking computer programs and scripts now make it possible to generate robust datasets of reporter signal intensities from many hundreds of cells without the potential biases of quantifying cells by hand (Jaqaman et al., 2008; Carpenter et al., 2006). While these software tools are rapidly advancing, each imaging data set usually requires a customized image analysis pipeline and parameter optimization.

Cell cycle proliferation and the restriction point phenomenon

Commitment to either cell cycle progression or quiescence is mutually exclusive. Moreover the collection of molecular states that differ between quiescent cells and cells committed to S phase entry is extensive and varied (Coller, 2011). It's worth emphasizing here that quiescent cells are not characterized simply as the absence of proliferation-associated activities. Quiescence is actively maintained not only through continual transcriptional repression of genes required for DNA replication and mitosis, but also through active expression

of anti-apoptotic, anti-senescence, and anti-differentiation genes (Coller et al., 2006; Legesse-Miller et al., 2012; Sang et al., 2008; Litovchick et al., 2007).

The commitment to proliferation is a binary decision that is marked by the onset of DNA replication, an irreversible process. For this reason the transition from G1 to S phase is under tight and multifaceted controls; disruption in those controls drive many aspects of cancer cell phenotypes. Moreover, partial replication of chromosomal DNA is particularly dangerous in actively proliferating cells, because the eventual dissolution of replication forks that do not ultimately meet one another during normal termination leads to double-stranded chromosome breaks (Zeman and Cimprich, 2014). Thus, cells that start replication must be fully prepared to finish replication in a time-frame compatible with the biochemical limitations of the replication program (number of initiation sites, replication fork stability and speed, etc.).

To ensure adequate preparation before S phase onset and a robust start and finish for DNA replication, the G1/S transition is a “bistable switch.” Bistability is a steady state distribution of two populations which may interconvert in a rapid, switch-like manner. It characterizes many cell cycle transitions so that progression from one phase to the next is rapid, complete, and unidirectional (Tyson and Novak, 2008; Barr et al., 2016; Ferrell et al., 2011). In the case of the G1/S transition, bistability applies to the activation of the cyclin dependent kinase (Cdk) Cyclin E/Cdk2 which triggers replication initiation (Yuan et al., 2014). A series of molecular feedback and feedforward relationships ensure that very little Cdk2 is active during early-to-mid G1 but in late G1, Cdk2 activity is sharply upregulated and stably maintained until later in S phase. These include: Cyclin E synthesis, degradation of a Cdk2 inhibitor protein ($p27^{KIP}$), Cdc6-dependent loading of the replicative DNA helicase to license replication origins, and Cyclin E/Cdk2 activation. Cdk2 activation is abrupt, but not at the exact same time in different cells. At any time in a population there may be subpopulations of cells with different discrete Cdk2 activity levels. The experimental challenges posed by this intercellular variability in the timing of rapid, irreversible, transitions from one phase to the next are greatly alleviated by single cell analyses.

Cells commit to either quiescence (G0) or future S phase entry at the restriction point. The term “restriction point” or “R-point” was first proposed by Arthur Pardee in 1974 based on the timing of DNA synthesis in populations of hamster fibroblasts after a cell cycle block and release (Pardee, 1974). The restriction point was the cell cycle point past which cells were irreversibly committed to S phase entry, regardless of whether or not extracellular mitogens were removed (Zetterberg et al., 1995). It is sometimes described as the “point of no return” in the cell cycle with respect to S phase entry. Mammalian cells in culture require external mitogens for proliferation, and since the DNA content of quiescent cells is the same as G1 cells, and mitogen stimulation leads to DNA synthesis before mitosis, it seems obvious that cells exit to quiescence from G1. What has not always been obvious is precisely *when* during the cell cycle mitogens are sensed to execute the commitment to quiescence versus proliferation nor what the precise molecular nature of the decision itself is (Hitomi and Stacey, 2001).

Pardee noted the limitations of measuring a cell population for cell cycle commitment and acknowledged the possibility that intercellular heterogeneity or the presence of fast-responding subpopulations would be missed in his study (Pardee, 1974). A subsequent single cell microscopy study in 1985 by Zetterberg and Larsson indicated that the only time mitogens are essential for the commitment to proliferation is in G1 phase (Zetterberg and Larsson, 1985). In these pioneering experiments, the authors conducted time lapse microscopy of proliferating mouse fibroblasts that were transiently deprived of mitogens. They found that the only cells that responded to mitogen withdrawal (by markedly delaying the next cell division) were very “young” cells in the first few hours after mitosis. They also noted intercellular variability in G1 length. Their observations have guided discussions of cell cycle commitment as an exclusively G1 event for the past 30 years.

Cell cycle commitment during re-entry to G1 from quiescence

The mechanisms by which mitogens stimulate passage through the restriction point and cell cycle commitment initiate at the plasma membrane with mitogen receptors (Figure 2.2A). Of

central relevance, external mitogens activate signal transduction activities including the Ras GTPase (Massagué, 2004). Ras activation stimulates a pathway culminating in activated gene expression through transcription factors such as c-Myc, serum response factor, and others (Blagosklonny and Pardee, 2002; Shaulian and Karin, 2002; Zhang et al., 2016). Among the principle proliferation genes under control of these transcription factors are those encoding D-type cyclins (hereafter Cyclin D). Cyclin D protein complexes with either of two redundant cyclin-dependent protein kinases, Cdk4 or Cdk6, and cyclin binding activates Cdk4/6 to phosphorylate the Retinoblastoma (Rb) transcriptional repressor at one of many individual phosphorylation sites. Rb does not itself bind DNA but rather is recruited to specific genes through interaction with the family of DNA binding transcription factors known as the E2F family. E2F controls the expression of a suite of genes necessary for DNA replication, S phase progression, and mitosis. Rb binds E2F which results in active transcriptional repression of those E2F target genes. For many years, the prevailing paradigm – based largely on molecular assays of whole cell populations - has been that initial partial Rb phosphorylation by Cyclin D/Cdk4 (or Cyclin D/Cdk6) gradually releases E2F inhibition to activate transcription (Massagué, 2004; Giacinti and Giordano, 2006; Weinberg, 1995; Blagosklonny and Pardee, 2002; Johnson and Skotheim, 2013). One of the E2F target genes that is induced is *cyclin E*, and the Cyclin E protein binds and activates the Cdk2 protein kinase which then participates in Rb phosphorylation in a positive feedback loop; this feedback loop is further reinforced by the fact that E2F1 is one of the E2F target genes. Full Rb hyperphosphorylation completely releases Rb from E2F relieving repression of E2F target genes and allowing for activated E2F-dependent transcriptional induction and S phase entry.

Pardee proposed that cells exist in two states – either proliferating or quiescent – and that the G1 restriction point marked the shift from quiescence to proliferation. E2F activation

Figure 2.2

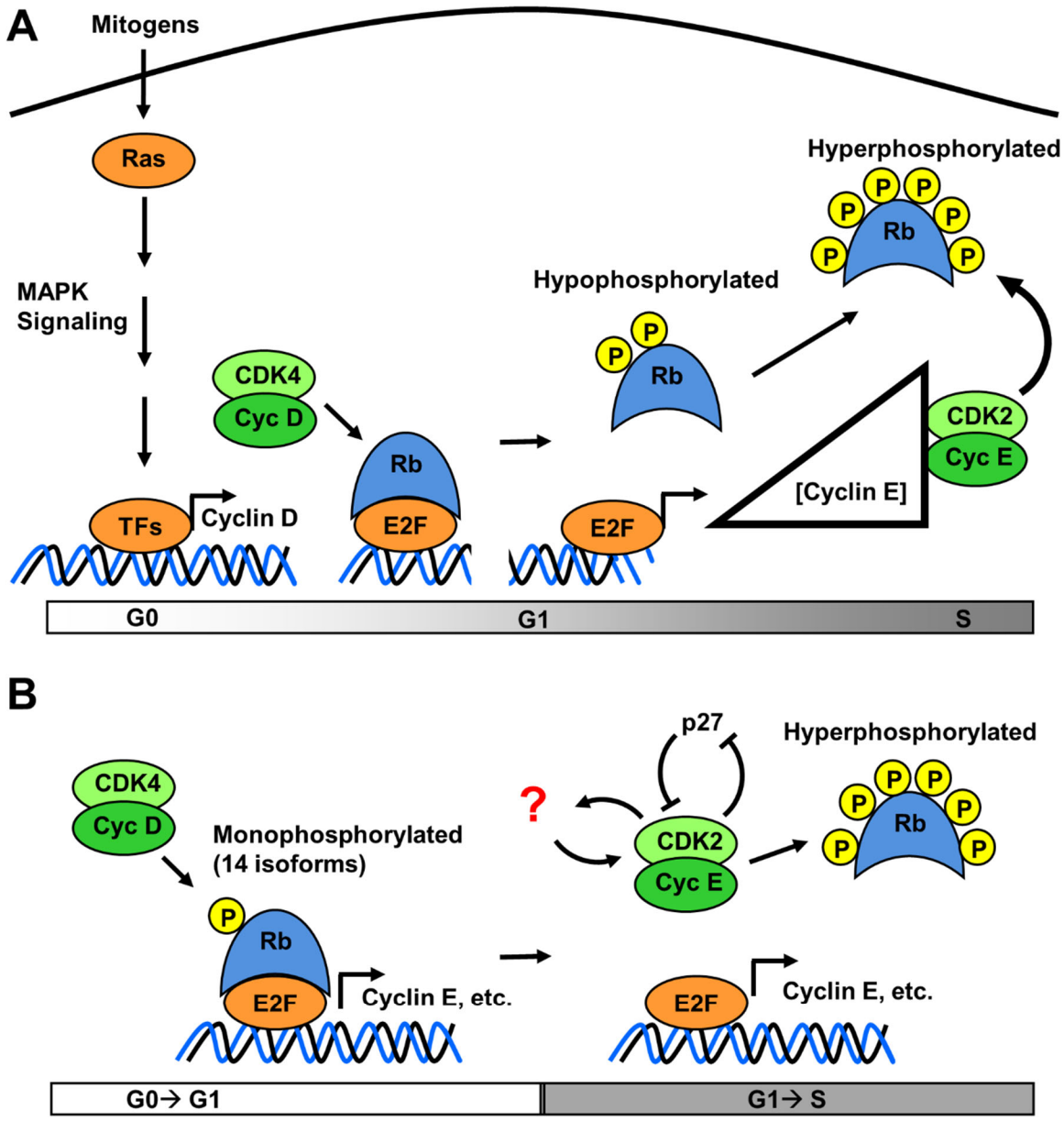

Figure 2.2. The restriction point during re-entry to G1 from quiescence
(A) The prevailing paradigm of the restriction point. Mitogens activate Ras signaling, downstream MAP Kinases, and ultimately Cyclin D transcription. Cyclin D complexes with CDK4 and CDK6 to partially phosphorylate Rb, and this hypophosphorylation causes release from E2F and partially activates Cyclin E expression. Cyclin E complexes with CDK2 to hyperphosphorylate Rb, creating a positive feedback loop where progressively increasing Cyclin E levels increase Rb phosphorylation leading to increased Cyclin E transcription and S phase

commitment. (B) An alternate model for the restriction point. Cyclin D-CDK complexes only monophosphorylate Rb on 14 unique sites. The monophosphorylated Rb remains E2F-bound, but at least some aspects of Rb-mediated gene repression are relieved moving cells from G0 to G1. Multiple sustained mitogen-dependent inputs (p27 degradation, origin licensing, etc.) activate Cyclin E-CDK2 complexes which rapidly hyperphosphorylate Rb in a switch-like fashion to drive commitment to S phase.

emerged later as a popular marker of post-restriction point cells which have committed to division. The prevailing model of gradual and progressive Rb phosphorylation during G1 was not easily reconciled with an all-or-none proliferation decision however. Methods that measure entire populations of cells – such as DNA synthesis by general thymidine incorporation or immunoblotting cell lysates for Rb hyperphosphorylation, report only a global average of any subpopulations, making it difficult to precisely detect a switch between two states. To overcome this hurdle and focus specifically on E2F control, Yao *et al*. used single cell flow cytometry with fluorescent E2F or Cyclin D transcriptional reporters to correlate mitogen-induced gene expression with the switch triggering cell cycle commitment during re-entry from quiescence (G0) (Yao et al., 2008). They synchronized cells in G0 by mitogen withdrawal then re-stimulated with serum. Transcriptional activity displayed an all or none bistable response resulting in two distinct cell populations. That is, each individual cell either remained quiescent with no reporter transcription, or displayed maximally-active expression. Significantly, there were no intermediate states and no partial commitment to the cell cycle. Sustained mitogen stimulation shifted the probability that any individual cell committed to S phase entry. This shifting probability was detectable as changes in the distribution of the population between the two states. Single cell flow cytometry clearly distinguished and quantified the two subpopulations of maximal or minimal response.

The study by Yao *et al.* was also the first demonstration of a bistable commitment point directly related to E2F activity. A feature of this bistability was that cell cycle commitment measured by reporter activation required sustained and strong E2F stimulation, but once activated, was largely irreversible. Low levels of mitogens were insufficient to pass the restriction point and activate E2F. On the other hand, withdrawing mitogens after a cell passed the restriction point with high E2F transcriptional activity neither reduced E2F reporter activity nor prevented S phase entry. Thus, quiescent cells require a threshold of E2F activity to re-

enter the cell cycle, and committed cells retain their high E2F activity even if the environment favoring proliferation changes.

One mechanism that maintains E2F activity once it crosses the commitment point is feedforward regulation of the *E2F1* gene itself. E2F1 transcription is stimulated not only by E2F but also by the c-Myc transcription factor (Leung et al., 2008) which is stabilized by mitogen signaling (Sears et al., 2000). The dynamics of mitogen activated E2F1 expression were precisely monitored by Dong *et al*. with an updated fluorescent E2F1 transcriptional reporter for single cell live imaging to compare the contributions of Cyclin/Cdk and Myc to E2F dependent cell cycle commitment (Dong et al., 2014). Importantly, they tracked the behavior of individual cells over time, and correlated commitment to divide with each cell's history of reporter activity. At any time before irreversible commitment to the cell cycle, the E2F transcriptional activity in a cell predicted the probability for commitment to cell division. Greater levels of transcription before the restriction point correlated with higher probability to re-enter the cell cycle, passing the restriction point.

A recent study further challenges the notion that E2F is progressively activated by progressive Rb phosphorylation via Cyclin D in early-to-mid G1 and then via Cyclin E in late G1 (Narasimha et al., 2014). A team of scientists from the Dowdy lab (Narasimha, Kaulich, Shaprio, *et al.*) used isoelectric focusing gels and a series of phospho-specific Rb antibodies to show that Rb is exclusively monophosphorylated by Cyclin D throughout most of G1 phase (Figure 2.2B). Fully un-phosphorylated Rb was restricted to non-transformed cells under conditions of profound quiescence induced by mitogen deprivation or after terminal differentiation. Surprisingly, Rb was monophosphorylated at any one of the 14 individual Cdk sites by Cyclin D/Cdk4 (or Cyclin D/Cdk6), and the sites seemed to be functionally equivalent, though potential differences in their effects at different E2F-regulated genes remain to be investigated. Importantly, no intermediate Rb phospho-isoforms appeared at any time during G1. Moreover, a sharp Cyclin E mRNA increase coincided with Cdk2 activation and abrupt switch-like Rb

hyperphosphorylation at ≥ 10 sites. Each of the 14 different Cyclin D-induced monophosphorylated Rb isoforms remained bound to E2F, suggesting that some degree of active repression at E2F-regulated genes may be maintained throughout G1 even after Cyclin D/Cdk4-mediated Rb phosphorylation (Narasimha et al., 2014). The apparent requirement for Cyclin E/Cdk2 to rapidly convert monophosphorylated Rb to fully hyperphosphorylated Rb suggests a strict division of labor between Cyclin D- and Cyclin E-activated kinases under normal conditions. The model proposed is that Cyclin D-mediated Rb phosphorylation is not the sole late G1 event that marks passage through the restriction point. Cyclin D may instead promote entry from quiescence into early G1 while other events are likely required to drive cells through G1 past the restriction point.

The prime candidate for the event needed for restriction point passage was long-held to be cyclin E transcription which is under Rb-E2F control. Cyclin E protein activates Cdk2 protein kinase which both hyperphosphorylates Rb and can trigger DNA replication initiation. Certainly, high Cdk2 activity corresponds with both Rb hyperphosphorylation and post-restriction point behavior (i.e. mitogen-independent cell cycle progression) (Narasimha et al., 2014). Multiple recent studies using time-lapse microscopy of single cells have found inconsistencies with the Cdk2 and Rb-centric model that have not yet been fully resolved. In one study pharmacological Cdk2 inhibition did not block fibroblast cell passage through the restriction point, and cyclin E accumulation appeared later than the calculated restriction point time of 3-4 hours post-mitosis (Ekholm et al., 2001). Similarly Rb phosphorylation was not elevated until several hours *after* cells had already committed to mitogen-independent proliferation (Martinsson et al., 2005). The Cdk2 inhibitor used in that study, roscovitine, inhibits enzymes in addition to Cdk2 however, though it is not yet clear how important the other kinases are for restriction point passage (Bach et al., 2005). Highly selective Cdk2 inhibition in untransformed epithelial cells using chemical genetics suggested a positive role for Cdk2 in restriction point passage (Merrick et al., 2011). Thus, although a sharp increase in Cdk2 activity is required for Rb hyperphosphorylation and for

origin firing in S phase (at least in cells passing through G1 from quiescence), it is not clear that Cyclin E/Cdk2 activity alone normally causes commitment to future S phase entry.

Classic studies with overproduced Rb mutant forms that block G1 progression, overproduced cyclin that accelerates G1 progression, or genetic Cyclin and Cdk null alleles should be carefully interpreted in light of our current understanding about the redundancies among Rb and cyclin family members. The question remains if Rb hyperphosphorylation itself is the principal molecular determinant of restriction point passage or if it is a downstream consequence of restriction point passage or some combination of both models. Cell type and whether the cells are actively proliferating or first entering the cycle from quiescence may be important determinants of when and how the commitment is made (discussed below).

Regardless of whether Cdk2 causes restriction point passage or is a subsequent reflection of that commitment, the correlation between an increase in Cdk2 activity and commitment to S phase entry is widely accepted. The molecular mechanisms that drive the increase in cyclin E/Cdk2 activity are all in feedforward relationships with Cdk2 to reinforce bistability (Figure 2.2B). One of these relationships is Cdc6-dependent DNA replication origin licensing, and Cdc6 is itself stabilized by Cdk2 phosphorylation in late G1 (Mailand and Diffley, 2005; Machida et al., 2005; Shreeram et al., 2002; Nevis et al., 2009). A second major Cdk2 regulator is the $p27^{KIP}$ protein which is both a direct inhibitor of Cdk2 kinase activity and also a substrate of Cyclin E/Cdk2. p27 is abundant in quiescent cells but is partially degraded shortly after cell cycle re-entry from G0 in early G1 which reduces, but does not eliminate p27 (Rizzardi and Cook, 2012). In late G1, the remaining p27 is eliminated by Cyclin E/Cdk2-induced degradation (Rizzardi and Cook, 2012). In another example of single cell biosensor use to track cell proliferation decisions, Oki *et al.* followed both the initial p27 drop from G0 to G1 and the subsequent elimination at G1/S by time-lapse fluorescence microscopy and flow cytometry of cells expressing a fluorescent p27 fusion. Altogether, this collection of distinct mitogen-dependent molecular events cooperate in late G1 to activate Cyclin E/Cdk2, and the

feedforward mechanisms serve to maintain high activity through the G1/S transition (Cappell et al., 2016).

Cell cycle decisions in actively-proliferating populations.

The proliferation decision committing cells to complete the cell cycle or exit to quiescence has until recently, been thought to occur only in G1 (Zetterberg et al., 1995). However, single cell studies suggest the cell proliferation decision can occur during a window of G2 in the previous cell cycle in actively proliferating cells. Hitomi and Stacy first demonstrated that mitogen-induced Ras activity is required in G2 to complete the next cell cycle (Hitomi and Stacey, 1999). Spencer *et al*. subsequently explored this G2 mitogen requirement by removing mitogens from proliferating cultures during time lapse fluorescence microscopy (Spencer et al., 2013). They observed a large subpopulation of cell in mitosis or early G1 when the mitogens were withdrawn that were already committed to complete one more cell cycle.

A key component of this study was the use of a fluorescent fusion protein that responds to changes in Cdk2 activity, a Cdk2 “biosensor”. At the start of G1 (i.e. just after mitosis), new cells were either already on a trajectory to increase biosensor activity or they started G1 with measurably lower activity that remained low for many hours. Cells born with the already increasing kinase activity contained hyperphosphorylated Rb and were apparently irreversibly committed to completing the next cell cycle, even if mitogens were withdrawn or mitogen signaling was inhibited in early G1. Mitogen withdrawal, mitogen pathway inhibition or high levels of a Cdk2 inhibitor during the preceding G2 phase reduced biosensor activity in the subsequently-born daughter cells and blocked progression into S phase in the following cell cycle (though cells completed the ongoing G2, M phase, and cytokinesis). Conversely, cells born with naturally low Cdk2 activity entered a prolonged G1/G0-like state and required sustained mitogen signaling through early G1 to commit to cell division (similar to the Zetterberg and Larsson restriction point study) before committing to G1 progression. Sister cells were born with the same biosensor activity and cell cycle commitment, supporting the idea of a decision

occurring in the previous cell cycle. The low activity cells were interpreted as transiently exiting to quiescence and then re-entering the cell cycle at G1 whereas the high activity cells were pre-committed to finishing the next cell cycle.

Tracking cells from G2 through division and monitoring subpopulations in the next G1 was only possible by single cell analysis. Moreover live imaging of the fluorescent reporter in single cells revealed the two subpopulations of cells with different Cdk2 activity levels and subsequently different G1 phases. Interestingly, different cell lines had different relative amounts of the two subpopulations; transformed cell lines had more of the increasing Cdk2 cells and non-transformed more of the low Cdk2 activity cells. These differences generally correlated with the propensity of the different cells to exit the cell cycle, a characteristic that varies with cell cycle and especially transformation status.

A second study by Naetar *et al.* supports the role for a Cdk2-driven G2 decision window committing cells to the next cell cycle (Naetar et al., 2014). These authors withdrew mitogens from cells that they had pre-synchronized in G2 and used flow cytometry to measure DNA synthesis in the following cell cycle to test commitment to the next cell cycle. Removing serum mitogens during G2 caused cell cycle exit in the following G1 as expected. However, simultaneously inhibiting protein phosphatase 2A (PP2A) during the G2 mitogen withdrawal prevented cell cycle exit in the following G1. The cells committed irreversibly to completing the next cell division even though they entered G1 without mitogens present. Specific Cdk2 inhibition by chemical genetics or dominant-negative Ras expression coincident with PP2A inhibition during G2 mitogen withdrawal imposed the expected cell cycle exit in the following G1. It seems that G2 specific PP2A-dependent protein dephosphorylation of substrates phosphorylated by Cdk2 and Ras-dependent kinases is required to re-establish mitogen dependence in early G1 phase. The requirement for mitogen dependent Ras signaling in G2 for commitment to the next cycle is also consistent with the pioneering single cell studies by Hitomi and Stacy (Hitomi and Stacey, 1999). Thus, a cellular decision to proliferate or become

quiescent can occur during the previous cell cycle in a window of G2 receptive to mitogens. The notion that the events in the previous cell cycle control the outcome of the next cycle is a relatively new concept in the field.

The notion that a G2 proliferation decision can produce distinct subpopulations of G1 cells with different molecular characteristics likely includes molecular distinctions beyond the activity of Cdk2 and its regulators. One possibility for an additional molecular distinction is the chromatin loading of replicative DNA helicases, known as Minichromosome maintenance complexes (MCM), to license DNA replication origins (Skarstad and Katayama, 2013; Remus and Diffley, 2009). MCM loading is restricted to G1 and thought to be largely irreversible in that the only mechanism known for MCM unloading occurs during replication completion itself. (Kuipers et al., 2011; Maric et al., 2014; Moreno et al., 2014). Therefore, differences in G2 proliferation decisions may be reflected in the kinetics or patterns of G1 MCM loading. In support of this idea Håland *et al.,* using an innovative flow cytometry technique to measure protein chromatin association in single cells, compared the timing of MCM loading to the timing of Rb chromatin release (i.e. Rb hyperphosphorylation) (Håland et al., 2015). Cells re-entering G1 from G0 only loaded MCM complexes after Rb chromatin release (MCM loading only after the restriction point). On the other hand, cells entering G1 from a preceding mitosis were distributed into two populations: cells with loaded MCM before Rb chromatin release and cells with loaded MCMs after Rb chromatin release (MCM loading both before and after the restriction point). The potential for cycling cells with two modes of MCM regulation in G1 is consistent with the idea of two populations after the G2 decision window.

A second study suggesting distinct G1 subpopulations focused on the inactivation of the APC^{Cdh1} ubiquitin ligase at the G1/S transition. Cappell *et al.* co-expressed the Cdk2 biosensor from Spencer *et al.* with a second biosensor derived from the FUCCI system (Cappell et al., 2016). Cells with increasing kinase activity in G1 not only spent little time in G1 but they also rapidly inactivated APC^{Cdh1}. Conversely, the subpopulation of cells with low kinase activity and

an extended G1/G0 inactivated APC^{Cdh1} with delayed and variable timing. Interestingly, the G1 subpopulation of G2 committed cells could be further divided into multiple smaller populations with variable responses to DNA damage, oxidative and osmotic stresses. We expect future single cell live cell imaging studies will discover even more unique subpopulations in many cell cycle phases (Darzynkiewicz et al., 2004).

Multiple proliferation decision points – multiple mechanisms?

The suggestion that mitogen-dependent proliferation commitments can occur in G2 rather than G1 raises new questions about the molecular mechanisms that drive proliferation decisions. Cell cycle commitments during both the G2 decision window and the G1 restriction point require mitogen signaling through the Ras GTPase pathway (Dobrowolski et al., 1994; Peeper et al., 1997; Mulcahy et al., 1985; Hitomi and Stacey, 1999), but what are the key molecular targets of this pathway in either setting? Is Cyclin D/Cdk4 activity important for cells to commit to proliferation in G2? While the details of the G2 decision window are incompletely understood, we suggest that: (1): The G1 restriction point and the G2 decision window operate by related but not identical molecular mechanisms. (2): The G1 restriction point is most important during the transition from G0 to cell cycle re-entry in G1, while the G2 decision window functions in continuously cycling cells. We also favor the idea that actively proliferating cells - especially non-transformed cells – can spontaneously and transiently divert to quiescence, and that their eventual progression through G0/G1 requires passage through the same G1 restriction point as mitogen-starved and re-stimulated cells (Figure 2.3).

In cells re-entering G1 from quiescence, mitogen-dependent Cyclin D expression supports an Rb-E2F molecular state that is required, but not sufficient, for subsequent G1 progression. Progression from this permissive state past the G1 restriction point requires sustained mitogen signaling and a collection of interconnected and reinforcing mechanisms that stimulate Cdk2 activation. E2F-stimulated Cyclin E expression is one of these mechanisms, but p27 degradation at the G0/G1 transition and again in late G1, and MCM loading (which supports

Cdk2 activity by an as-yet unknown mechanism) are also important contributors to Cdk2 activation (McIntosh and Blow, 2012). In addition, Cdk2 is cytoplasmic in at least some quiescent cells which prevents it from acquiring an essential activating phosphorylation by a nuclear kinase (Nevis et al., 2009; Lunn et al., 2010). Mitogen-stimulated signaling causes Cdk2 to translocate to the nucleus for activation, but Cdk2 is constitutively nuclear and phosphorylated in actively proliferating cells. Thus at least one additional requirement to activate Cdk2 in cells entering G1 from G0 is already met by cells entering G1 from the preceding cell cycle.

The Myc transcription factor also has different roles at the G1 and G2 proliferation decisions. For passage through the G1 restriction point, Ras-driven Myc accumulation regulates and cooperates with E2F transcriptional activity to control a suite of proliferation-related genes (Dong et al., 2014; Leung et al., 2008; Hölzel et al., 2001). For commitments made during G2 however, Myc is apparently important primarily for Cyclin E transcription, possibly to prime G2 cells for high Cyclin E/Cdk2 activity after mitosis (Naetar et al., 2014). Neither Cyclin D nor other E2F target genes including PCNA, CCNA2 (Cyclin A), and E2F1 are transcribed in G2 under the same conditions (Naetar et al., 2014). This observation suggests the G2 decision window, unlike the G1 restriction point during cell cycle re-entry, does not heavily rely on Rb-E2F control as a primary mechanism. Moreover cells lacking all three Rb family members, “triple knockout” mouse embryonic fibroblasts, require mitogen signaling in G2, but not G1, for proliferation (Foijer et al., 2005, 2008). We suggest that E2F transcription is not required in G2 for commitment to the following cell cycle, but rather continues to promote cell cycle transcription in the following G1 in cells which are already committed to division.

The G2 decision window ultimately leads to increasing and self-reinforcing Cdk activity as the switch that determines proliferation or quiescence in the next cell cycle. Of note, Cdk2 activity itself peaks in S phase, but many Cdk2 functions can also be carried out by Cdk1, so the proliferation commitment may be set by a combination of Cdk2 and Cdk1 activity in G2 phase

Figure 2.3

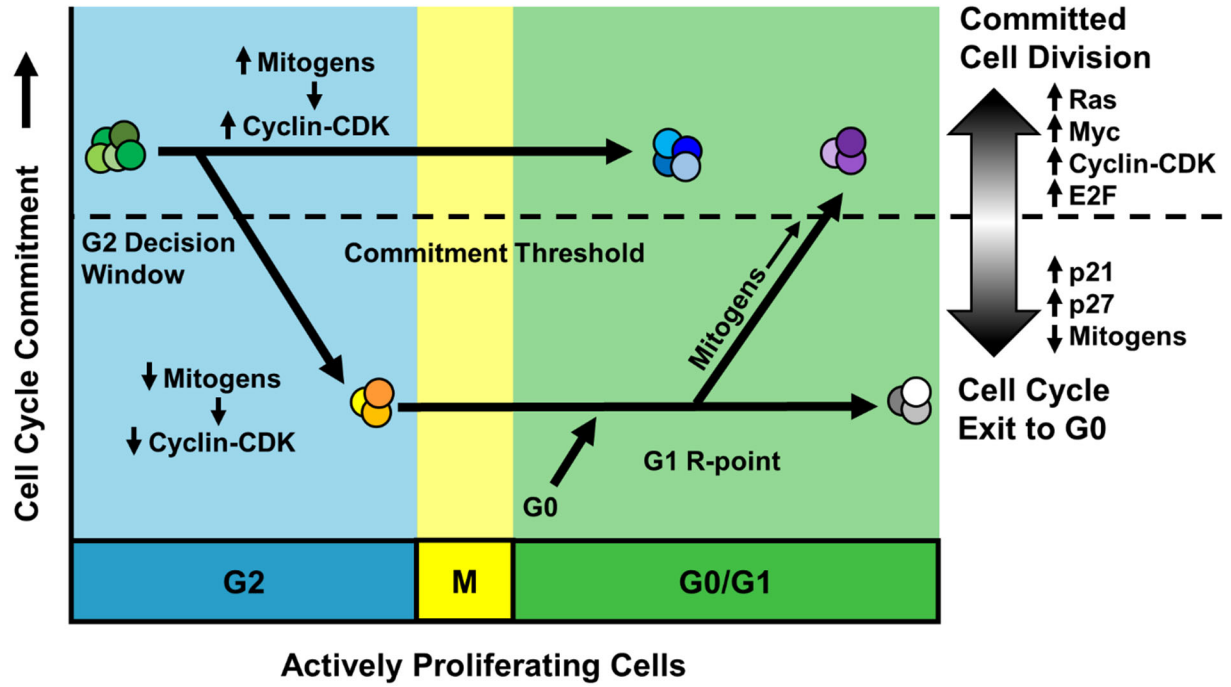

Figure 2.3 Multiple proliferation decisions in actively dividing cells
Actively dividing cells have two distinct proliferation decision points. The first is a window during G2, in which cells with CDK activity above a critical threshold pre-commit to completing the next cell cycle with a short G1. A subpopulation of G2 cells with reduced mitogen signaling and/or low Cyclin-CDK activity do not commit to the next cell cycle. These cells have a long, variable length subsequent G1/G0-like phase and are presented with a second proliferation decision at the G1 restriction point. Sustained mitogen signaling promotes increased CDK activity above the commitment threshold which is self-sustaining through multiple feedback and feedforward relationships. In the absence of sustained signaling and increasing CDK activity, cells exit to G0. The probability of cells committing to the cell cycle or exiting to G0 is the cumulative probability of multiple molecular events.

(L'Italien et al., 2006). The precise downstream target(s) of Cdk mediating the G2 proliferation decision are not clear, but it does not appear to be E2F-stimulated transcription in G2 (Naetar et al., 2014). Spencer *et al.* provided evidence that an important determinant of high or low Cdk activity in G2 is the abundance of the CDK inhibitor, p21 (which is related to p27 but regulated by different mechanisms) (Spencer et al., 2013). Cells with high p21 and low Cdk activity in G2 entered a variable, but prolonged G1/G0-like state in the following cell cycle, and cycling cells lacking p21 altogether proliferated with high Cdk2 activity (Perucca et al., 2009; Spencer et al., 2013). The relative contributions of CDK inhibitors, kinase activity, and Rb-E2F-controlled transcription to the ultimate commitment to proliferation are likely influenced not only by the differences between mitogen signaling for cell cycle re-entry from quiescence and mitogen-dependent cell cycle progression in proliferating cells by also by cell type and cell context.

G2-committed cells consistently pass quickly through the subsequent short G1 phase (Naetar et al., 2014; Spencer et al., 2013). Interestingly, G1 length varies considerably between different human cell types in culture: human embryonic stem cells spend as little as 2-3 hours in G1 whereas many differentiated cell lines spend 12 hours or more in G1 (Kapinas et al., 2013). It is intriguing to speculate that in a population of cells with very short G1 lengths, all the cells make the proliferation commitment in the G2 decision window and never face the G1 restriction point. Both cancer cells with short G1 lengths and embryonic stem cells have high levels of CDK activity, which may guarantee consistent G2 commitment in nearly every cell cycle (Malumbres and Barbacid, 2001; Kapinas et al., 2013). Mutations that cause high CDK activity might dictate G2 commitment to the next cell cycle, and consequently a short G1 phase.

Outlook

Technological advances in microscopy, flow cytometry, and fluorescent reporters have made it increasingly clear that individual cells make different proliferative decisions, even when they are genetically identical to one another and are cultured together. These intercellular differences are likely to be more pronounced in tissues where variations in cellular

microenvironments affect local proliferation signals. For example, the intestinal epithelium comprises a broad range of proliferative stem cells and differentiated cells that respond to diverse spatial signaling cues (Simons and Clevers, 2011). Understanding the behavior of a cell population requires a nuanced appreciation that each cell responds to intrinsic or extrinsic cues by shifting its probability of entering or exiting the cell cycle. Thus, statistical models that take these probabilities into account will be particularly useful predictive tools (Klein and Simons, 2011). Mathematical models of cell cycle transitions have been in development for several years, and the increasingly-sophisticated ability to acquire real-life parameters for molecular events using robust quantitative single cell approaches will both test and refine these models (Barr et al., 2016; Huard et al., 2012; Tyson and Novák, 2015; Weis et al., 2014).

One long-term goal held by many in the field is deep mechanistic understanding of proliferation decisions and the factors that affect the probabilities of progressing from G1 to S phase or exiting from G1 to quiescence. An important contributor to the achievement of that goal will be combinations of assays that reveal the relationships among molecular events and cell behaviors. For example, simultaneously tracking two or more biosensors in the same cell is the best way to determine the order of two events and if one is likely the cause of the other (Stewart-Ornstein and Lahav, 2016; Coleman et al., 2015; Cappell et al., 2016). Furthermore combining different types of single cell assays, such as live cell imaging of fluorescent biosensors with single-cell transcriptomics or genomics, ties the recent molecular behavior of one cell with its later fate (Skinner et al., 2016; Toledo et al., 2013; Zhang and Pellman, 2015; Zhang et al., 2015). We anticipate that ongoing technological and conceptual breakthroughs will ultimately yield practical benefits such as precision cancer diagnoses and treatments, interventions into degenerative diseases and aging, and cell-based therapies.

CHAPTER 3: RAPID DNA REPLICATION ORIGIN LICENSING PROTECTS STEM CELL PLURIPOTENCY[2]

Introduction

Metazoan DNA replication requires initiation at thousands of DNA replication origins during S phase of every cell cycle. Origins are genomic loci where DNA helicases first unwind DNA and DNA synthesis begins. Origins are made competent for replication during G1 phase of each cell cycle by the loading of Minichromosome Maintenance (MCM) complexes onto DNA. MCM is the core component of the replicative helicase, and the process of MCM loading is termed origin licensing. Total MCM levels remain constant throughout the cell cycle, but the levels of DNA-loaded MCM change as cells progress through the cell cycle. Cells can begin MCM loading as early as telophase, and loading continues throughout G1 until the G1/S transition, the point of maximum DNA-loaded MCM(Kimura et al., 1994; Todorov et al., 1995). Throughout S phase, individual MCM complexes are activated for DNA unwinding as origins "fire". MCM complexes travel with replication forks and are progressively unloaded as replication forks terminate (Figure 3.1A)(Deegan and Diffley, 2016; Remus and Diffley, 2009; Siddiqui et al., 2013).

The control of origin licensing is critical for genome stability. Origins must not be re-licensed after S phase begins because such re-licensing can cause a genotoxic phenomenon known as re-replication which may result in double strand breaks, gene amplification, aneuploidy, and general genome instability(Arias and Walter, 2007; Truong and Wu, 2011). To

[2]Modified from: Matson, J. P., Dumitru, R., Coryell, P., Baxley, R. M., Chen, W., Twaroski, K., Webber, B. R., Tolar, J., Bielinsky, A.-K., Purvis, J. E. and Cook, J. G. (2017) 'Rapid DNA replication origin licensing protects stem cell pluripotency', eLife, 6, p. e30473. doi: 10.7554/eLife.30473.

avoid re-replication, MCM loading is tightly restricted to G1 phase by multiple overlapping mechanisms that destroy or inactivate MCM loading proteins to prevent any new origin licensing On the other hand, cells typically load 5-10-fold more MCM complexes in G1 than they strictly require under ideal circumstances, and the additional MCM loading ensures timely and complete genome duplication even if replication hurdles are encountered in S phase (Ibarra et al., 2008; Woodward et al., 2006; Ge et al., 2007). It is possible for cells to proliferate with less than optimal MCM loading, but such cells are hypersensitive to DNA damage and replication stress(Blow et al., 2011; McIntosh and Blow, 2012).

MCM loading to license origins is restricted to G1, but G1 length varies widely among different cell types. For example, specialized developmental and immune cell cycles have minimal G1 lengths of mere minutes(O'Farrell et al., 2004; Kinjyo et al., 2015; Kermi et al., 2017). In cultured human embryonic stem cells, G1 is only 2-3 hours, and this short G1 is both a hallmark of and has been implicated in maintaining pluripotency(Soufi and Dalton, 2016; Kareta et al., 2015b). G1 lengthens early in differentiation, and in cultured somatic cells is often greater than 12 hours (Calder et al., 2013). Thus, different proliferating cells have drastically different amounts of time available to complete MCM loading before making the G1-to-S phase transition. In addition, pluripotent stem cells respond to differentiation stimuli specifically in G1 phase, suggesting that the balance among cell cycle phases influences differentiation potential(Gonzales et al., 2015; Pauklin and Vallier, 2013).

Given that MCM loading is restricted to G1 and the wide variation of G1 lengths, we postulated that the absolute amount of loaded MCM in S phase is a product of both the time spent in G1 and the rate of MCM loading. The combination of these two parameters has implications for genome stability because loading more or less MCM in G1 influences S phase length and how effectively S phase cells can accommodate both endogenous and exogenous sources of replication stress(Shima et al., 2007; Pruitt et al., 2007). These implications are relevant both when cell cycle distributions change during development and during oncogenesis

Figure 3.1

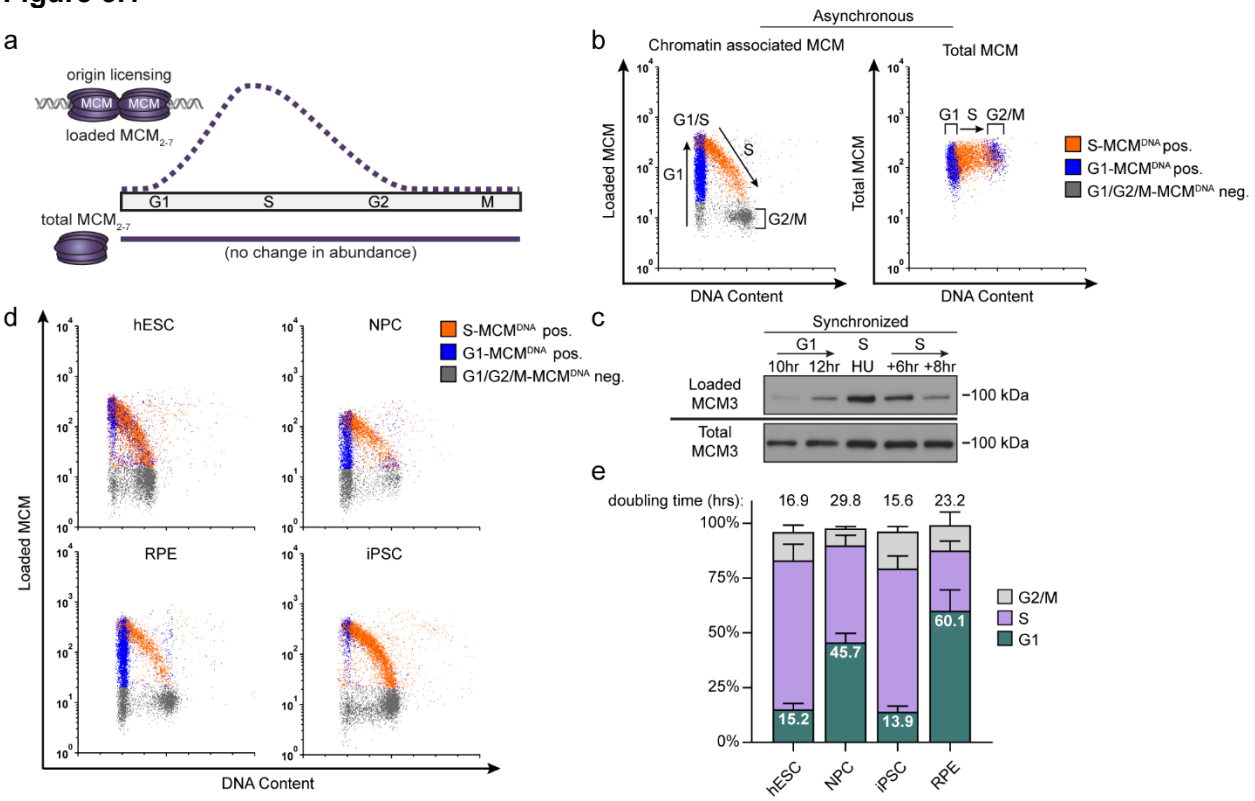

Figure 3.1. Pluripotent stem cells load MCMs faster than differentiated cells.
(**a**) DNA-loaded MCM levels increase in G1 and decrease in S phase whereas total MCM protein levels are constant throughout the cell cycle.
(**b**) Flow cytometric analysis of DNA-loaded and total MCM in asynchronously proliferating RPE1-hTERT cells. Cell cycle phases are defined by DNA content and DNA synthesis. Left: Cells were labeled with EdU, extracted with nonionic detergent to remove unbound MCM, fixed, and stained with anti-MCM2 (a marker for the MCM_{2-7} complex), DAPI (total DNA), and for EdU incorporation (active DNA synthesis). Orange cells are S-phase with DNA-loaded MCM, blue cells are G1-phase with DNA-loaded MCM, and grey cells are G1/G2/M phase cells without DNA-loaded MCM. Right: Cells were treated as on the left except that they were fixed prior to extraction to detect total MCM2.
(**c**) T98G cells were synchronized in G0 by contact inhibition and serum deprivation, then released into G1 for 10 or 12 hrs, or re-synchronized in early S with hydroxyurea (HU), and released into S for 6 or 8 hrs. MCM3 in chromatin-enriched fractions (Loaded) or whole cell lysates (Total) was detected by immunoblotting.
(**d**) Chromatin flow cytometry of the indicated asynchronous cell lines measuring DNA content (DAPI), DNA synthesis (EdU incorporation), and loaded MCM (anti-MCM2). Blue Cells are G1-MCM^{DNA}-positive and EdU-negative, orange are S phase-MCM^{DNA}-positive; grey are G1/G2/M-MCM^{DNA}-negative.
(**e**) Stacked bar graph of cell cycle phase distribution from cells in (d); mean with error bars ± SD (n=3 biological replicates). The doubling times were calculated experimentally using regression analysis in GraphPad Prism.

after S phase begins(Remus and Diffley, 2009; Arias and Walter, 2007; Truong and Wu, 2011). since many cancer cell lines also have short G1 phases. The actual rate of MCM loading in human cells has not yet been quantified however, and little is known about how the amount, rate or timing of MCM loading varies between cells with different G1 lengths. Here we utilized single cell flow cytometry to measure MCM loading rates in asynchronous populations of pluripotent and differentiated cells. We discovered that rapid MCM loading is intrinsic to pluripotency, slows universally during differentiation, and rapid replication licensing suppresses differentiation. These findings demonstrate that the rate of MCM loading is subject to developmental regulation, and we suggest that rapid origin licensing is a new hallmark of pluripotency.

Results

Pluripotent cells load MCM significantly faster than differentiated cells.

We considered two possibilities for how cells with varying G1 lengths load MCM onto DNA. One possibility is that cells with short G1 phases load MCM at the same rate as cells with long G1 phases resulting in less total loaded MCM. Alternatively, cells with short G1 phases could load MCM faster than cells with long G1 phases and reach similar levels of loaded MCM. To distinguish between these scenarios, we developed an assay to measure DNA-loaded MCM in individual cells of asynchronously proliferating populations by adapting a previously-reported flow cytometry method(Håland et al., 2015; Moreno et al., 2016). We extracted immortalized epithelial cells (RPE1-hTERT) with nonionic detergent to remove soluble MCM. We then fixed the remaining chromatin-bound proteins for immunofluorescence with anti-MCM2 antibody as a marker of the $MCM_{2\text{-}7}$ complex, and for DNA content (DAPI) and DNA synthesis (EdU) to measure cell cycle phases (Figure 3.1B, left). We used a sample without primary antibody as a control (relevant flow cytometry gating schemes are shown in Figure 3.2). For chromatin flow cytometry, MCM signal below the antibody threshold is colored grey ("G1/G2/M-MCM^{DNA} neg"), whereas detectable MCM signal is colored either blue in G1 cells ("G1-MCM^{DNA} pos") or orange

in S phase cells ("S-MCM^{DNA} pos"). As expected, total MCM protein levels do not substantially change during the cell cycle (Figure 3.1B, right)(Todorov et al., 1995). For comparison to commonly used cell fractionation methods to assess MCM dynamics, we also probed immunoblots of chromatin-enriched fractions, and noted a similar MCM expression, G1 loading, and S phase unloading pattern (Figure 3.1C)(Cook et al., 2002; Mendez and Stillman, 2000). Interestingly, individual G1 cells (blue stripe) have a very broad range of DNA-loaded MCM levels with a more than 100-fold difference between minimum and maximum (Figure 3.1B, left). MCMs are unloaded during S phase, ending in G2/M with undetectable MCM on DNA (Figure 3.1B, left). Moreover loaded MCM is resistant to extraction in high salt buffer which removes peripherally-bound chromatin proteins (Figure 3.3F-H), similar to yeast MCM complexes loaded *in vitro* (Bowers et al., 2004; Randell et al., 2006). We validated MCM2 antibody specificity using quiescent G0 synchronized cells (MCM unloaded), and we also observed the same broad G1 signal distribution using MCM3 antibody (Figure 3.3A-D).

Loaded MCM complexes are extremely stable on DNA, both *in vivo* and *in vitro*(Cocker et al., 1996; Evrin et al., 2009; Remus et al., 2009; Bowers et al., 2004). In human cells, MCMs can persist on DNA for more than 24 hours during a cell cycle arrest and are typically only unloaded during S phase(Kuipers et al., 2011). These properties result in MCM loading that occurs unidirectionally throughout G1 phase(Symeonidou et al., 2013). The unidirectional nature of MCM loading means that G1 cells with low MCM levels are in early G1, and G1 cells with high MCM levels are in late G1. Since we observed a broad distribution of MCM loading throughout G1 including many cells with low levels of loaded MCM, we conclude that RPE1-hTERT cells load MCM relatively slowly during their ~9 hr G1.

We then used this method to analyze MCM loading in asynchronous cells with different G1 lengths. H9 human embryonic stem cells (hESCs) have a short G1 phase and spend most of the cell cycle in S phase. In contrast to the differentiated epithelial cells, the majority (~80%) of

Figure 3.2

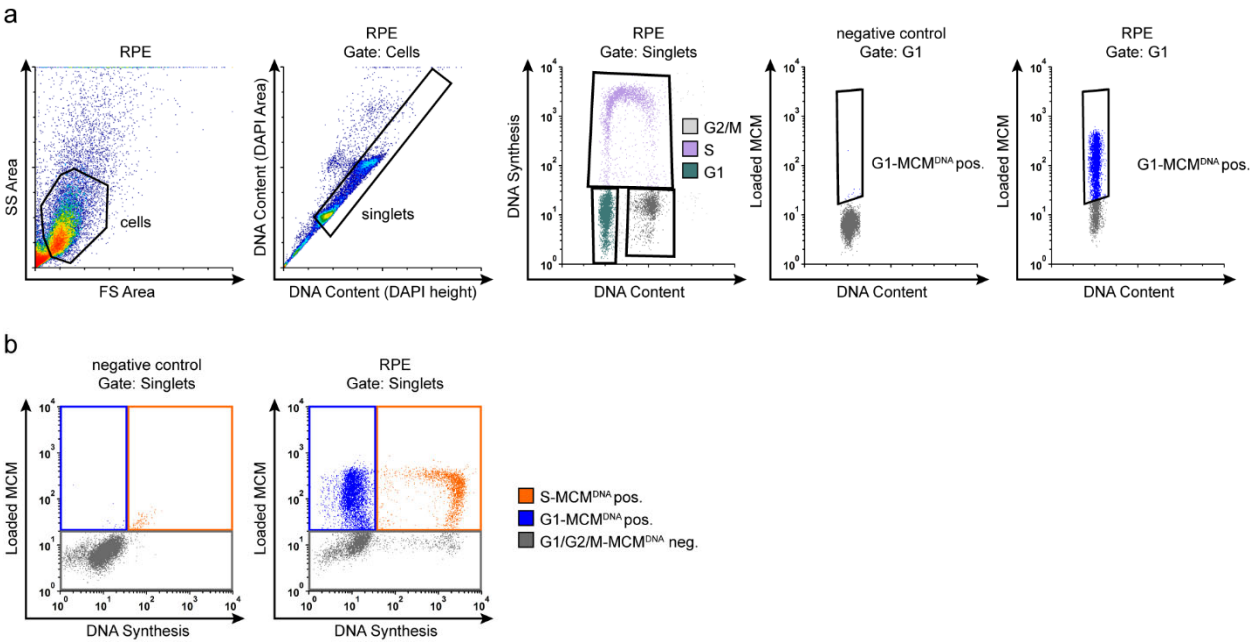

Figure 3.2. Flow Cytometry Gating

(**a**) Example flow cytometry gating with chromatin extracted ARPE-19 (RPE) cells from Figure 3.1d, measuring Loaded MCM (anti-MCM2), DNA Synthesis (EdU incorporation) and DNA content (DAPI). Gating to discriminate cells from debris was on FS-area vs SS-area, singlets (individual cells) from clumps of cells was on DAPI height vs DAPI area, cell cycle phases were determined on DAPI-area vs EdU-647. Non-specific background staining by the secondary antibody was accounted for by using a negative control sample stained without primary antibody, only secondary antibody to gate on cells positive for DNA-loaded MCM on DAPI-Area vs MCM2-488.

(**b**) Example flow cytometry color gating with chromatin extracted ARPE-19 cells from Figure 1d. Left: Negative control to define background staining without EdU incubation or MCM2 primary antibody. Cells were stained with DAPI, subjected to EdU detection chemistry, and stained with secondary antibody. Cells with greater EdU or MCM values than the majority of this background stained sample were gated as positive cells for DNA-Loaded MCM or DNA synthesis (EdU). Right: Chromatin flow cytometry of ARPE-19 measuring DNA content (DAPI), DNA synthesis (EdU-647), and loaded MCM (anti-MCM2). Gates define color schemes for color dot plots.

(**c**) Gating for early S phase for cells in Figure 4d, EdU +, MCM^{DNA}+, G1 DNA Content.

Figure 3.3

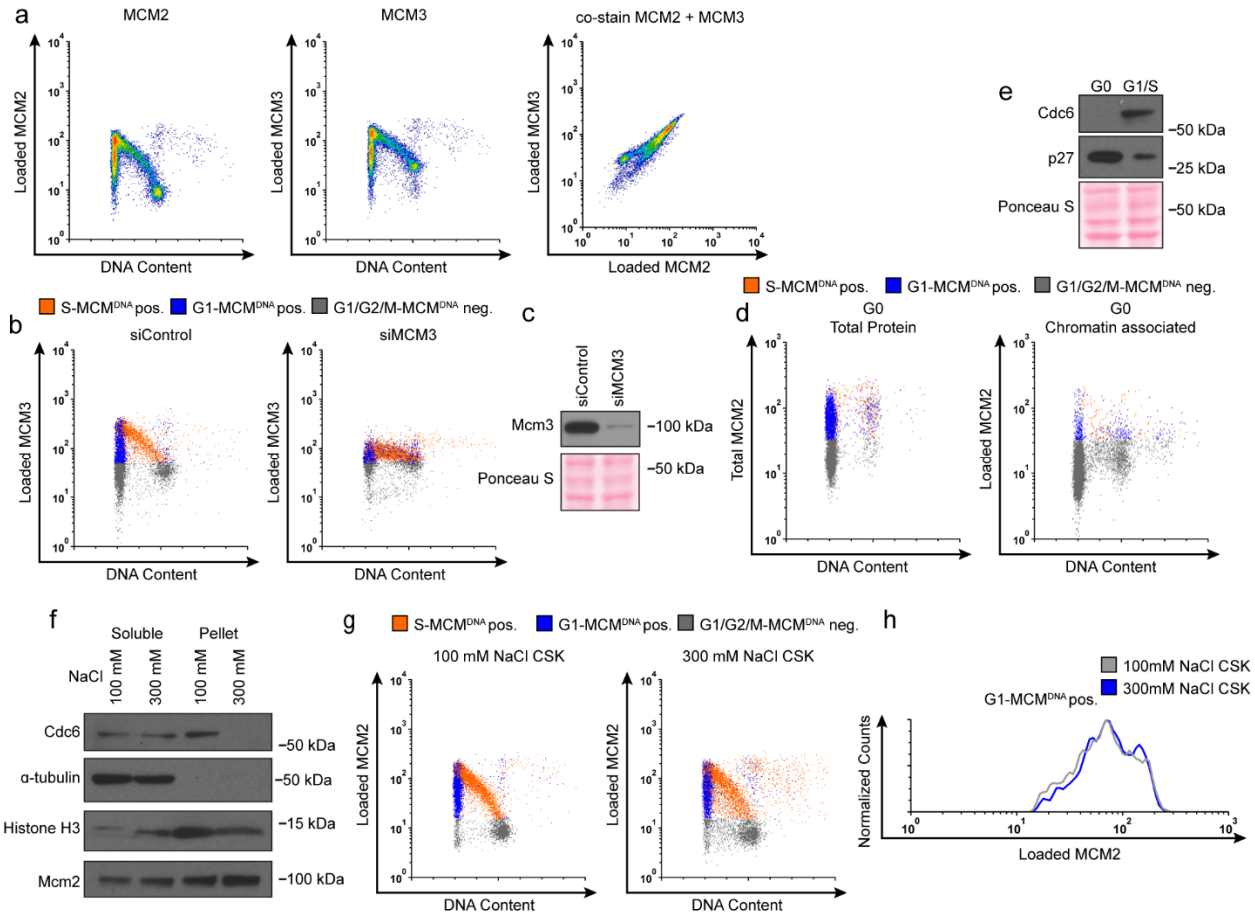

Figure 3.3. Validation of MCM antibodies for chromatin flow cytometry.
(**a**) Chromatin flow cytometry of RPE1 cells stained for loaded MCM2 (anti-MCM2), loaded MCM3 (anti-MCM3), and DNA content (DAPI). All 3 plots are the same sample. Cells stained with monoclonal MCM2 antibody for loaded MCM2 co-stain equally well for a polyclonal MCM3 antibody for loaded MCM3.
(**b**) Chromatin flow cytometry of RPE1 cells treated with 100 nM siControl or a 100 nM pool of siMCM3 for 72 hrs, measuring DNA content (DAPI), DNA synthesis (EdU incorporation), and loaded MCM3 (anti-MCM3). Loaded MCM3 levels decrease with siMCM3 treatment, demonstrating antibody specificity.
(**c**) Immunoblot of cells from (b).
(**d**) RPE1 cells synchronized in G0 by contact inhibition. Left: Total protein flow cytometry of G0 cells measuring total MCM (anti-MCM2), DNA synthesis (EdU incorporation) and DNA content (DAPI). Right: Chromatin flow cytometry of G0 cells measuring loaded MCM (anti-MCM2), DNA synthesis (EdU incorporation) and DNA content (DAPI). G0 cells lack loaded MCM, demonstrating antibody specificity.
(**e**) Immunoblot of cells for (d) demonstrating G0 synchronization.
(**f**). Immunoblots of cells fractionated into soluble protein and pellet (chromatin associated protein) using a normal salt CSK buffer (100mM NaCl) or high salt CSK buffer (300 mM NaCl). High salt 300 mM NaCl strips away weakly chromatin associated proteins, including Cdc6, but not loaded MCM.
(**g**) Chromatin flow cytometry of cells lysed with normal 100 mM NaCl CSK or high salt 300 mM NaCl CSK.

(**h**) Histograms of only the G1-MCM^{DNA} –positive cells from (g). The loaded MCM in G1 remains constant with high salt, demonstrating the chromatin flow cytometry measures DNA loaded MCM. Note the harsh 300 mM salt makes flow cytometry samples more difficult, therefore we use the 100 mM NaCl for all other flow cytometry experiments, which measures loaded MCM equally well.

G1 hESCs had high levels of loaded MCM; very few G1 cells had low levels of loaded MCM (blue cells, Figure 3.1D). This difference suggests that hESCs load MCM rapidly to achieve abundant DNA-loaded MCM in a short time. To test if MCM loading varies in differentiated cells, we differentiated hESCs into neural progenitor cells (NPCs) to generate an isogenic pair of pluripotent and differentiated cells. In contrast to hESCs, differentiated NPCs had a longer doubling time and a wide distribution of DNA-loaded MCM in G1 (blue cells, Figure 3.1D); they also spend approximately five time longer in G1 (Figure 3.1E; e.g. 15% of a 17 hr hESC cell cycle is 2.5 hrs in G1 vs to 45% of a 30 hr NPC cell cycle is 13.6 hrs in G1). Since the NPCs had many cells with low levels of DNA-loaded MCM, we conclude that these differentiated cells load MCM more slowly than hESCs.

To generate another isogenic pair of pluripotent and differentiated cells we reprogramed ARPE-19 primary retinal pigmented epithelial cells (RPE) into induced pluripotent stem cells (iPSCs). The iPSCs had hallmark features of pluripotency as measured by microscopy, bisulfite sequencing, gene expression, and teratoma formation (Figure 3.4A-E), and their G1 phases were typically seven times shorter than their differentiated parents (Figure 3.1E). Like hESCs, the pluripotent iPSCs had predominantly high levels of DNA-loaded MCM in G1 (Figure 3.1D). Importantly, both of the pluripotent cell lines reached approximately equal levels of DNA-loaded MCM at the start of S phase as their differentiated counterparts did, but in in less time (the absolute MCM loading intensities are comparable when samples are processed and analyzed with identical instrument settings). Taken together, these data demonstrate that pluripotent cells load MCMs rapidly in G1, but differentiated cells load MCMs slowly.

We then quantified the relative MCM loading rates in pluripotent and differentiated cells using ergodic rate analysis, a mathematical method that can derive rates from fixed, steady state populations(Kafri et al., 2013). Ergodic analysis can measure any unidirectional rate parameter from a steady state distribution, and is not limited to the cell cycle (e.g. car traffic jams)(Gray and Griffeath, 2001). The ergodic analysis as applied to the cell cycle means that

Figure 3.4

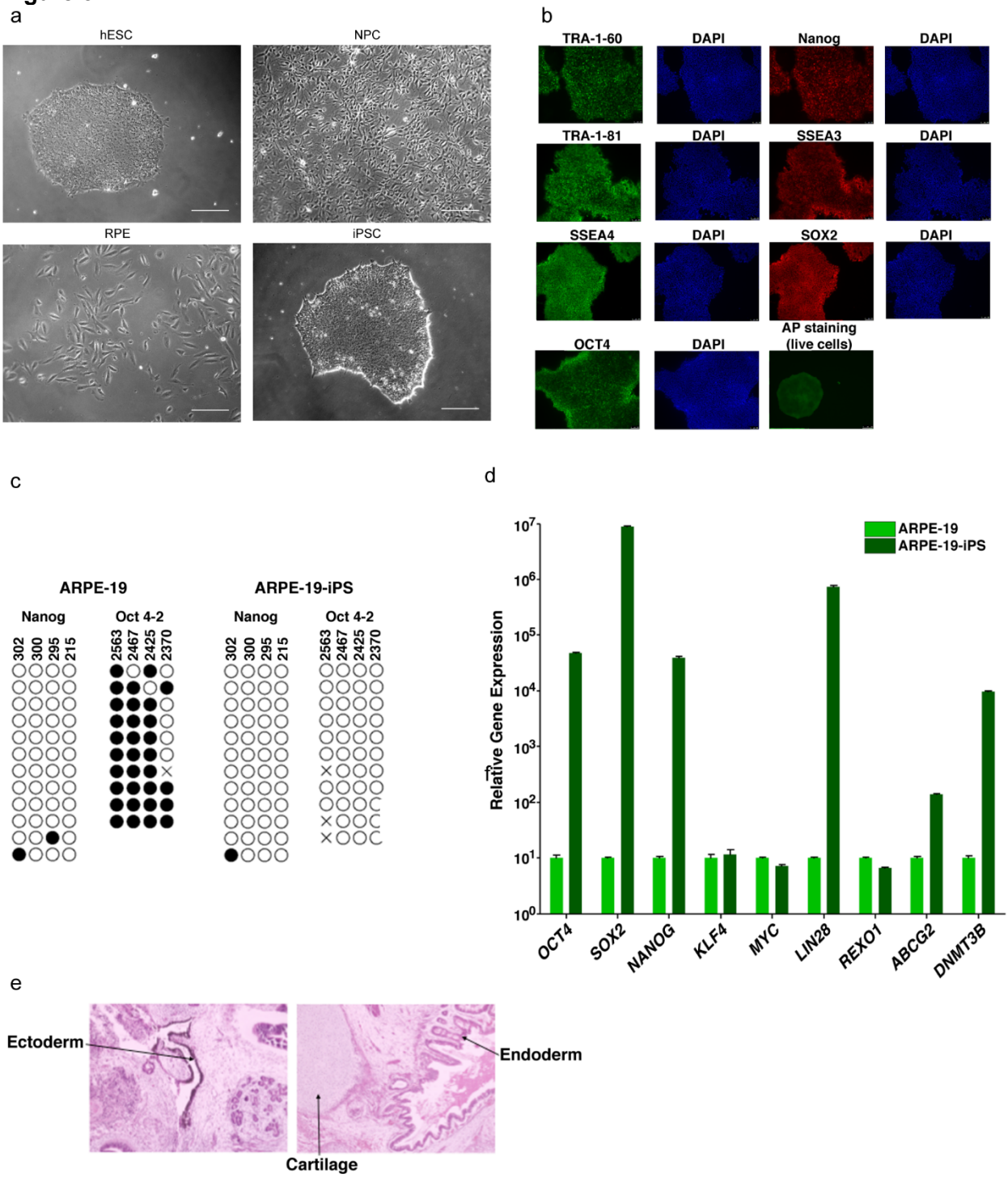

Figure 3.4. Characterization of pluripotent and differentiated cells.
(**a**) Representative phase contrast images in greyscale of indicated cell lines from Figure 3.1d. Scale bar is 50 µm.
(**b**) Immunofluorescence analysis of iPS cells visualizing TRA-1-60, TRA-1-81, SSEA or OCT4 (in green) and Nanog, SSEA3 or SOX2 (in red). DAPI counterstaining for DNA indicates the

nuclei of individual cells in each colony. Live alkaline phosphatase (AP) staining was also performed as a positive indicator of stem cells.
(**c**) Bisulfite sequencing analysis of the NANOG and OCT4-2 promoter regions in ARPE-19 and ARPE-19-iPS cells is indicated. Methylated CpGs are indicated with a closed circle, and unmethylated CpGs are indicated with an open circle. An 'X' indicates a mismatch or gap in the bisulfite sequence. The CpG position relative to the downstream transcription start site is shown above each row.
(**d**) Quantitative RT-PCR analysis showing the relative gene expression of OCT4, SOX2, NANOG, KLF4, MYC, LIN28, REXO1, ABCG2 and DNMT3B in ARPE-19 and ARPE-19-iPS cells (normalized to GAPDH). Error bars indicate standard error.
(**e**) Hematoxylin and eosin staining of teratoma sections from immunodeficient mice injected with ARPE-19-iPS cells show cartilage, as well as endoderm and ectoderm teratoma formed by ARPE-19-iPS.

within a steady state population with a constant doubling time and cell cycle distribution, the number of cells at any point in the cell cycle is inversely related to the rate they move through that point. For any measured parameter, the density of cells indicates rate: low cell density on a flow cytometry plot indicates a fast rate passing through that cell cycle state whereas high cell density indicates a slow rate. This phenomenon is analogous to a high density of slow-moving cars observed at a given point on a road in a traffic jam compared to a low density of fast-moving cars on an open highway. We visualized MCM loading as histograms of the MCM^{DNA} intensities in only the G1 cells for ergodic rate analysis (G1-MCM^{DNA}, Figure 3.5A, B and Figure 3.6).

To compute MCM loading rate per hour, we experimentally determined the cell cycle distributions and doubling times of each cell population (Figure 3.6). Pluripotent cells reached near equal levels of loaded MCM at the G1/S transition in less time than differentiated cells. To quantify the actual MCM loading rate difference, we subdivided the G1-MCM^{DNA} population into 10 equally-sized bins, calculated the MCM loading rate for each bin, then the overall average MCM loading rate for each G1 population. These calculations revealed that pluripotent hESCs loaded MCM 6.5 times faster per hour than differentiated NPCs and pluripotent iPSCs loaded MCM 3.9 times faster per hour than differentiated RPEs (Figure 3.5). Thus, pluripotent cells with short G1 phases load MCMs significantly faster than differentiated cells with long G1 phases.

Differentiation, G1 length, and MCM loading rate are coupled.

We hypothesized that MCM loading is fundamentally linked to pluripotency because MCM loading rate decreased during differentiation and increased during reprogramming. This idea predicts that slowed MCM loading is a phenomenon common to differentiation towards all germ layers. To test that hypothesis, we initiated differentiation in hESCs towards the three embryonic germ layers (neuroectoderm, mesoderm and endoderm), collecting cells at 24 hour and 48 hours after inducing differentiation (Figure 3.8). We confirmed progress towards each lineage by the expected gene expression changes, particularly induction of lineage-specific

Figure 3.5

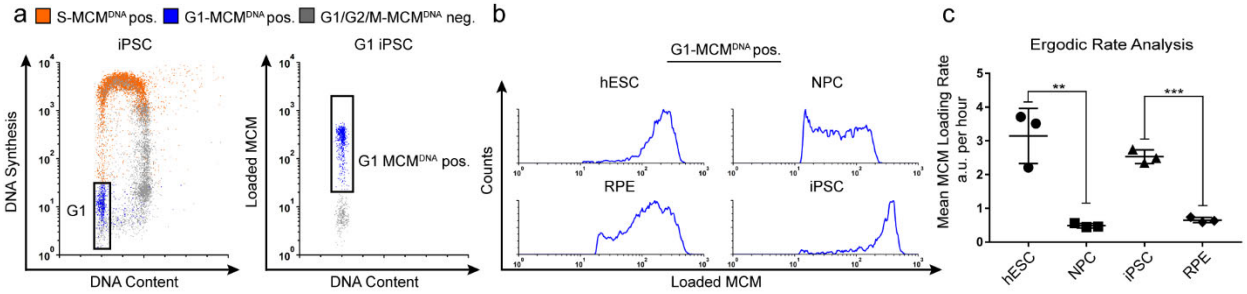

Figure 3.5. Quantification of MCM loading rate by ergodic rate analysis.
(**a**) Gating scheme for chromatin flow cytometry of iPSCs measuring DNA content (DAPI), DNA synthesis (EdU incorporation), and loaded MCM (anti-MCM2); this sample is from Fig 3.1d.
(**b**) Histograms of only the G1-MCM^{DNA} –positive cells from the four chromatin flow cytometry samples in Fig 3.1d.
(**c**) Calculated mean MCM loading rate per hour by ergodic rate analysis; mean with error bars ± SD. (n=3 biological replicates), unpaired two tailed t-test. **p=0.0049. ***p=0.001. See Methods for details.

Figure 3.6

a

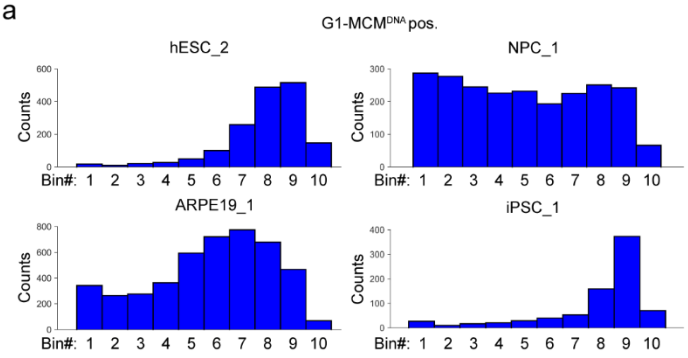

b

$$w_n = \alpha \frac{2 - F}{f_n}$$

c

	G1-MCM-DNA cell number	Total cell number	F
F_iPSC_1	799	9976	0.0801
F_iPSC_2	1438	9720	0.1479
F_iPSC_3	1255	10868	0.1155
F_H9_1	1454	10314	0.1410
F_H9_2	1637	10745	0.1523
F_H9_3	1113	10714	0.1039
F_ARPE19_1	4551	9655	0.4714
F_ARPE19_2	6363	10162	0.6262
F_ARPE19_3	4002	9901	0.4042
F_NPC_1	2244	6702	0.3348
F_NPC_2	1659	6592	0.2517
F_NPC_3	2030	7331	0.2769

d

	doubling time (hours)
iPSC	15.64
H9	16.91
ARPE-19	23.19
NPC	29.8
	alpha
alpha_iPSC	0.0443
alpha_H9	0.041
alpha_ARPE-19	0.0299
alpha_NPC	0.0233

Figure 3.6. Ergodic Rate Analysis binning.

(**a**) Histograms from G1-MCM^{DNA+} samples in Figure 2B, binned into 10 regions for ergodic rate analysis (see Methods).

(**b**) Ergodic rate equation based on (Kafri et al., 2013). w_n is the rate in each bin n, α is a constant accounting for doubling time, F is the fraction of cells in G1-MCM^{DNA+} out of all cells, f_n is the fraction of cells in each bin n out of G1-MCM^{DNA+} (see Methods).

(**c**) Value of F for 3 biological replicates for each cell line, used to calculate Figure 3.5c. (**d**) Doubling time and alpha values used to calculate rate in Figure 3.5c.

Figure 3.7

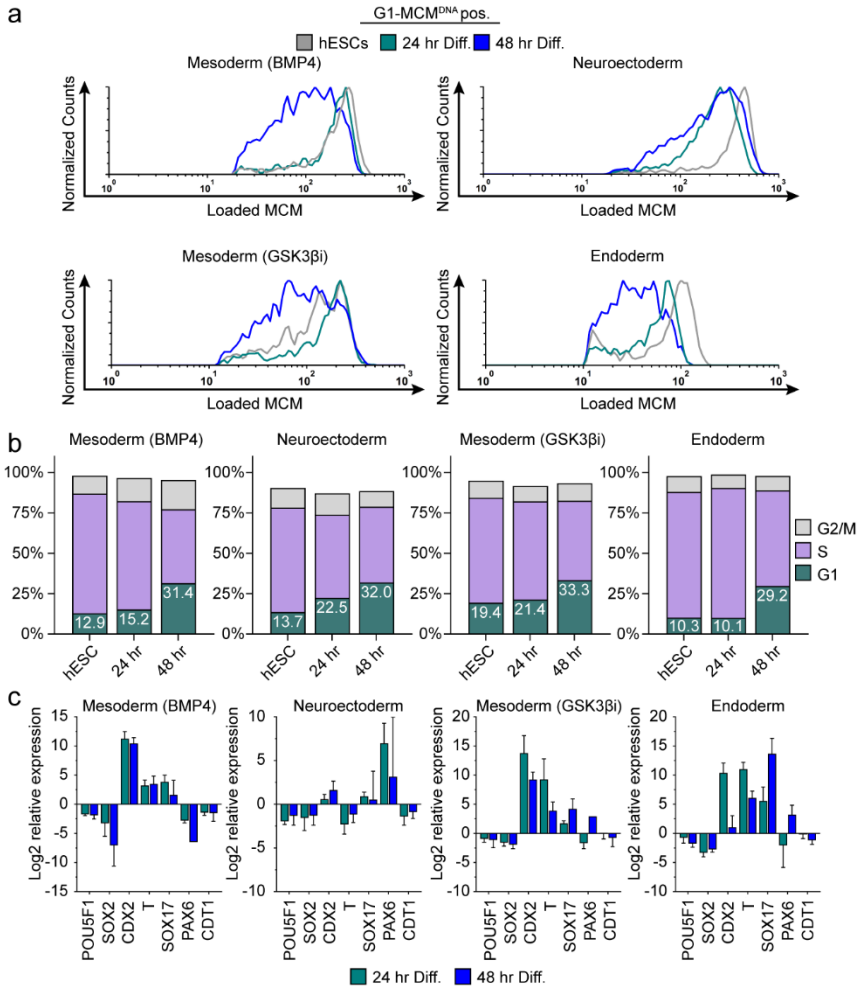

Figure 3.7. Differentiation universally decreases MCM loading rate.
(**a**) Chromatin flow cytometry of hESCs induced to differentiate towards mesoderm (BMP4), neuroectoderm, mesoderm (GSK3βi), or endoderm for 24 or 48 hrs. Histograms show only G1-MCM^{DNA} cells as in Figure 2b. See methods for differentiation protocols. Cell counts for 24 hr and 48 hr were normalized relative to corresponding hESC samples.
(**b**) Stacked bar graphs of cell cycle distribution for cells in (a).
(**c**) Gene expression analysis of differentiation markers by quantitative PCR of the samples in 3a; $\log_2$ expression is relative to the undifferentiated cells. Data are mean ±SD of two biological replicates.

Figure 3.8

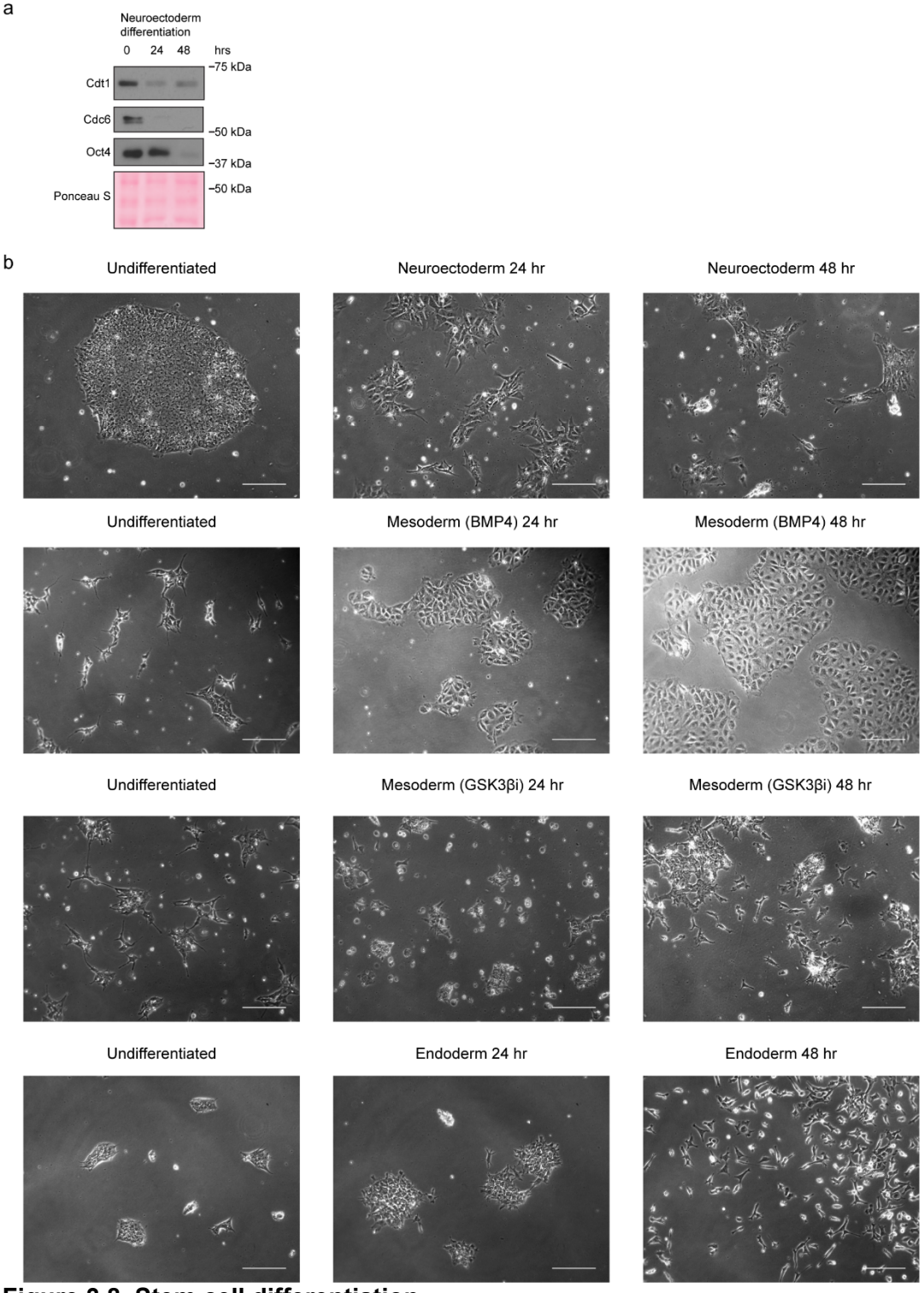

Figure 3.8. Stem cell differentiation.
(**a**) Immunoblots of neuroectoderm differentiation, as in Figure 3.7a.
(**b**) Representative phase contrast images in greyscale during the indicated differentiation protocols from Figure 3.7a. Scale bar is 50 μm.

markers and modest reduction of pluripotency markers – even at these very early time points (Figure 3.7C). We assessed MCM loading rates during differentiation by flow cytometry as before. The MCM loading rate clearly decreased for all germ layers rapidly within the first 48 hours of initiating differentiation (Figure 3.7A, compare the grey histograms for undifferentiated G1 cells to the green and blue histograms). The decrease in MCM loading rate also coincided with the increase in the proportion of G1 cells for each lineage. For example, within 24 hours of neuroectoderm differentiation, G1 had already lengthened and MCM loading had slowed, but during mesoderm (BMP4) differentiation both G1 lengthening and slowed MCM loading took 48 hrs (Figure 3.7A and B). The closely-coordinated changes that we universally observed during differentiation suggest that MCM loading rate is coupled to G1 length. Importantly, these results demonstrate that the rate of origin licensing by MCM loading is developmentally regulated.

We next asked if G1 length and MCM loading rate are *obligatorily* coupled, or if the link can be short-circuited by artificially advancing the G1/S transition. To distinguish between these possibilities, we constructed an RPE1-hTERT derivative with a *CYCLIN E1* cDNA under doxycycline-inducible control. Cyclin E1 overproduction reproducibly shortened G1 length, consistent with previous studies (Figure 3.9A, B)(Resnitzky et al., 1994; Ekholm-Reed et al., 2004). Strikingly, cells overproducing Cyclin E1 (designated as "↑Cyclin E1") not only spent less time in G1 but also began S phase with much lower amounts of loaded MCM compared to the control; this new subpopulation appeared in the central triangular region of the plots that is typically clear of S phase cells (Figure 3.9C, D orange S-MCM^{DNA}pos). Cyclin E1 overproduction dramatically increased the proportion of these MCM-low early S phase cells by six-fold from 9.9% of control S phase cells to 63.6% of ↑Cyclin E1, S phase cells (Figure 3.9C, D). We also conclude that the MCM loading rate did not increase to accommodate the shorter G1 because the MCM loading pattern in G1 remained constant and the ↑Cyclin E1 cells had on average at least two-fold less DNA-loaded MCM in early S phase than control cells (Figure 3.9F-H).

Figure 3.9.

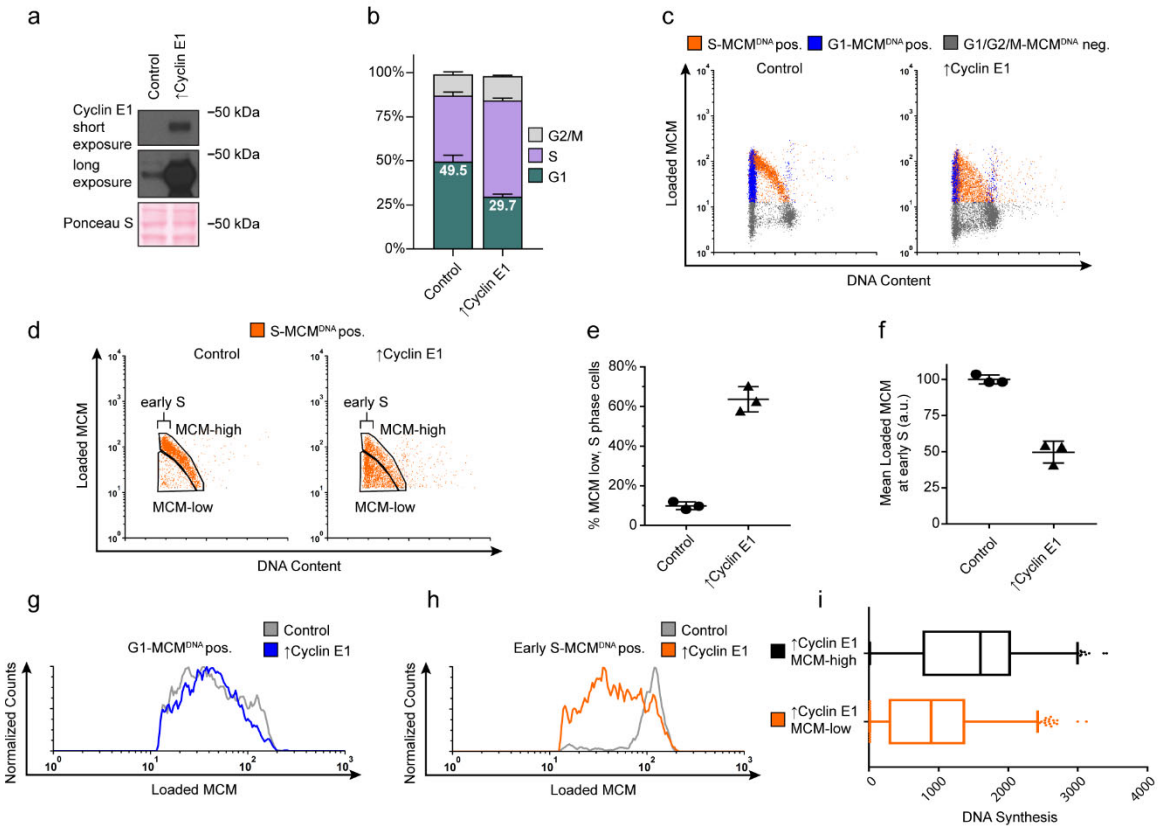

Figure 3.9. Cyclin E overproduction uncouples MCM loading and G1 length.
(**a**) Immunoblots of a stable derivative of RPE1-hTert cells bearing an integrated doxycycline-inducible *cyclin E* construct treated with 100 ng/mL doxycycline for 72 hrs to overproduce Cyclin E1 (↑Cyclin E1) or with vehicle control
(**b**) Stacked bar graphs of cell cycle distribution measured by flow cytometry for cells shown in (a); mean with error bars ± SD (n=3 biological replicates).
(**c**) Chromatin flow cytometry of control or cyclin E-overproducing cells measuring DNA content (DAPI), DNA synthesis (EdU incorporation), and loaded MCM (anti-MCM2).
(d) S-MCM^{DNA}+ cells from samples in (c) divided into populations that began S phase with high or low MCM^{DNA}. Early S cells are S phase cells with G1 DNA content.
(e) The percentage of MCM-low S phase cells relative to all S-MCM^{DNA}+ cells from three biological replicates; mean with error bars ± SD, unpaired two tailed t-test. ***p=0.002.
(**f**) Mean loaded MCM in early S phase, (S-MCM^{DNA}+, G1 DNA content) from three biological replicates; mean with error bars ± SD, unpaired two tailed t-test. ***p=0.0004.
(**g**) Histogram of G1-MCM^{DNA}+ cells from samples shown in (c). Counts for ↑Cyclin E1 are normalized to the control.
(**h**) Histogram of early S cells from samples shown in (d). Counts for ↑Cyclin E1 are normalized to the control. These data are one of the replicates quantified in (f).
(**i**) EdU intensity from ↑Cyclin E1, MCM-high or MCM-low cells from (d) as a box-and-whiskers plot. Center line is median, outer box edges are 25th and 75th percentile, whiskers edges are 1st and 99th percentile, individual data points are lowest and highest 1%, respectively. Median EdU incorporation of MCM-high ↑Cyclin E1 cells is 1.8 fold greater than MCM-low, mean EdU incorporation is 1.6 fold greater in MCM-high than MCM-low, average of 3 biological replicates. Samples compared by unpaired, two tailed t-test, **p=0.0027, **p=0.0033, respectively.

Furthermore, the ↑Cyclin E, MCM-low cells incorporated significantly less EdU per unit time than MCM-high cells did (1.6 fold lower mean, 1.8 fold lower median), indicating that low levels of loaded MCM are insufficient for normal S phase progression (Figure 3.9I). The early S phase cells with the least MCM loaded also had the least DNA synthesis by EdU intensity (data not shown). Thus, shortening G1 length without increasing MCM loading rate causes G1 cells to enter S phase prematurely without the full complement of DNA-loaded MCM.

Previous studies have shown that CDKs can inhibit MCM loading by directly inhibiting MCM loading factors, such as by stimulating Cdt1 degradation (Cdc10 dependent transcript 1), a protein essential for MCM loading (Ekholm-Reed et al., 2004; Sugimoto et al., 2004; Tanaka and Diffley, 2002). Cdt1 levels in lysates of asynchronous cells indeed decreased upon Cyclin E1 overproduction (Figure 3.10A). On the other hand, since Cdt1 is stable in G1 phase and degraded in S phase, the lower Cdt1 signal could have reflected less Cdt1 in the lysate due to the higher proportion of S phase cells; this indirect effect could apply to any cell cycle-regulated protein in cell populations with different cell cycle distributions. To test that idea, we measured total Cdt1 protein levels specifically in G1 by flow cytometry (Figure 3.10B). Cyclin E overproduction did not significantly reduce Cdt1 G1 levels relative to control (1.1 fold higher mean, 1.2 higher median, Figure 3.10C). We validated the Cdt1 antibody for immunofluorescence flow cytometry (Figure 3.10D-F). We conclude that Cyclin E/Cdk2 inhibits MCM loading indirectly, at least in part, by shortening G1 and decreasing the time available for MCM loading.

Fast loading hESCs have more Cdt1 in G1.

Loading MCM complexes onto DNA requires the six subunit Origin Recognition Complex (ORC), Cdc6, and Cdt1. We hypothesized that fast MCM loading in pluripotent stem cells is achieved by increased levels of the loading proteins. To test this idea, we probed protein lysates of asynchronous cells to compare the amount of MCM loading proteins between isogenic cell lines. Total Mcm2 and ORC protein levels remained constant (Figure 3.11A). The other MCM

Figure 3.10

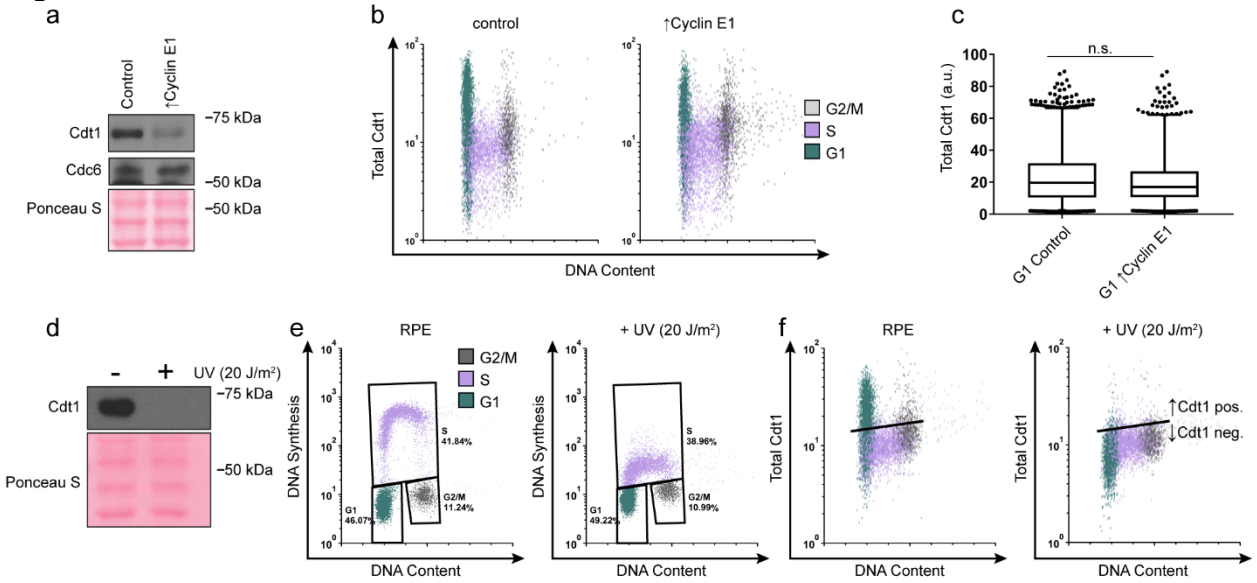

Figure 3.10. G1 Cdt1 levels remain constant with Cyclin E overproduction.
(**a**) Immunoblots of whole cell lysates from cells treated as in (Figure 3.9a).
(**b**) Total Cdt1 detected by flow cytometry of cells treated as in (b) measuring DNA content (DAPI), DNA synthesis (EdU incorporation), and Cdt1 (anti-Cdt1). Green cells are G1 cells, Purple cells are S phase cells (EdU positive), Grey cells are G2/M and >4C DNA content.
(**c**) Box-and-whiskers plots of G1 Cdt1 concentration per cell from (H). Center line is median, outer box edges are 25th and 75th percentile, whiskers edges are 1st and 99th percentile, individual data points are lowest and highest 1%, respectively. G1 Cdt1 intensity in controls is 1.1-fold greater mean and 1.2-fold greater median than G1 ↑Cyclin E1. Samples were not significantly different, compared by two-tailed, unpaired t test, p=0.1907, p=0.3525, respectively; average of 3 biological replicates.
(**d**) Immunoblot of whole cell lysate from RPE1-htert cells treated with or without 20 J/m^2 of UV irradiation, collected 1 hr after irradiation. UV irradiation induces DNA repair coupled PCNA loading, subsequently targeting Cdt1 for degradation.
(**e**) Flow cytometry of control and UV irradiated cells as in (a), measuring DNA content (DAPI), DNA synthesis (EdU incorporation), and Cdt1 (anti-Cdt1). Plots demonstrate decreased DNA synthesis after UV irradiation.
(**f**) The same samples as in (e). Cdt1 is degraded upon UV induced DNA repair, demonstrating Cdt1 antibody specificity for immunofluorescence flow cytometry.

Figure 3.11

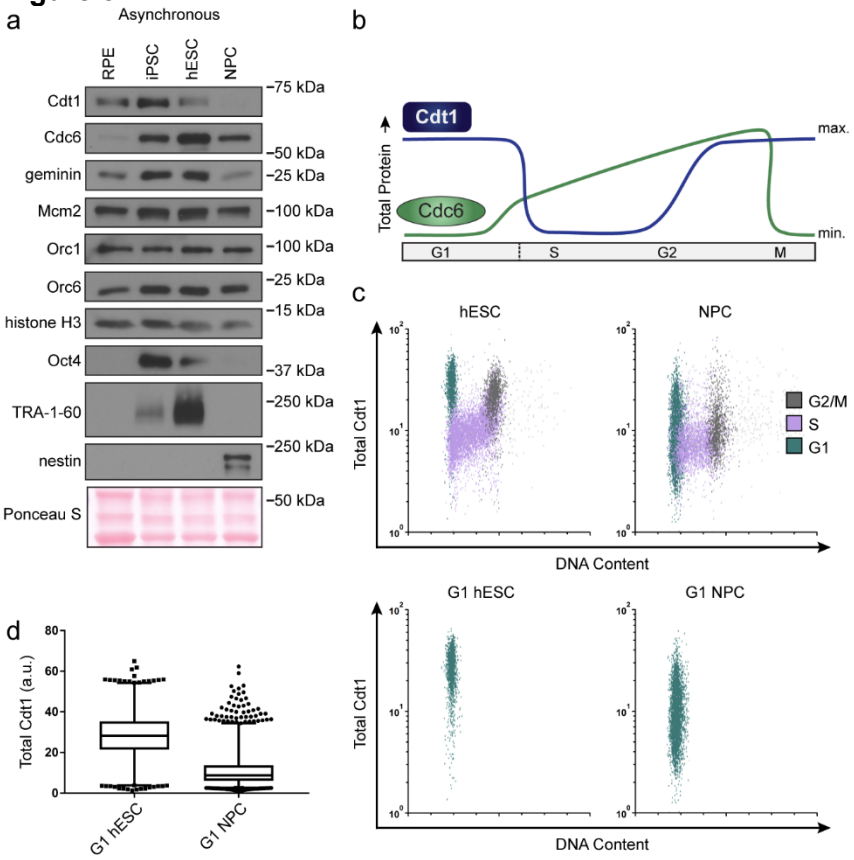

Figure 3.11. hESCs have high levels of Cdt1 in G1.
(**a**) Immunoblots of whole cell lysates from the indicated asynchronous cell lines.
(**b**) Expected changes in total protein levels of Cdt1 and Cdc6 during the human cell cycle.
(**c**) Total Cdt1 detected in asynchronous cells by flow cytometry measuring DNA content (DAPI), DNA synthesis (EdU incorporation), and Cdt1 (anti-Cdt1). Green cells are G1, purple cells are S phase (EdU positive), grey cells are G2/M and >4C DNA content. Lower plots are G1 cells only (green).
(**d**) Box-and-whiskers plots of G1 Cdt1 concentration per cell from (C). Center line is median, outer box edges are 25th and 75th percentile, whiskers edges are 1st and 99th percentile, individual data points are lowest and highest 1%, respectively. Median G1 Cdt1 in hESCs is 2.9 fold greater, mean is 2.2 fold greater than G1 Cdt1 in NPCs, mean p=0.0504 median p=0.0243, average of 3 biological replicates.

loading factors normally change in their abundance during the cell cycle due to regulated proteolysis. Cdc6 protein levels are low in G1 and high in S phase (Figure 3.11B). Conversely, Cdt1 protein levels are high in G1 and low in S phase (Figure 3.11B)(Mailand and Diffley, 2005; Pozo and Cook, 2016). Since an asynchronous population of pluripotent cells spends significantly more time in S phase than differentiated cells do, we expected Cdc6 levels to be higher in asynchronous pluripotent cells compared to their isogenic counterparts. Cdc6 was indeed higher in pluripotent cells, as was Geminin, a protein regulated in a similar manner as Cdc6 (Figure 3.11A)(McGarry and Kirschner, 1998). To our surprise, even though the majority of asynchronous pluripotent cells were in S phase, a time when Cdt1 is degraded, Cdt1 levels were higher in asynchronous pluripotent cells than in isogenic differentiated cells (Figure 3.11A). A similar observation was reported for mouse embryonic stem cells(Ballabeni et al., 2011). These data imply that Cdt1 levels are higher in G1 phase of pluripotent cells than G1 of differentiated cells, providing a potential explanation for fast MCM loading in pluripotent cells.

To directly measure Cdt1 levels specifically in G1, we collected asynchronous hESCs and NPCs then fixed and stained them for Cdt1, EdU and DAPI. S phase Cdt1 degradation in hESCs is similar to differentiated cells with very low levels in S phase (purple, Figure 3.11C). In contrast, the hESCs had a large population of cells with high Cdt1 levels in G1 (green cells) and significant amounts of Cdt1 in G2/M phase (grey cells), whereas the NPCs had a broad and overall lower Cdt1 distribution in G1 and very little Cdt1 in G2/M (Figure 3.11D). The G1 hESCs consistently harbored significantly more Cdt1 than G1 NPCs did (2.9 fold higher median, 2.2 fold higher mean, 3 replicates (Figure 3.11D)). We note that *CDT1* mRNA is modestly but consistently higher in asynchronous hESCs compared to differentiated derivatives, and that Cdt1 protein levels decrease during early differentiation coincident with the slowdown in licensing rate, but before loss of Oct4 (Figure 3.7C and Figure 3.8). We postulate that the higher amount of this essential MCM loading protein specifically in G1 contributes to the fast MCM loading rate in hESCs.

Manipulating MCM loading factors alters MCM loading rates.

Cdt1 is essential for MCM loading(Pozo and Cook, 2016); therefore reducing Cdt1 levels should slow MCM loading. If MCM loading rate is linked to G1 length, then slowing MCM loading by reducing Cdt1 levels could also lengthen G1. To test this prediction, we used siRNA to reduce Cdt1 in hESCs and measured changes in both MCM loading rate and G1 length (Figure 3.12A, B). As expected, Cdt1 depletion reduced MCM loading rate in hESCs (Figure 3.12C). Strikingly, G1 length increased coincidentally with the decrease in MCM loading rate (Figure 3.12D). These data corroborate the close link between MCM loading rate and G1 length in hESCs.

As a complement to slowing MCM loading in hESCs with a short G1, we also attempted to accelerate origin licensing in cells with a long G1 by overproducing essential licensing proteins. We first constructed an RPE_hTERT derivative with ~two-fold inducible Cdt1 overproduction, but this manipulation was insufficient to accelerate MCM loading (Figure 3.13B). We also tested ectopic myc-tagged Cdc6 expressed constitutively in RPE cells (Figure 3.13E); this addition also had only minimal effects on MCM loading rate (Figure 3.13G, compare the grey and green histograms). We considered however, that human Cdc6 is unstable throughout much of G1 phase because it is targeted for degradation by APC^{Cdh1} (Petersen et al., 2000; Mailand and Diffley, 2005). We therefore expressed a previously-described Cdc6 mutant that is resistant to APC^{CDH1} mediated destruction both alone and combination with inducible Cdt1 (Figure 3.12E and Figure 3.13A)(Petersen et al., 2000; Mailand and Diffley, 2005). We have previously demonstrated that tagged Cdc6 and Cdt1 are functional(Cook et al., 2002; Coleman et al., 2015; Chandrasekaran et al., 2011). Expression of the stable Cdc6-mut was sufficient to increase MCM loading rates (Figure 3.12G, compare the blue histogram to the grey and green histograms); Cdt1 overproduction had little additive effect on MCM loading rate in RPE cells (Figure 3.13B). Interestingly accelerating MCM loading by this method did not shorten G1 in

Figure 3.12

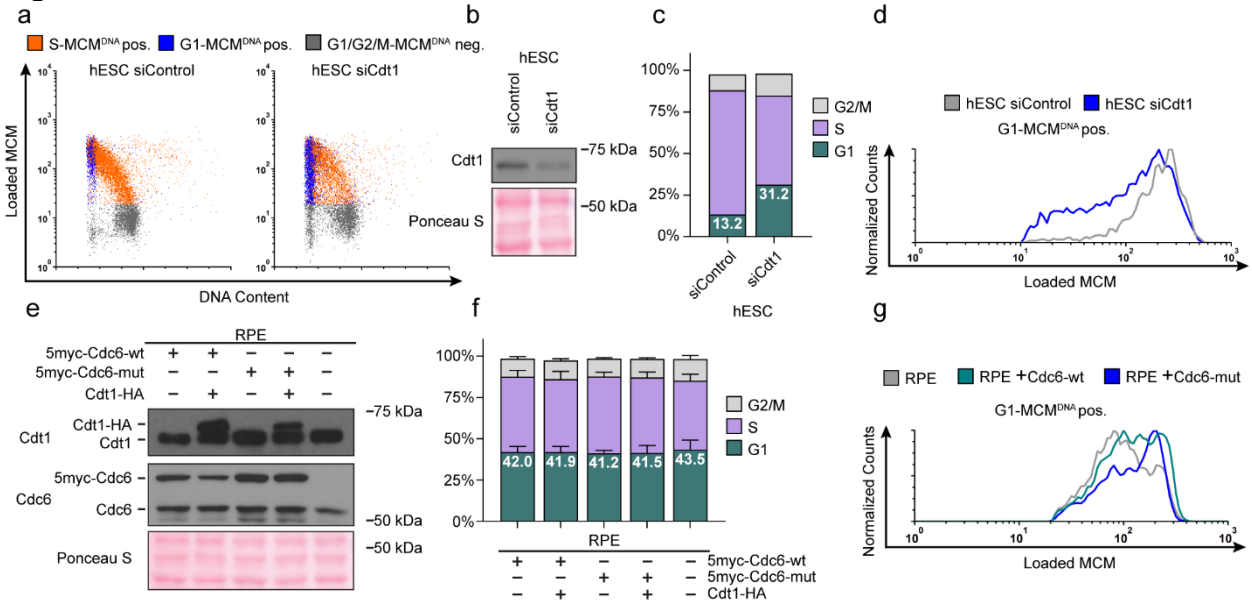

Figure 3.12. Fast MCM loading rate promotes short G1 length in hESCs.
(**a**) Immunoblot of total protein for hESCs treated with 25 nM siCdt1 or 100 nM siControl for 24 hr and labeled with EdU for 30 min prior to harvest.
(**b**) Chromatin flow cytometry of cells from (a) as in Figure 3.1d.
(**c**) Histograms of loaded MCM in G1-MCM^{DNA} cells. Counts for siCdt1 are normalized to the corresponding siControl sample.
(**d**) Stacked bar graph of cell cycle distributions for samples in (a); representative of 2 biological replicates.
(**e**) Immunoblots of RPE1 cells with combinations of: constitutive production of 5Myc-Cdc6-wt or 5myc-Cdc6-mut (which is not targeted for degradation by APC^{CDH1}, R56A, L59A, K81A, E82A, N83A) and an integrated doxycycline-inducible Cdt1-HA construct treated with 100 ng/mL doxycycline for 48 hrs to overproduce Cdt1-HA.
(**f**) Stacked bar graphs of cell cycle distribution measured by flow cytometry for cells shown in (e); mean with error bars ± SD (n=3 biological replicates).
(**g**) Histogram of loaded MCM in G1-MCM^{DNA} cells in RPE1 cells from (e). Counts of Cdc6-wt and Cdc6-mut are normalized to RPE.

Figure 3.13

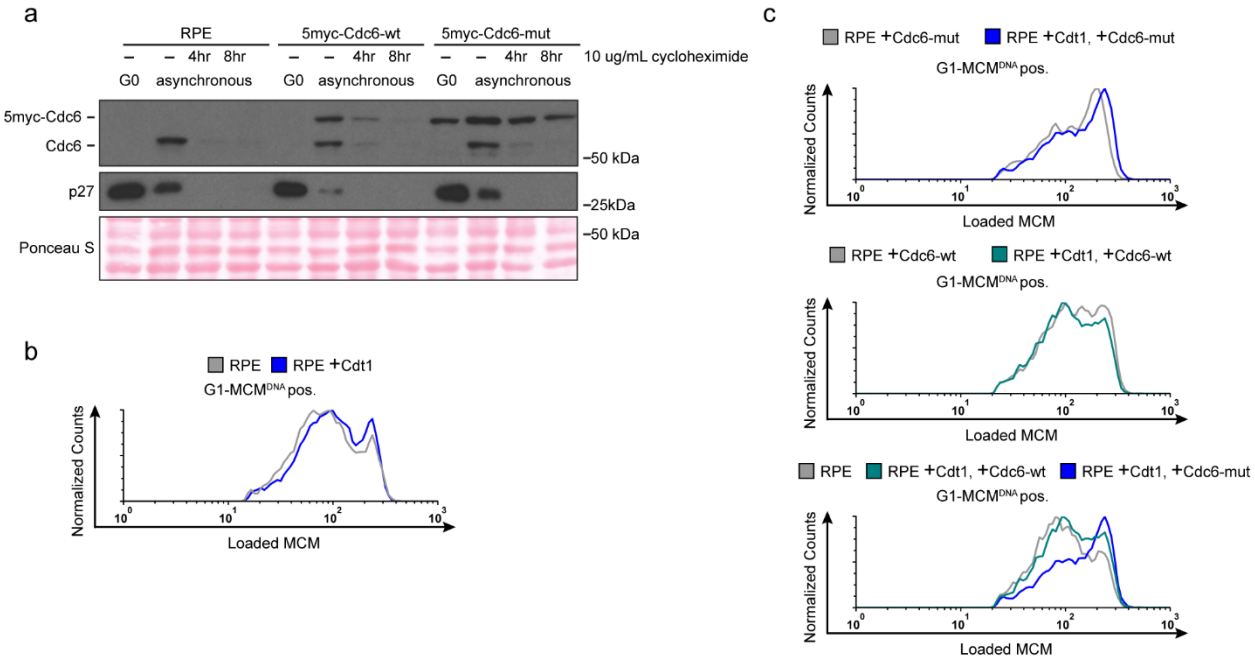

Figure 3.13. Manipulating MCM loading factors alters MCM loading rates.
(**a**) Validation of the 5myc-Cdc6-mut. Immunoblots of total cell lysates of RPE, RPE +5myc-Cdc6-wt or RPE +5myc-Cdc6-mut. Cells were synchronized in G0 by contact inhibition. Asynchronous cells were treated with 10 ug/mL cycloheximide for 4 or 8 hr. Cdc6-mut is more stable in cycloheximde and is resistant to APCCDH1-induced degradation in G0 cells.
(**b**) Histogram of loaded MCM in G1-MCMDNA positive cells in RPE cells expressing ectopic Cdt1 compared to control. There is little increase in MCM loading rate. Counts of Cdt1-expressing cells (blue,+Cdt1) are normalized to parent RPE controls (grey).
(**c**) Histogram of loaded MCM in G1-MCMDNA-positive cells in RPE cells from (Figure 3.12e) with the indicated combinations of Cdc6 and Cdt1 expression. Counts in experimental samples (green and blue) are normalized to their respective controls (grey).

RPEs (Figure 3.12F), further demonstrating that the length of G1 phase and the rate of MCM loading to license origins can be uncoupled. Slow MCM loading may delay S phase entry through the licensing checkpoint (Teer et al., 2006; Shreeram et al., 2002; Nevis et al., 2009; Ge and Blow, 2009), but rapid MCM loading itself is not sufficient to trigger S phase entry, other restriction point phenomenon are required.

Rapid MCM loading protects hESC pluripotency

Our demonstration that slower MCM loading occurs universally during early differentiation suggested a functional link between the rate of MCM loading and pluripotency maintenance. We considered that slowing MCM loading might promote differentiation. To explore this idea, we prematurely slowed MCM loading in hESCs by Cdt1 depletion prior to inducing their differentiation (Figure 3.14E). After Cdt1 depletion, we stimulated differentiation towards mesoderm with BMP4(Bernardo et al., 2011). After 48 hours, we quantified Oct4 and Cdx2 by immunostaining. (Figure 3.14A, Figure 3.15). The pluripotency transcription factor Oct4 and the homeobox transcription factor Cdx2 reciprocally repress one another's expression, creating a clear distinction between Oct4 positive-Cdx2 negative pluripotent cells and Oct4 negative-Cdx2 positive differentiating cells(Niwa et al., 2005). We quantified mean fluorescence intensity of both Oct4 and Cdx2 in >18,000 cells per condition with a customized, automated CellProfiler pipeline, plotting the signal intensities for each cell in a density scatter plot (Figure 3.14B, C). Stimulating control hESCs with 10 ng/mL of BMP4 slightly shifted the population towards differentiation, but most cells remained pluripotent with high Oct4 levels at this time point. Strikingly, hESCs pretreated with Cdt1 siRNA to prematurely slow MCM loading gained a substantial population of Oct4 negative-Cdx2 positive differentiating cells relative to controls that were treated similarly. To quantify the extent of differentiation, we divided the Cdx2 intensity of each cell by its Oct4 intensity, creating a single differentiation score (Figure 3.14D). After 10 ng/ml BMP4 treatment, Cdt1-depleted hESCs had significantly higher scores, indicating that prematurely slowing MCM loading promoted differentiation ($p<0.0001$, two-tailed Mann-Whitney

Figure 3.14

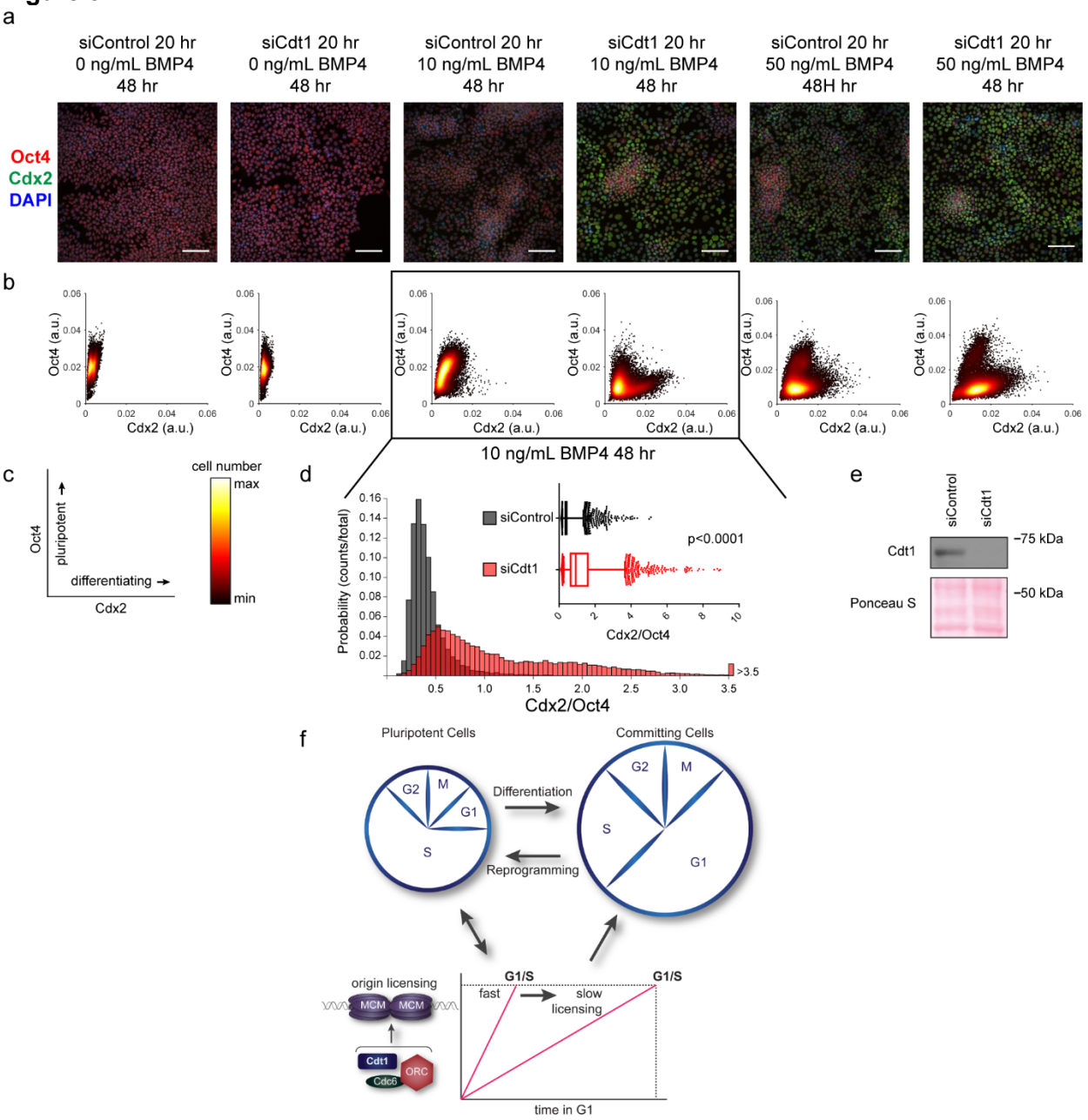

Figure 3.14. Slow MCM loading promotes differentiation.
(**a**) Immunofluorescence microscopy of hESCs treated with 100 nM of siControl or 100 nM of siCdt1 for 20 hr and then treated with BMP4 as indicated. Cells were fixed and stained with DAPI (blue), Cdx2 antibody (green), and Oct4 antibody (red). Images are one region of 18 fields-of-view per condition; scale bar is 100 μm (see Methods).
(**b**) Density scatterplots of mean fluorescence intensity (arbitrary units) of Oct4 and Cdx2 staining for each cell in each condition, >18,000 cells were quantified per condition.
(**c**) Diagram of the relationship between Oct4 and Cdx2 in pluripotent and differentiated cells as plotted in (b); color bar for scatterplots in (b).
(**d**) Histogram of mean fluorescence intensity ratio Cdx2/Oct4 for all cells in siControl and siCdt1 treated with 10 ng/mL BMP4 for 48 hrs. Rightmost histogram bin contains all values greater than 3.5. The inset is a box-and-whiskers plot of the same data, center line is median, outer box

edges are 25th and 75th percentile, whiskers edges are 1st and 99th percentile, individual data points are lowest and highest 1%, respectively. Medians are 0.3722, 0.9319, and means are 0.4285, 1.194 for siControl and siCdt1, respectively. Samples compared by two tailed Mann-Whitney test, ****p<0.0001.
(**e**) Immunoblot for Cdt1 in whole cell lysates at 20 hr of siRNA treatment, prior to BMP4 treatment.
(**f**) Illustration of the relationship between differentiation and MCM loading rate changes.

Figure 3.15

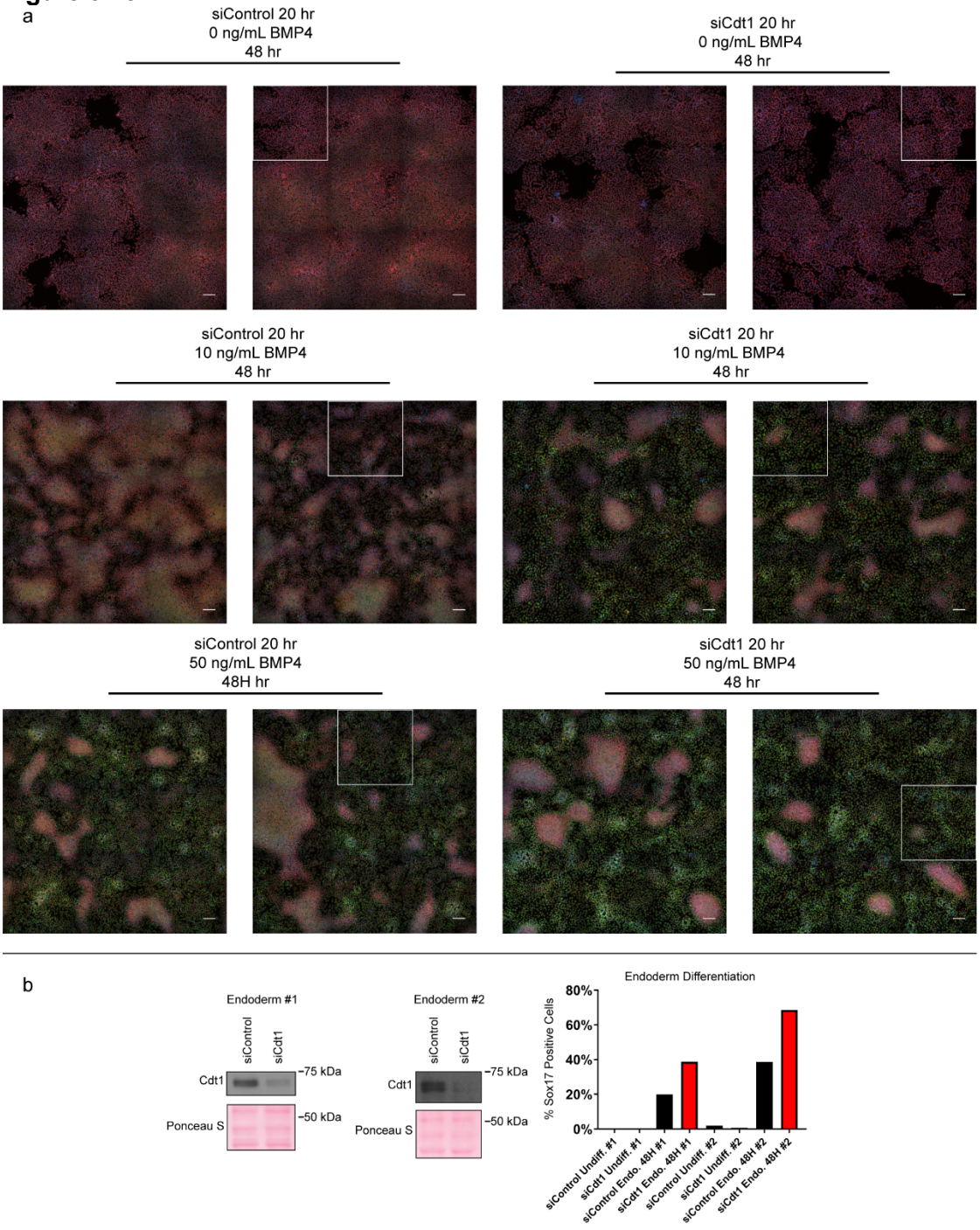

Figure 3.15. Complete microscopy dataset and endoderm differentiation.
(**a**) Complete immunofluorescence microscopy data for Figure 7. White boxes mark the areas shown in Figure 7b; scale bars are 100 μM.
(**b**) Immunoblots for Cdt1 in whole cell lysates of hESCs treated with 100 nM siControl or siCdt1 for 24 hr prior to initiating differentiation toward endoderm, two biological replicates. Bar graph indicates the percentage of Sox17-positive cells, n > 2,300 cells per condition.

test). Both control cells and Cdt1-depleted cells differentiated more fully at a higher concentration of 50 ng/mL BMP4, but the Cdt1-depleted cells still differentiated further than the controls ($p<0.0001$, two-tailed Mann-Whitney test, Figure 3.14B and Figure 3.17A). Other combinations of BMP4 concentrations or treatment times also resulted in a consistent, significant increase in differentiation in cells pretreated to slow MCM loading ($p<0.0001$, two-tailed Mann-Whitney test, data not shown). Importantly, the phenotype was conserved across multiple differentiation lineages, as prematurely slowing MCM loading prior to endoderm differentiation also increased the number of cells positive for the endoderm transcription factor Sox17 relative to controls at the same time point (Figure 3.15B). To test if the pluripotency maintenance was due to Cdt1's role in origin licensing and not its mitotic or other functions(Varma et al., 2012), we slowed licensing by depleting the orthogonal MCM loading protein, Cdc6 (Figure 3.16A-D). A more modest Cdc6 knockdown correlated with a weaker, but detectable effect on MCM loading. Interestingly, this degree of licensing inhibition had no effect on G1 length. Despite the short G1 length, slowing MCM loading by depleting Cdc6 significantly promoted differentiation (Figure 3.17B-F, $p<0.0001$, two-tailed Mann-Whitney test. Thus, we conclude that slow MCM loading generally promoted differentiation and by extension, that rapid MCM loading preserves pluripotency.

Discussion

In this study we demonstrate that rapid MCM loading to license replication origins is an intrinsic property of pluripotent cells. Human embryonic stem cells have a remarkably fast MCM loading rate, and reprogramming to create induced pluripotent stem cells increases MCM loading rate. Moreover, MCM loading slows concurrently with the G1 lengthening and extensive cell cycle remodeling that accompany the early stages of differentiation (Figure 3.14F). To our knowledge this is the first demonstration that the rate of MCM loading is developmentally regulated. Developmental regulation of MCM loading rate is consistent with previous work

Figure 3.16

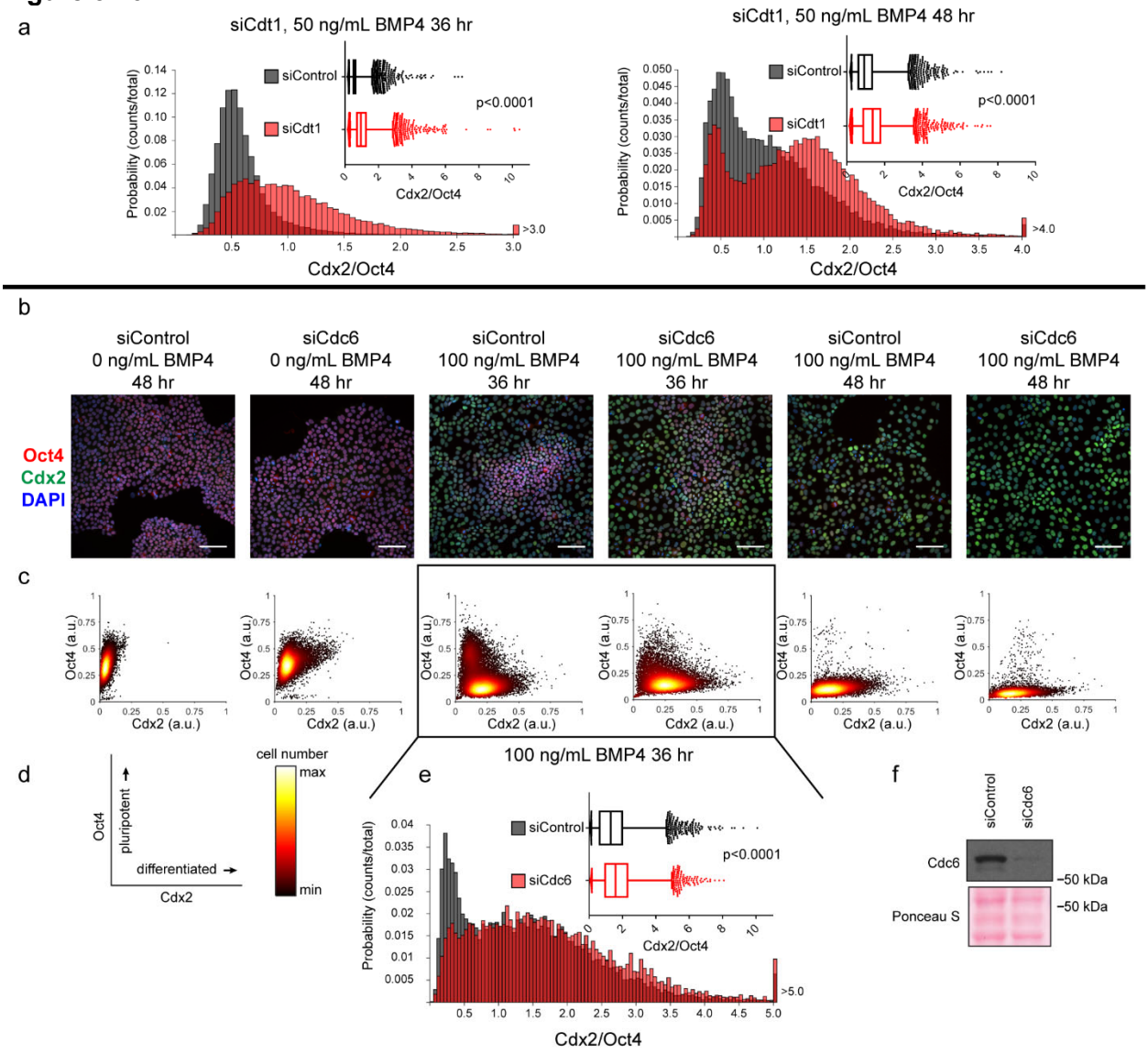

Figure 3.16. Slow MCM loading promotes differentiation.

(**a**) Histogram of mean fluorescence intensity ratio Cdx2/Oct4 for all cells in siControl and siCdt1 treated with 50 ng/mL BMP4 for 36 or 48 hrs. Rightmost histogram bin contains all values greater than 3.0 or 4.0 respectively. The inset is a box-and-whiskers plot of the same data, center line is median, outer box edges are 25th and 75th percentile, whiskers edges are 1st and 99th percentile, individual data points are lowest and highest 1%, respectively. Medians for 50 ng/mL 36 hrs are 0. 0.5418, 0.9465, and means are 0. 0.5993, 1.05 for siControl and siCdt1, respectively. Medians for 50 ng/mL 48 hrs are 0.916, 1.368, and means are 1.055, 1.387 for siControl and siCdt1, respectively. Samples compared by two tailed Mann-Whitney test, ****p<0.0001.

(**b**) Immunofluorescence microscopy of hESCs treated with 100 nM of siControl or 100 nM of siCdc6 for 32 hr and then treated with BMP4 as indicated. Cells were fixed and stained with DAPI (blue), Cdx2 antibody (green), and Oct4 antibody (red). Images are one region of 27 fields of view per condition; scale bar is 100 μm. (see methods).

(**c**) Density scatterplots of mean fluorescence intensity (arbitrary units) of Oct4 and Cdx2 staining for each cell in each condition, >7,900 cells were quantified per condition.

(**d**) Diagram of the relationship between Oct4 and Cdx2 in pluripotent and differentiated cells as plotted in (b); color bar for scatterplots in (b).
(**e**) Histogram of the mean fluorescence intensity ratio Cdx2/Oct4 for all cells in siControl and siCdc6 treated with 100 ng/mL BMP4 for 36 hrs. Rightmost histogram bin contains all values greater than 5.0. the inset is a box-and-whiskers plot of the same data, center line is median, outer box edges are 25th and 75th percentile, whiskers edges are 1st and 99th percentile, individual data points are lowest and highest 1%, respectively. Medians are 1.296, 1.58, and means are 1.433, 1.728 for siControl and siCdc6, respectively. Samples compared by two tailed Mann-Whitney test, ****p<0.0001.
(**e**) Immunoblot for Cdc6 in whole cell lysates at 32 hr of siRNA treatment, prior to BMP4 treatment.

Figure 3.17

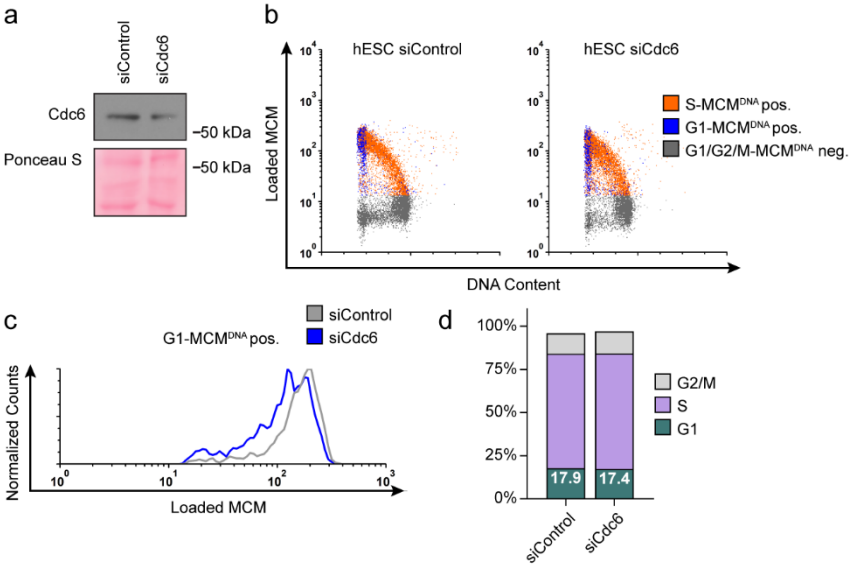

Figure 3.17. Reducing MCM loading rate by an alternative siRNA.
(**a**) Immunoblot of total protein for hESCs treated with 100 nM siControl for 32 hr or 100 nM siCdc6 pool for 32 hr and pulse-labeled with EdU for 30 min prior to harvest.
(**b**) Chromatin flow cytometry of cells from (a) stained with DAPI and anti-MCM2 and subjected to EdU detection.
(**c**) Histogram MCM^{DNA} intensity in G1 cells. Counts for siCdc6 are normalized to the corresponding siControl sample.
(**d**) Stacked bar graph of cell cycle distributions for samples in (a).

showing higher levels of total Cdt1 in asynchronous mouse ESCs than in differentiated cells(Ballabeni et al., 2011). The regulated decrease in MCM loading rate is critical during differentiation, as rapid MCM loading protects pluripotency, and prematurely slowing MCM loading promotes differentiation.

Pluripotent stem cells load MCM complexes rapidly to reach similar total amounts of loaded MCM at the G1/S transition in less time than their isogenic differentiated counterparts. Although we did not detect substantial MCM loading in telophase, as suggested previously(Dimitrova et al., 2002), it is clear that telophase loading is an option in some cells and a requirement in cells with no detectable G1 such as *S. pombe* and in the first nuclear divisions in *D. melanogaster*(Nishitani et al., 2000; Farrell and O'Farrell, 2014). Stem cells achieve faster MCM loading, at least in part, by particularly high Cdt1 levels in G1. These high levels are achieved not only by a modest difference in *CDT1* mRNA (Figure 3.7C) but also post-transcriptionally by specific re-accumulation of Cdt1 protein in the preceding G2 phase (Figure 3.11C). Cdt1 stability in G2 phase has been attributed to geminin-mediated protection from the SCF^{Skp2} E3 ubiquitin ligase in non-stem cells(Tsunematsu et al., 2013; Ballabeni et al., 2004; Clijsters et al., 2013). It is not clear however that geminin levels are particularly high in stem cells relative to differentiated cells (aside from differences expected from cell cycle distribution changes (Figure 3.11A)(Ballabeni et al., 2011)), so it seems unlikely that geminin drives higher Cdt1 levels in stem cells. Skp2 levels also do not change in the earliest stages of stem cell differentiation(Egozi et al., 2007). Cdt1 is protected in late S phase and G2 by cyclin A/Cdk1 activity(Rizzardi et al., 2015), and we thus consider it likely that the documented high CDK activity in stem cells contributes to Cdt1 stabilization in G2(Sela et al., 2012; Neganova et al., 2009). The anticipatory Cdt1 accumulation to promote MCM loading in G1 was originally proposed from experiments in cancer-derived cell lines(Clijsters et al., 2013; Ballabeni et al., 2004). Our observations in stem cells suggest this strategy is employed by non-transformed cells during developmental stages that require short G1.

Other factors besides Cdt1 accumulation may also accelerate MCM loading. The hESCs we assayed have 2-3 fold greater Cdt1 protein levels in G1 relative to NPCs yet load MCM 6.5 times faster per hour than NPCs. One Cdt1 molecule can (*in vitro*) load multiple MCM complexes since Cdt1 is released into the soluble phase immediately after completing a loading reaction(Ticau et al., 2015). Stem cells may experience less Cdc6 degradation in early G1 due to nearly constitutive Cyclin E/Cdk2 activity and/or attenuated APC^{Cdh1} activity, corroborated by our observation that a Cdc6 mutant that is not targeted by APC^{Cdh1} increases MCM loading rate in cells with long G1 phases (Figure 3.12G)(Ballabeni et al., 2011; Neganova et al., 2009; Filipczyk et al., 2007). Additionally, stem cells are enriched for euchromatin, an environment that may be particularly permissive for rapid MCM loading(Chen and Dent, 2013).

Rapid MCM loading may itself contribute to mechanisms that maintain short G1 phases in pluripotent cells. The origin licensing checkpoint links the amount of loaded MCM to G1 length by controlling Cdk2 activity. In that regard, overproducing Cyclin E “short-circuited” the licensing checkpoint in slow loading differentiated cells. This checkpoint has thus far only been demonstrated in p53-proficient differentiated mammalian cells(Ge and Blow, 2009), but the G1 lengthening of hESCs after Cdt1 depletion suggests that pluripotent stem cells also have a functioning licensing checkpoint. Cells with fast MCM loading could satisfy this checkpoint quickly, activate Cyclin E/Cdk2, and thus spend less time in G1. Mechanisms that support short G1 length preserve pluripotency in hESCs (and promote reprogramming to iPSCs) since cells are most sensitive to differentiation cues in G1; in that regard, extending G1 phase in hESCs can increase differentiation propensity(Pauklin and Vallier, 2013; Filipczyk et al., 2007; Coronado et al., 2013; Soufi and Dalton, 2016). Recent work with quintuple knockout mice lacking all D and E type cyclins also reported that Cyclin E/Cdk2 further contributes to maintaining pluripotency by stabilizing the Oct4, Sox2, and Nanog transcription factors(Liu et al., 2017). Fast MCM loading may have evolved as an intrinsic property of pluripotent cells to maintain high Cdk2 activity and keep G1 phase short.

Cyclin/Cdk activity is not the sole connection between the cell cycle and pluripotency. Non-CDK cell cycle-associated proteins regulate expression of key pluripotency genes including *SOX2* and *NANOG*(Pauklin et al., 2016; Gonzales et al., 2015; Li et al., 2012). Pluripotency transcription factors themselves regulate expression of cell cycle genes including those encoding cyclins, CDK inhibitors, and E2F3a(Lee et al., 2010; Kanai et al., 2015; Choi et al., 2012). On the other hand, pluripotency and cell cycle functions can be genetically uncoupled in experiments where manipulating the cell cycle didn't alter pluripotency and vice versa(Scognamiglio et al., 2016; Kareta et al., 2015a). We observe that licensing inhibition can accelerate differentiation even without greatly lengthening G1 (Figure 3.16, 3.17) which may point to an additional direct and cell cycle-independent link between MCM loading rate and differentiation.

We note that early differentiation is not the only setting in which rapid MCM loading during a short G1 may be relevant. Like hESCs, activated T cells have very fast cell cycles with short G1 phases(Kinjyo et al., 2015). Oncogenic transformation is also frequently associated with G1 shortening. It may be that the pathways linking differentiation to MCM loading rate are also coopted in some cancers to induce rapid licensing. On the other hand, a subset of cancers may proliferate in a perpetually underlicensed state that contributes to the genome instability characteristic of transformed cells. Future investigations will elucidate the molecular relationships among developmental signaling pathways, MCM loading rate, and cell cycle remodeling.

Materials and Methods

Cell Culture

Cell lines were authenticated by STR profiling (ATCC) and confirmed to be mycoplasma negative. T98G, HEK293T, and RPE1-hTERT were cultured in Dulbecco's Modified Eagle Medium (DMEM) supplemented with 2 mM L-glutamine and 10% fetal bovine serum (FBS) and incubated in 5% CO2 at 37 °C. ARPE-19 (male) were cultured in 1:1 DMEM:F12 supplemented

with 2 mM L-glutamine and 10% fetal bovine serum and incubated in 5% CO2 at 37 °C. T98G, HEK293T, RPE1-hTERT, and ARPE-19 cells were from the ATCC and were passaged with trypsin and not allowed to reach confluency. WA09 (H9 hESCs) were cultured in mTeSR1 (StemCell Technologies) with media changes every 24 hours on Matrigel (Corning) coated dishes and incubated in 5% CO2 at 37 °C. H9s had normal diploid karyotype at passage 32 and were used from passage 32-42. ARPE-iPSCs were cultured in Essential 8 (Life Technologies) with media changes every 24 hours on Matrigel (Corning) coated dishes and incubated in 5% CO2 at 37 °C. iPSCs were used from passage 20-25 and had normal karyotype. Both hESCs and iPSCs were routinely passaged every 4 days as aggregates using ReLeSR, according to manufacturer's instructions (StemCell Technologies). The hESCs and iPSCs were only passaged as single cells in 10 μM Y-27632 2HCl (Selleck Chemicals) for experiments, as described previously (Watanabe et al., 2007). NPCs were cultured in Neural Progenitor Medium (StemCell Technologies) with media changes every 24 hours on poly-L-ornithine/Laminin (Sigma Aldrich) coated dishes and incubated in 5% CO2 at 37 °C. NPCs were passaged with StemPro Accutase (Gibco) weekly.

Total lysate and chromatin fractionation

Cells were collected via trypsinization. For total protein lysates, cells were lysed on ice for 20 minutes in CSK buffer (300 mM sucrose, 100 mM NaCl, 3 mM $MgCl_2$, 10 mM PIPES pH 7.0) with 0.5% triton x-100 and protease and phosphatase inhibitors (0.1 mM AEBSF, 1 μg/ mL pepstatin A, 1 μg/ mL leupeptin, 1 μg/ mL aprotinin, 10 μg/ ml phosvitin, 1 mM β-glycerol phosphate, 1 mM Na- orthovanadate). Cells were centrifuged at 13,000 xg at 4 °C for 5 minutes, then the supernatants were transferred to a new tube for a Bradford Assay (Biorad) using a BSA standard curve. Chromatin fractionation for immunoblotting was performed as described previously(Cook et al., 2002; Mendez and Stillman, 2000), using CSK buffer with 1 mM ATP, 5 mM $CaCl_2$, 0.5% triton x-100 and protease and phosphatase inhibitors to isolate insoluble proteins and S7 nuclease (Roche) to release DNA bound proteins. A Bradford Assay (Biorad)

was performed for equal loading. For 100 mM or 300 mM NaCl soluble/pellet fractionation, cells were lysed in standard CSK (100 mM NaCl) or high salt CSK (300 mM NaCl) with 0.5% triton X-100 with protease and phosphatase inhibitors for 5 minutes on ice. Then cells were centrifuged at 2000 xg for 3 minutes, supernatants transferred to a new tube as the soluble fraction. The remaining pellet was suspended in 2x SDS loading buffer (2% SDS, 5% 2-mercaptoethanol, 0.1% bromophenol blue, 50 mM Tris pH 6.8, 10% glycerol) as the pellet fraction. Bradford assay was performed on the soluble fraction for equal loading.

Immunoblotting

Samples were diluted with SDS loading buffer (final: 1% SDS, 2.5% 2-mercaptoethanol, 0.1% bromophenol blue, 50 mM Tris pH 6.8, 10% glycerol) and boiled. Samples were run on SDS-PAGE gels, then the proteins transferred onto polyvinylidene difluoride membranes (Thermo Fisher) or nitrocellulose (GE Healthcare). Membranes were blocked at room temperature for 1 hour in either 5% milk or 5% BSA in Tris-Buffered-Saline-0.1%-tween-20 (TBST). After blocking, membranes were incubated in primary antibody overnight at 4 °C in either 1.25% milk or 5% BSA in TBST with 0.01% sodium azide. Blots were washed with TBST then incubated in HRP-conjugated secondary antibody in either 2.5% milk or 5% BSA in TBST for 1 hour, washed with TBST, and then membranes were incubated with ECL Prime (Amersham) and exposed to autoradiography film (Denville). Equal protein loading was verified by Ponceau S staining (Sigma Aldrich). Antibodies used for immunoblotting were: Mcm2, (BD Biosciences, Cat#610700), Mcm3, (Bethyl Laboratories, Cat#A300-192A), Cdt1, (Cell Signaling Technologies, Cat#8064S), Cdc6, (Santa Cruz Biotechnology, Cat#sc-9964), Oct4, (Abcam, Cat#ab19857),Cyclin E1, (Santa Cruz Biotechnology, Cat#sc-198), Orc1, (Bethyl Laboratories, Cat#A301-892A), Orc6, (Santa Cruz Biotechnology, Cat#sc-32735), geminin, (Santa Cruz Biotechnology, Cat#sc-13015), Histone H3, (Cell Signaling Technologies, Cat#4499S), TRA-1-60, (Invitrogen, Cat#41-1000), nestin, (Abcam, Cat#ab22035), p27 (Santa Cruz Biotechnology, Cat#sc-528), α-tubulin (Sigma Aldrich, Cat#9026).

Flow Cytometry

For EdU labeled samples, cells were incubated with 10 uM EdU (Santa Cruz Biotechnology) for 30 minutes prior to collection. For total protein flow cytometry, cells were collected with trypsin and resuspended as single cells, washed with PBS, and fixed with 4% paraformaldehyde (Electron Microscopy Sciences) in PBS for 15 minutes at room temperature, then 1% BSA-PBS was added, mixed and cells were centrifuged at 1000 xg for 7 minutes (and for all following centrifuge steps) then washed with 1% BSA-PBS and centrifuged. Fixed cells were permeabalized with 0.5% triton x-100 in 1% BSA-PBS at room temperature for 15 minutes, centrifuged, then washed once with 1% BSA, PBS and centrifuged again before labeling. For chromatin flow cytometry, cells were collected with trypsin and resuspended as single cells, washed with PBS, and then lysed on ice for 5 minutes in CSK buffer with 0.5% triton x-100 with protease and phosphatase inhibitors. Next, 1% BSA-PBS was added and mixed, then cells were centrifuged for 3 minutes at 1000 xg, then fixed in 4% paraformaldehyde in PBS for 15 minutes at room temperature. For 100 mM NaCl vs 300 mM NaCl CSK, cells were processed as in chromatin flow cytometry above, except CSK containing 300 mM NaCl was used instead of the normal 100 mM NaCl. Next, 1% BSA-PBS was added, mixed and cells were centrifuged then washed again before labeling. The labeling methods for total protein samples and chromatin samples were identical. For DNA synthesis (EdU), samples were centrifuged and incubated in PBS with 1 mM $CuSO_4$, 1 μM fluorophore-azide, and 100 mM ascorbic acid (fresh) for 30 minutes at room temperature in the dark. 1% BSA-PBS + 0.1% NP-40 was added, mixed and centrifuged. Samples were resuspended in primary antibody in 1% BSA-PBS + 0.1% NP-40 and incubated at 37 °C for 1 hour in the dark. Next, 1% BSA-PBS + 0.1% NP-40 was added, mixed and centrifuged. Samples were resuspended in secondary antibody in 1% BSA-PBS + 0.1% NP-40 and incubated at 37 °C for 1 hour in the dark. Next, 1% BSA-PBS + 0.1% NP-40 was added, mixed and centrifuged. Finally, cells were resuspended in 1% BSA-PBS + 0.1% NP-40 with 1 μg/mL DAPI (Life Technologies) and 100 μg/mL RNAse A (Sigma Aldrich) and

incubated overnight at 4 °C in the dark. Samples were run on a CyAn ADP flow cytometer (Beckman Coulter) and analyzed with FCS Express 6 software (De Novo). The following antibody/fluorophore combinations were used: (1): Alexa 647-azide (Life Technologies), primary: Mcm2 (BD Biosciences, Cat#610700), secondary: Donkey anti-mouse-Alexa 488 (Jackson ImmunoResearch), DAPI. (2): Alexa 488-azide (Life Technologies), primary: Cdt1 (Abcam, Cat#610700), secondary: Donkey anti-rabbit-Alexa 647 (Jackson ImmunoResearch), DAPI. (3): Alexa 647-azide (Life Technologies), primary: Mcm3 (Bethyl Cat#A300-192A), secondary: Donkey anti-rabbit-Alexa 488 (Jackson ImmunoResearch), DAPI. (4): primary: Mcm3 (Bethyl Cat#A300-192A), Mcm2 (BD Biosciences, Cat#610700), secondary: Donkey anti-mouse-Alexa 488, Donkey anti-rabbit-Alexa 647 (Jackson ImmunoResearch), DAPI. Cells were gated on FS-area vs SS-area. Singlets were gated on DAPI area vs DAPI height. The positive/negative gates for EdU and MCM were gated on a negative control sample, which was treated with neither EdU nor primary antibody, but incubated with 647-azide and the secondary antibody Donkey anti-mouse-Alex 488 and DAPI to account for background staining (Figure 3.2).

Doubling Time

Doubling time was calculated by plating equal number of cells as described above and counting cell number over time using a Luna II automated cell counter (Logos Biosystems) at 24, 48, and 72 hours after plating. Three or four wells were counted as technical replicates at each timepoint. GraphPad Prism's regression analysis was used to compute doubling time, and multiple biological replicates were averaged for a final mean doubling time. ARPE-19s were counted 4 times, hESCs and NPCs 3 times, and iPSCs 2 times.

Cell Synchronization and treatments

To synchronize cells in G1, T98G cells were grown to 100% confluency, washed with PBS, and incubated for 72 hr in 0.1% FBS, DMEM, L-glutamine. After serum-starvation, cells were re-stimulated by passaging 1:3 with trypsin to new dishes in 20% FBS, DMEM, L-

glutamine, collecting cells 10 hr and 12 hr post-stimulation. To synchronize T98G cells in early S phase, cells were treated as for G1, except 1 mM Hydroxyurea (Alfa Aesar) was added to the media upon re-stimulating and cells were collected 18 hr post-stimulation. To synchronize cells in mid-late S, cells were treated as in early S, then at 18 hr post-stimulation cells were washed with PBS and released into 10% FBS, DMEM, L-Glutamine, collecting 6 hr, 8 hr post release. To synchronize RPE1-hTERT cells in G0, cells were grown to 100% confluency, then incubated for 48 hr in 10% FBS, DMEM, L-glutamine. For RPE1 in G1/S, G0 cells were trypsinized and passaged 1:6 with trypsin to new dishes in 10% FBS, DMEM, L-glutamine, and collected with trypsin 22 hrs later. For cycloheximide (Sigma) treatment, asynchronous RPE cells were treated with 10 ug/mL for 4 hr or 8 hr as indicated. For UV irradiation, asynchronous RPE cells were treated with 20 J/m^2 of UV with a Stratalinker (Stratagene) and collected 1 hr later.

Cloning

The pInducer20-Cyclin E plasmid was constructed using the Gateway cloning method (Invitrogen). The *att*B sites were added to Cyclin E1 cDNA by PCR using Rc/CMV cyclin E plasmid as a template and BP-cycE-F (5' GGGGACAAGTTTGTACAAAAAAGCAGGCTACCATGAAGGAGGACGGCGGC) and BP-cycE-R primers (5' GGGGACCACTTTGTACAAGAAAGCTGGGTTCACGCCATTTCCGGCCCGCT) (Hinds et al., 1992). The PCR product was recombined with pDONR221 plasmid using BP clonase (Invitrogen) according to the manufacturer's instructions and transformed into DH5α to create pENTR221-Cyclin E1. Then the LR reaction was performed between pInducer20 and pENTR221-Cyclin E1 using LR Clonase (Invitrogen) according to manufacturer's instructions and transformed into DH5α to create pInducer20-Cyclin E1. The pInducer20 plasmid was converted to blasticidin resistance (pInducer20-blast2) by Gibson Assembly (New England Biolabs) following manufacturer's protocol. pInducer20 was cut with AgeI and assembled with PCR products with the following primers:

AgeI-rta3-F: 5- GCTCGGATCTCCACCCCGTACCGGTCCTGCAGTCGAATTCAC

AgeI-IRES-blast-R: 5- ACAAAGGCTTGGCCATGGTT TAAGCTTATCATCGTGTTTTTCA

Blast-F:5- TGAAAAACACGATGATAAGCTTAAACCATGGCCAAGCCTTTGT

Blast-AgeI-Ind-R: 5- GTTCAATCATGGTGGACCGG CTATTAGCCCTCCCACACATAACCA

The pLenti CMV blast plasmid was a template for the blasticidin resistance gene. A tagged Cdt1-HA was cloned into pInducer20-blast using Gateway cloning as described above. The Cdc6 mutant unable to bind APC^{CDH1} (5myc-Cdc6-mut) was described previously: R56A, L59A, K81A, E82A, N83A(Petersen et al., 2000). pCLXSN-5myc-Cdc6-wt was cloned to 5myc-Cdc6-mut by two sequential Gibson assemblies (NEB) according to manufacturer's instructions. Primers used:

CDC6-KEN-F: 5-

CTCCACCAAAGCAAGGCAAGGCGGCCGCAGGTCCCCCTCACTCACATACAC

CDC6-KEN-R: 5-

GTGTATGTGAGTGAGGGGGACCTGCGGCCGCCTTGCCTTGCTTTGGTGGAG

CDC6-DBOX-F: 5-

AAGCCCTGCCTCTCAGCCCCGCCAAACGTGCCGGCGATGACAACCTATGCAA

CDC6-DBOX-R: 5-

TTGCATAGGTTGTCATCGCCGGCACGTTTGGCGGGGCTGAGAGGCAGGGCTT

Cell Line construction and inducible protein production

To package retrovirus, pCLXSN 5myc-Cdc6 wt or mut were co-transfected with pCI-GPZ and VSVG plasmids into HEK293T using 50 µg/mL Polyethylenimine-Max (Aldrich Chemistry).To package lentivirus, pInducer20-Cyclin E1 or pInducer20-blast2-Cdt1-HA were co-transfected with ΔNRF and VSVG plasmids into HEK293T using 50 µg/mL Polyethylenimine-Max (Aldrich Chemistry). Viral supernatant was transduced with 8 ug/mL Polybrene (Millipore) onto RPE1-hTERT cells overnight. Cells were selected with 500 ug/mL neomycin (Gibco) or 5 ug/mL blasticidin (Research Products International) for 1 week. To overproduce Cyclin E1, cells were treated with 100 ng/mL doxycycline (CalBiochem) for 72 hr in 10% FBS, DMEM, L-

glutamine. Control cells were the Inducer20-Cyclin E1 without doxycycline. To overproduce Cdt1, cells were treated with 100 ng/mL doxycycline for 48 hr in 10% FBS, DMEM, L-glutamine, control cells were without doxycycline.

siRNA transfections

For siRNA treatment, Dharmafect 1 (Dharmacon) was mixed in mTeSR1 with the appropriate siRNA according to the manufacturer's instructions, then diluted with mTeSR1 and added to cells after aspirating old media. The final siRNA concentrations were: 100 nM siControl (Luciferase), 25 or 100 nM siCdt1, or a mixture of two siCdc6 (2144 and 2534 at 50 nM each). The Cdt1 siRNA mix was incubated on cells for either 20 or 24 hours, then changed to new mTeSR1 without siRNA. The Cdc6 siRNA mix was incubated on cells for 24 hours, then changed to new mTeSR1 without siRNA for 8 hours (32 total hours). The Cdt1, Cdc6 and Luciferase siRNA were described previously (Coleman et al., 2015; Nevis et al., 2009). For siRNA treatment of RPE cells, Dharmafect 1 (Dharmacon) was mixed in Optimem (Gibco) with the appropriate siRNA according to manufacturer's instructions, then diluted with DMEM, 10% FBS, L-glutamine and added to cells after aspirating old media. The next day the siRNA mix was aspirated and replaced with fresh DMEM, 10% FBS, L-glutamine, collecting samples 72 hrs after the start of siRNA treatment. The siRNA were siControl (Luciferase) at 100 nM or a mixture of two MCM3 siRNA (2859 and 2936 at 50 nM each).

siMCM3-2859 5'- augacuauugcaucuucauugdTdT

siMCM3-2936 5'- aacauaugacuucugaguacudTdT

Differentiation

Mesoderm (BMP4): hESCs were passaged as single cells at $7x10^3$ /cm^2 in mTeSR1 with 10 μM Y-27632 2HCl onto Matrigel-coated plates. 24 hours later, the media was changed to start differentiation with fresh mTeSR1 with 100 ng/mL BMP4 (R&D Systems), and 24 hours later the media was changed to fresh mTeSR1 with 100 ng/mL BMP4 for 48 total hours of differentiation.

Neuroectoderm: hESCs were differentiated using a monolayer-based protocol in Neural Induction Medium: hESCs were passaged as single cells at $5.2x10^4$ /cm^2 in STEMdiff™ Neural Induction Medium (StemCell Technologies) with 10 μM Y-27632 2HCl onto Matrigel coated plates, and plating started the differentiation. 24 hours later, the media was changed to fresh Neural Induction Medium for another 24 hours for 48 hours total differentiation. To derive NPCs, hESCs were differentiated in Neural Induction medium (StemCell Technologies) using the Embryoid Body Neural Induction protocol according to manufacturer's instructions, similar to previous reports (Robinson et al., 2016). Once generated, NPCs were maintained in Neural Progenitor Medium (StemCell Technologies).

Mesoderm (GSK3βi): hESCs were passaged as single cells at $3x10^4$ /cm^2 in mTeSR1 with 10 μM Y-27632 2HCl onto Matrigel coated plates. 24 hours later, the media was changed to start differentiation. Cells were washed with Advanced RPMI 1640 (Gibco), then incubated in Advanced RPMI 1640 with B27 minus insulin (Gibco), 2 mM L-glutamine, and 8 μM CHIR-99021 (Selleck Chemicals). At 24 hours after changing the media, cells were washed with Advanced RPMI 1640 then incubated in Advanced RPMI 1640 with B27 minus insulin (Gibco), 2 mM L-glutamine, without CHIR-99021 for 24 hours for a total of 48 hours of differentiation. Endoderm: hESCs were passaged as single cells at $4x10^3$ /cm^2 in mTeSR1 with 10 μM Y-27632 2HCl onto Matrigel-coated plates. The next day the media was changed to fresh mTeSR1 without Y-27632 2HCl. 24 hours later, the media was changed to start differentiation. The cells were washed with Advanced RPMI 1640 (Gibco), then incubated in Advanced RPMI 1640 with 0.2% FBS, 2 mM L-glutamine, 100 ng/mL Activin A (R&D Systems) and 2.5 μM CHIR-99021. At 24 hours after changing the media, cells were washed with Advanced RPMI 1640 then incubated in Advanced RPMI 1640 with 0.2% FBS, 2 mM L-glutamine, 100 ng/mL Activin A, without CHIR-99021 for 24 hours for a total of 48 hours of differentiation.

Phase contrast microscopy

Phase contrast images were acquired with an Axiovert 40 CFL inverted microscope, 20x objective.

Immunofluorescence Microscopy

For immunofluorescence microscopy, hESCs were plated as single cells in mTeSR1 with 10 μM Y-27632 2HCl in Matrigel-coated, 24 well, #1.5 glass bottom plates (Cellvis) at $7x10^3$ /cm^2 for siCdt1, Mesoderm (BMP4), at $5x10^3$ for siCdc6, Mesoderm (BMP4), and at $4x10^3$ /cm^2 for siCdt1, Endoderm. Cells were incubated with siCdt1 for 20 hours (Mesoderm (BMP4)), 24 hours (Endoderm) or siCdc6 for 32 hours (Mesoderm (BMP4)) all in parallel with siControl as described above (siRNA transfections). After siRNA treatment, cells were differentiated as described above (Differentiation) with the following modifications: For Mesoderm (BMP4), multiple BMP4 concentrations and treatment times were used as indicated (Figure 3.15). For treatment less than 48 hours, cells were incubated in mTeSR1 after siRNA treatment until starting differentiation. (Example: 12 hours of mTeSR1 then 36 hours of BMP4, for a total of 48 hours). For endoderm, the first RPMI/Activin/CHIR-99021 was immediately after siRNA, without a day of incubation in mTeSR1. After differentiation, cells were fixed in 4% paraformaldehyde in PBS for 15 minutes at room temperature, washed with PBS, and permeabalized with 5% BSA, PBS, 0.3% triton x-100 at 4 °C overnight. Next, cells were incubated in primary antibody in 5% BSA, PBS, 0.3% triton x-100 at 4 °C overnight. Cells were washed with PBS at room temperature, then incubated in secondary antibody in 5% BSA, PBS, 0.3% triton x-100 at room temperature for 1 hour. Cells were washed with PBS, then incubated in 1 μg/mL DAPI in PBS for 10 minutes at room temperature, then washed with PBS. For Mesoderm (BMP4)the primary antibodies were Oct4 (Millipore, Cat#MABD76) and Cdx2 rabbit (Abcam, Cat#ab76541), the secondary antibodies were goat anti-mouse-Alexa 594, donkey anti-rabbit-Alexa 488. For endoderm the primary antibody was Sox17 (R&D Systems, Cat#AF1924), the secondary antibody was donkey anti-goat-Alexa 594 (Jackson ImmunoResearch). Cells were imaged in

PBS on a Nikon Ti Eclipse inverted microscope with an Andor Zyla 4.2 sCMOS detector. Images were taken as 3x3 scan of 20x fields with a 0.75 NA objective, stitched with 15% overlap between fields using NIS-Elements Advanced Research Software (Nikon). Shading correction was applied within the NIS-Elements software before acquiring images. Raw images were quantified using a custom CellProfiler pipeline.

qPCR (Figure 3.7)

RNA lysates were prepared using Norgen Biotek's Total RNA Purification Kit (Cat. 37500). Lysates were first treated with Promega RQ1 RNase-Free DNase (Promega), and then converted to cDNA using Applied Biosystem's High-Capacity RNA-to-cDNA Kit (Cat. 4387406). Quantitative real-time PCR (qPCR) with SYBR Green (Bio-Rad; SsoAdvanced Universal SYBR Green Supermix, Cat. 1725271) was carried out to assess gene expression. All results were normalized to *ACTB*. Primers for qPCR were ordered from Eton Bioscience. Primers:

POU5F1-F: 5'-CCTGAAGCAGAAGAGGATCACC,

POU5F1-R 5'-AAAGCGGCAGATGGTCGTTTGG,

CDX2-F 5'-ACAGTCGCTACATCACCATCCG,

CDX2-R 5'-CCTCTCCTTTGCTCTGCGGTTC,

T-F 5'-CTTCAGCAAAGTCAAGCTCACC,

T-R 5'-TGAACTGGGTCTCAGGGAAGCA,

SOX17-F 5'-ACGCTTTCATGGTGTGGGCTAAG,

SOX17-R 5'-GTCAGCGCCTTCCACGACTTG,

CDT1-F 5'-GGAGGTCAGATTACCAGCTCAC,

CDT1-R, 5'-TTGACGTGCTCCACCAGCTTCT,

SOX2-F 5'-CTACAGCATGATGCAGGACCA,

SOX2 -R 5'-TCTGCGAGCTGGTCATGGAGT,

PAX6-F 5'-AATCAGAGAAGACAGGCCA,

PAX6-R 5'-GTGTAGGTATCATAACTC,

ACTB-F 5'-CACCATTGGCAATGAGCGGTTC,

ACTB-R 5'-AGGTCTTTGCGGATGTCCACGT.

Generating ARPE-19-iPS cells

ARPE-19-iPS cells were derived from the human retinal pigment epithelial cell line ARPE-19 by reprogramming with CytoTune-iPS 2.0 Sendai reprogramming kit (Invitrogen) following the manufacturer's instructions.

Briefly, two days before Sendai virus transduction, 100,000 ARPE-19 cells were plated into one well of a 6-well plate with ATCC-formulated DMEM:F12 medium and were transduced with the CytoTune™ 2.0 Sendai reprogramming vectors at the MOI recommended by the manufacturer 48 hours later (d0). The medium was replaced with fresh medium every other day starting from one day after transduction (d1). At day 7, transduced cells were replated on Matrigel coated 6-well plates. Cells were fed with Essential 8 medium every day. Colonies started to form in 2-3 weeks and were ready for transfer after an additional week. Undifferentiated colonies were manually picked and transferred to Matrigel coated 6-well plates for expansion. After two rounds of subcloning and expansion (after passage 10), RT-PCR was used to verify whether iPS cells were vector-free with the primer sequences published in the manufacturer’s manual.

After iPS cells became virus-free, they were submitted to the University of Minnesota Cytogenomic Laboratory for karyotype analysis. This analysis indicated that the ARPE-19-iPS cells have normal karyotypes.

Immunofluorescence characterization of ARPE-19-iPS cells

To examine pluripotency markers, iPS cells were fixed with 4% paraformaldehyde for 20 minutes. If nuclear permeation was required, cells were treated with 0.2% triton-x-100 in phosphate-buffered saline (PBS) for 30 minutes, blocked in 3% bovine serum albumin in PBS for 2 hours, and incubated with the primary antibody overnight at 4˚C. Antibodies targeting the following antigens were used: TRA1-60 (MAB4360, 1:400), TRA1-81 (MAB4381, 1:400), stage-

specific embryonic antigen-4 (MAB4304, 1:200), and stage- specific embryonic antigen-3 (MAB-4303, 1:200), all from Millipore/Chemicon (Billerica, MA), OCT3/4 (AB27985, 1:200) from Abcam (Cambridge, MA), and NANOG (EB068601:100) from Everest (Upper Heyford, Oxfordshire, UK). Cells were incubated with secondary Alexa Fluor Series antibodies (all 1:500, Invitrogen) for 1 hour at room temperature and then with DAPI for 10 minutes. Images were examined using an Olympus FluoView 1000m IX81 inverted confocal microscope and analyzed with Adobe Photoshop CS6. Direct alkaline phosphatase (AP) activity was analyzed as per the manufacturer's recommendations (Millipore).

Bisulfite sequencing and methylation analysis

Genomic DNA was isolated using the DNeasy Blood and Tissue kit (Qiagen) per manufacturer's recommendations for isolation from mammalian cells. Bisulfite conversion was performed using the Epitect Bisulfite kit (Qiagen) according to the manufacturer's protocol for low amounts of DNA. Single-step PCR amplification of the NANOG and OCT4 promoter regions were conducted using Accuprime Supermix II (Invitrogen). Amplification products were visualized by gel electrophoresis and bands were excised and purified using the QIAquick Gel Extraction kit (Qiagen). Purified PCR products were inserted into the PCR4-TOPO vector (Invitrogen) and individual clones were sequenced. Alignment and methylation analysis were performed using the online QUMA program (http://quma.cdb.riken.jp/). Sequenced clones with at least 90% non-CpG cytosine conversion and at least 90% sequence homology were retained for analysis.

Quantitative reverse transcriptase PCR (Figure 3.3)

RNA was isolated using RNeasy Mini kit (Qiagen) and treated with TURBO DNA-free (Ambion, Austin, TX). First-strand cDNA was synthesized using a Superscript III First-Strand Synthesis SuperMix (Invitrogen). Reverse transcriptase-PCR was performed using TaqMan Gene Expression Assays and TaqMan Universal PCR Master Mix, No AmpErase UNG (Applied Biosystems, Carslbad, CA) as per the manufacturer's protocol.

TaqMan gene expression assays used were OCT4 (Hs04260367-gH), SOX2 (Hs01053049-sl), NANOG (Hs04399610-g1), KLF4 (Hs00358836-m1), MYC (Hs00153408-m1), LIN28 (Hs00702808-s1), REXO1 (Hs00810654-m1), ABCG2 (Hs1053790-m1), DNMT3 (Hs00171876-m1), with GAPDH (Hs99999905-m1) used as an endogenous control. Expression levels were measured in duplicate. For genes with expression below the fluorescence threshold, the cycle threshold (Ct) was set at 40 to calculate the relative expression. Analysis was performed using an ABI PRISM 7500 sequence detection system (Applied Biosystems).

Teratoma analysis

ARPE-19-iPS cells contained in a mixture of DMEM/F12, Matrigel and collagen were implanted onto the hind flank of NSG mice (n=5) until a palpable mass formed. Teratoma tissue was excised for histological examination following embedding and staining by haematoxylin and eosin. Experiments were conducted with the approval of the Institutional Animal Care and Research Committee at the University of Minnesota.

Ergodic Rate Analysis

Ergodic Rate Analysis for cell cycle data was based on previously published work (Kafri et al., 2013). First, the raw data from flow cytometry files were extracted using FCSExtract Utility (Earl F Glynn) to comma separated value (.csv) files. The data in the .csv files were then gated in FCS Express 6 (De Novo Software) and the data for only G1-MCM^{DNA} were exported. MCM negative cells were excluded based on the negative control sample (see Flow Cytometry). The mean MCM loading rate was calculated in MATLAB (MathWorks). To calculate the mean MCM loading rate, the G1-MCM^{DNA} were subdivided into 10 equal sized bins, with rate calculated for each bin, and all 10 rates were averaged together for a mean MCM loading rate. The rate calculation was based on the formula from Kafri et al:

$$w_n = \alpha \frac{2 - F}{f_n}$$

w_n = MCM loading rate in bin n

α = ln(2) / doubling time (Figure 3.6)

F = number of G1-MCM^{DNA} cells / total number of cells in sample. F was calculated from FCS Express and entered into MATLAB manually (Figure 3.6).

f_n = number of cells in bin n / number of G1-MCM^{DNA} cells

The bins were created in MATLAB (Figure 3.6). To control for small day to day differences in raw data from staining intensities, the histogram edges were defined with the first bin starting at the lowest MCM value and the last bin ending at the highest MCM value, divided into 10 equal sized bins between the lowest and highest MCM value. The 10 w_n were then averaged for a final mean w per sample.

The mean MCM loading rate was calculated for 3 biological replicates for each cell line, and the replicates were averaged using GraphPad Prism for further statistical analysis. We cannot use ergodic rate analysis on actively differentiating cells (e.g. Figure 3.7) because they are not at steady state.

Quantification and Statistical Analysis

Statistical analysis was performed with GraphPad Prism 7 using unpaired, two-tailed t test (displayed as mean ±SD) or two-tailed Mann-Whitney test as indicated in figure legends. Significance levels were set at *p≤ 0.05, **p≤ 0.01, ***p≤ 0.001, ****p≤ 0.0001. All experiments were performed a minimum of 2 times, and representative data are shown in figures.

CHAPTER 4: INTRINSIC CHECKPOINT DEFICIENCY DURING CELL CYCLE RE-ENTRY FROM QUIESCENCE[3]

Introduction

Proliferating mammalian cells initiate DNA replication at thousands of DNA replication origins every cell cycle. Replication origins are chromosomal loci where DNA synthesis initiates in S phase. The Minichromosome Maintenance complex (MCM) is an essential component of the helicase that unwinds DNA to initiate replication. MCM loading dynamics are tightly regulated and coordinated with cell cycle progression for precise and complete genome duplication. Cells prepare for DNA replication in S phase by loading MCMs onto replication origins in the preceding G1 phase, a process called "origin licensing." The amount of DNA-loaded MCM increases as cells progress through G1 until reaching a maximum per cell at the G1/S transition (Siddiqui et al., 2013; Remus and Diffley, 2009). Once cells enter S phase, multiple overlapping mechanisms block any *new* origin licensing, thus restricting MCM loading to G1 phase (Truong and Wu, 2011; Arias and Walter, 2007). Cells block MCM loading outside of G1 phase to prevent genotoxic re-replication, which causes aneuploidy, double strand breaks, and genome instability (Neelsen et al., 2013; Truong and Wu, 2011; Arias and Walter, 2007). MCMs unwind DNA in S phase, travel with replication forks, and MCMs are unloaded throughout S phase as replication forks terminate (Maric et al., 2014; Moreno et al., 2014).

Cells may encounter replication stress and replication fork stalling in S phase from a variety of endogenous and exogenous sources. A stalled replication fork can be rescued if a

[3]Modified from unpublished work submitted to the Journal of Cell Biology: Jacob Peter Matson, Amy M. House, Gavin D. Grant, Huaitong Wu, Joanna Perez, Jeanette Gowen Cook. Intrinsic checkpoint deficiency during cell cycle re-entry from quiescence. 2019.

nearby licensed origin initiates a new fork to replicate the intervening DNA (Alver et al., 2014; Yekezare et al., 2013). Since MCM loading is tightly restricted to G1 phase, cells typically load excess MCM to license 5-10 fold more origins than they would require to complete S phase if there were no replication stress at all. These excess licensed origins function as “dormant origins”, and are activated as needed to respond to local replication stress and rescue stalled forks (Woodward et al., 2006; Ge et al., 2007; Ibarra et al., 2008). Cells with considerably less loaded MCM can still complete a normal S phase (Ge et al., 2007). Nonetheless, if cells enter S phase with less loaded MCM they are “underlicensed” with fewer dormant origins, and are hypersensitive to replication stress. In addition, animal models of underlicensing reveal its long-term consequences. Mice heterozygous for MCM null alleles or homozygous for hypomorphic MCM alleles have less MCM loading , increased replication stress, and defects in highly proliferative tissues such as hematopoietic cells and intestinal crypts (Alvarez et al., 2015; Pruitt et al., 2007). In addition, these mice with underlicensed cells are prone to genomic instability and cancer (Kunnev et al., 2010; Shima et al., 2007; Pruitt et al., 2007).

If dormant origins are critical to protect cells from replication stress and its consequent genome instability, then cells should have a control mechanism to ensure sufficient origin licensing. An origin licensing checkpoint in G1 phase of untransformed mammalian cells ensures abundant licensing in G1 phase before S phase entry (Shreeram et al., 2002; Nevis et al., 2009; Liu et al., 2009; Gillespie et al., 2007). Artificially reducing MCM loading in checkpoint proficient cells delays the late G1 activation of Cyclin E/Cyclin Dependent Kinase 2 (CDK2) (Nevis et al., 2009; McIntosh and Blow, 2012). Delayed Cyclin E/CDK2 activation delays the phosphorylation of multiple substrates that drive S phase entry. Delaying CDK2 activity lengthens G1 phase and ensures that cells do not enter S phase with low levels of origin licensing. Moreover, this checkpoint is p53-dependent (Nevis et al., 2009; Liu et al., 2009; Shreeram et al., 2002), thus a common genetic perturbation in transformed cancer cells likely compromises the normal coordination of origin licensing and S phase onset.

Given the importance of coordinating G1 length with the progress of origin licensing for robust S phase completion, we considered natural circumstances where G1 length changes. One example is the short G1 phase of pluripotent stem cells. We previously found that stem cells load MCM faster than differentiated cells with long G1 phases to achieve the same amount of loaded MCM at S phase entry (Matson et al., 2017). Another example is the long G1 after cell cycle re-entry from quiescence. Cell cycle quiescence, or "G0," is a reversible cell cycle exit to a non-dividing state. G0 is distinct from a G1 arrest; it is an active state requiring upregulation of anti-apoptotic, anti-senescent and anti-differentiation genes as well as repression of cell cycle genes (Coller et al., 2006; Sang et al., 2008; Litovchick et al., 2007; Sagot and Laporte, 2019). Cells re-entering G1 phase from G0 have a longer G1 than cells entering G1 from mitosis (Coller, 2007). The longer G1 phase during re-entry likely reflects the need to reactivate and express genes repressed in G0 as well as fundamental differences in G1 regulation.

The increased G1 length after G0 and the restriction of origin licensing to G1 phase suggests that origin licensing may be distinctly regulated in the longer G1 upon cell cycle re-entry. We entertained the notion that the increased G1 length may allow more time for MCM loading, causing a meaningful increase in DNA-loaded MCM when entering S phase compared to subsequent proliferating cell cycles. To test this idea, we used single cell flow cytometry to measure the amount of loaded MCM at S phase entry and live cell imaging to measure cell cycle timing to determine if the amount of loaded MCM differs between cell cycle re-entry and active proliferation. Surprisingly, we discovered instead that cells re-entering the cell cycle from G0 are underlicensed and hypersensitive to replication stress compared to proliferating cells. This finding is consistent with a recent report that the first S phase experiences higher spontaneous replication stress, though the source of that endogenous stress was not identified (Daigh et al., 2018). We report here that MCM loading is slow in the first G1 phase and that the first cell cycle has a severely compromised origin licensing checkpoint relative to the robust checkpoint in actively proliferating cells. This combination promotes premature S phase entry

and underlicensing. To our knowledge, these results demonstrate the first naturally underlicensed cell cycle and suggest that repeated cell cycle re-entry from G0 is particularly hazardous for long-term genome stability.

Results

G0 cells re-entering the cell cycle are underlicensed compared to actively proliferating cells.

Cells re-entering the cell cycle from G0 have a long G1 before S phase entry relative to actively proliferating cells (Coller, 2007). We hypothesized that the difference in G1 length and unique aspects of the G0 to G1 transition could alter the timing or amount of loaded MCM at S phase entry in normal human cells. The amount of MCM loaded at the onset of S phase determines replication stress tolerance and thus overall replication success. For this reason we focused on quantifying how much MCM is loaded at the onset of S phase (G1/S transition). Standard synchronization and immunoblotting is an inadequate approach however because G0 cells re-enter G1 phase semi-synchronously, particularly untransformed cells. Even in the first cycle, there is no time point near the G1/S transition after cell cycle re-entry that is not a mix of different phases (e.g. G1 and S phase cells), and the following second cell cycle is nearly asynchronous (Wang et al., 2017; Kwon et al., 2017). We therefore used a previously published and validated single cell flow cytometry assay to measure DNA-loaded MCM at the G1/S transition (Matson et al., 2017; Håland et al., 2015; Moreno et al., 2016; Carroll et al., 2018; Hiraga et al., 2017). We examined proliferating Retinal Pigmented Epithelial cells (RPE1) whose only genetic alteration is the introduction of telomerase (RPE1-hTert). We extracted soluble proteins with nonionic detergent, DNA-bound proteins were retained, then fixed and stained with anti-Mcm2 antibody as a marker for the whole MCM2-7 complex, DAPI to measure DNA content, and for the nucleotide analog 5-Ethynyl-2´-deoxyuridine (EdU) to measure DNA synthesis (Fig. 4.1). We defined MCM-positive cells based on an antibody negative control; grey cells in these plots are below this background for detecting DNA-loaded MCM (MCM^{DNA} neg.).

Figure 4.1

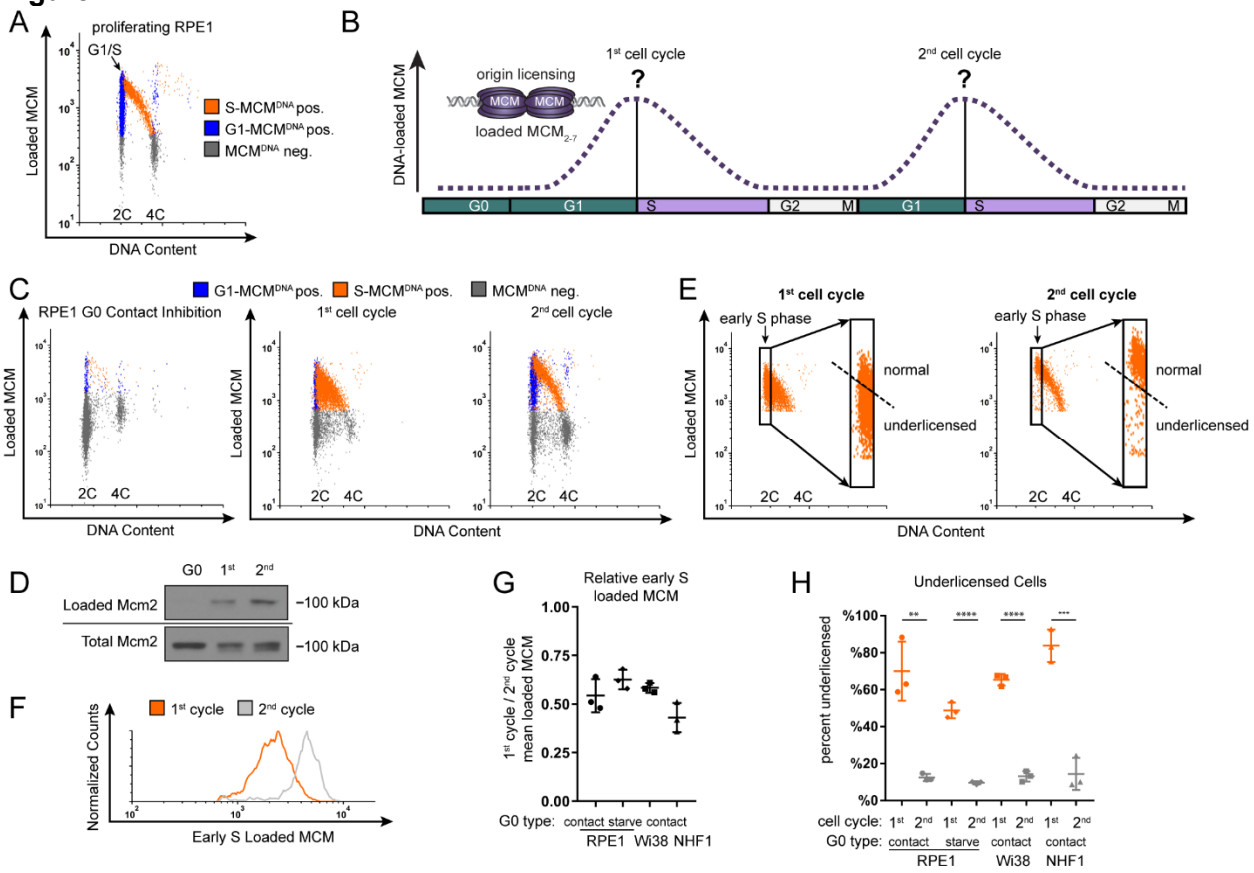

Figure 4.1. The first S phase after cell cycle re-entry from quiescence (G0) is underlicensed.

a. Flow cytometry of proliferating RPE1-hTert cells extracted with nonionic detergent to measure DNA bound protein (analytical flow cytometry for chromatin-bound proteins). Cells were labeled with 10 uM EdU for 30 minutes before harvesting then stained with anti-Mcm2 antibody to measure DNA-loaded MCM, DAPI to measure DNA content, and EdU to measure DNA synthesis. Gates to define colors are provided in Fig. 4.2A: orange cells are S phase, EdU-positive cells DNA-loaded MCM-positive, blue cells are G1 phase cells, EdU-negative with DNA-loaded MCM-positive, grey cells are all MCM-negative cells. Arrow indicates the G1/S transition.
b. Cartoon of MCM loading in the first and second cell cycles. The amount of MCM loaded at the point of S phase entry determines the likelihood of replication success (indicated by question marks). At the start of this study, MCM loading before the first S phase after the long G1 relative to MCM loading in second and subsequent cell cycles was unknown.
c. DNA loaded MCM, DNA content (DAPI), and DNA Synthesis (EdU) as in Fig. 4.1A. RPE1 cells were synchronized in G0 by contact inhibition with 10% fetal bovine serum and released from G0 into the cell cycle by replating. Cells were analyzed in G0, 24 hours after release (first cell cycle), and 48 hours after release (second cell cycle).
d. Immunoblot of cells treated as in Fig. 4.1C, Samples were fractionated into DNA loaded chromatin fractions and whole cell lysates then probed for MCM2.
e. Gating of early S cells from Fig. 4.1C, showing only the S phase-MCM^{DNA}-positive cells. Black rectangles define early S phase cells as MCM^{DNA}-positive with 2C DNA content. Inset: Displays only early S phase cells. Cells above the dashed line were normally licensed whereas cells below the line were underlicensed.

f. Histogram measuring DNA-loaded MCM in early S phase cells from Fig. 4.1E. The orange line is early S phase loaded MCM from first cell cycle, and the grey line is early S phase loaded MCM from second cell cycle.
g. Fold change in early S phase loaded MCM between first and second cell cycles of RPE1 G0 synchronized by contact inhibition from Fig. 4.1E, RPE1 G0 synchronized by mitogen starvation (Fig. 4.2I, J), and Wi38, and NHF1-hTert G0 synchronized by contact inhibition (Fig. 4.2E-H). Y axis is ratio of mean early S phase loaded MCM from first cell cycle divided by mean early S phase loaded MCM from second cell cycle, plotted center line is mean with standard deviation (SD) error bars, n=3 biological replicates.
h. Percentage of underlicensed cells from first and second cell cycles of cells in Fig. 4.1G, plotted center line is mean with standard deviation (SD) error bars, n=3 biological replicates. First and second cell cycles compared by unpaired, two tailed t test. RPE1 contact p=0.0035** RPE1 starve p<0.001****, Wi38 p<0.001****, NHF1 p=0.006***.

Figure 4.2

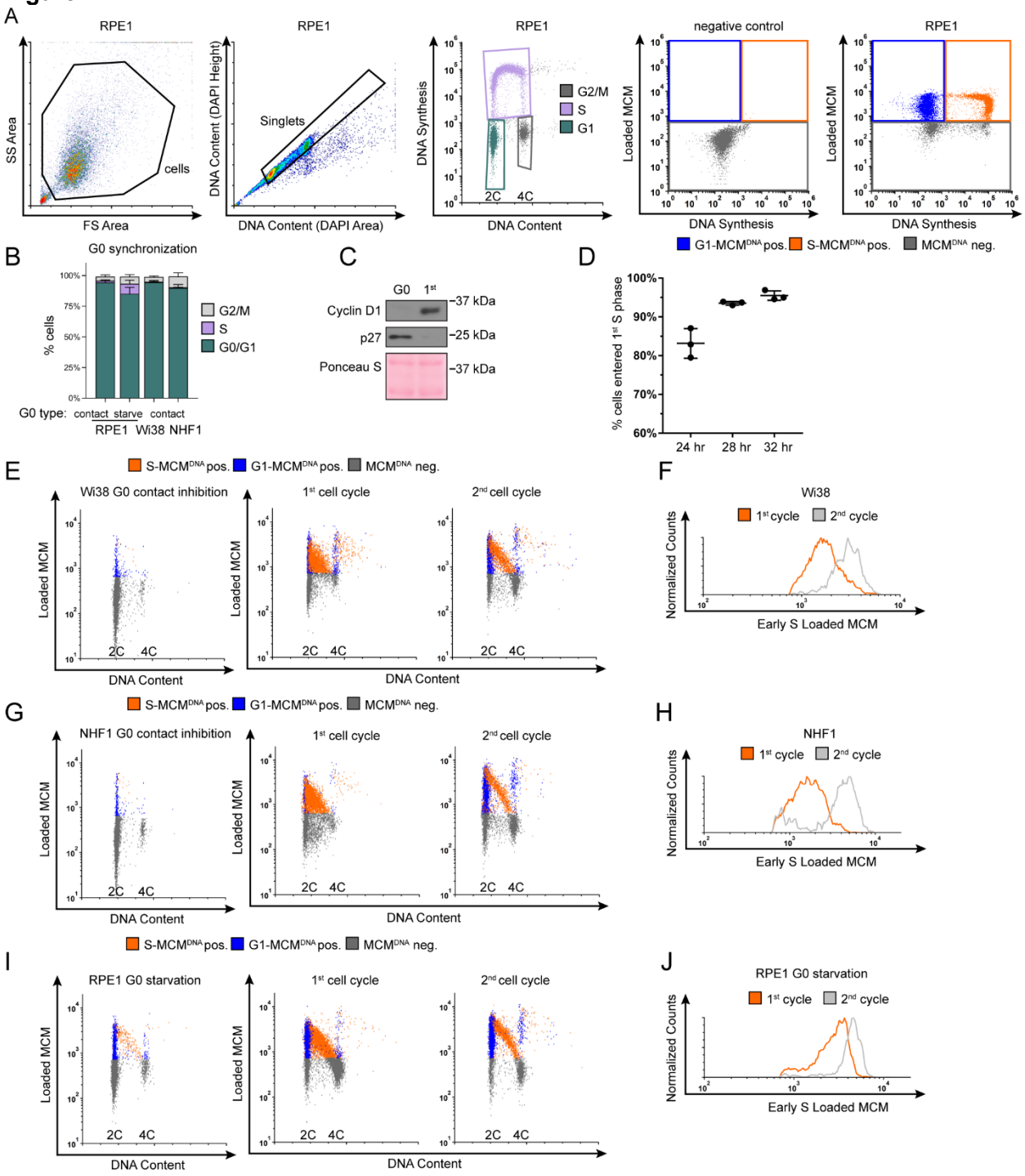

Figure 4.2. Flow cytometry gating and alternate cell lines

a. Flow cytometry gating to isolate cells for analysis. Proliferating RPE1 cells (Fig. 4.1A) were processed for analytical flow cytometry for chromatin-bound proteins, labeling DNA Content (DAPI), Loaded MCM (anti-Mcm2) and DNA Synthesis (EdU). Cells were labeled with 10 uM EdU for 30 minutes before harvesting. Gating to isolate cells from debris is Forward Scatter Area vs Side Scatter Area, cells gate. Gating to isolate single cells from doublets is DAPI Area vs DAPI Height, singlets gate. Gating to determine cell cycle phase distributions is DNA Content

vs DNA Synthesis. Color gating for S-MCM^{DNA} positive (orange), G1-MCM^{DNA} positive (blue) and MCM^{DNA} negative (grey) is on DNA Synthesis vs Loaded MCM using a negative control sample without Mcm2 primary antibody or EdU, but with Donkey anti Mouse-488 secondary antibody and 647-azide as a measure of background staining.
b. Cell cycle phase of RPE1 cells G0 synchronized by contact inhibition, Fig. 4.1C, RPE1 cells G0 synchronized by mitogen starvation, Fig. 4.21I, Wi38 cells G0 synchronized by contact inhibition, Fig. 4.2G, and NHF1-htert cells G0 synchronized by contact inhibition, Fig. 4.2E. Horizontal bars indicate means, error bars mark standard deviation (SD), n=3 biological replicates.
c. Immunoblot for Cyclin D1 or p27 on total protein lysate from RPE1 cells synchronized in G0 or released into the first cell cycle (24 hours) as in Fig. 4.1C.
d. Percentage of S phase cells defined by analytical flow cytometry. RPE1 cells were synchronized in G0 by contact inhibition were released into the cell cycle with 1 uM EdU at time of release, harvesting cells, 24, 28, and 32 hours after release from G0. S phase was determined by DAPI (DNA Content) and EdU (DNA Synthesis) cells as in Fig. 4.2A. Horizontal bars indicate means, error bars mark standard deviation (SD), n=3 biological replicates.
e. Flow cytometry of chromatin-bound protein on Wi38 cells synchronized in G0 by contact inhibition in 0.1% FBS for 72 hours and released from G0 into the cell cycle, harvesting 24 hours after release (first cell cycle) and 48 hours after release (second cell cycle). Flow cytometry measured DNA Content (DAPI), Loaded MCM (anti-Mcm2) and DNA Synthesis (EdU). Cells were labeled with 10 μM EdU for 30 minutes before harvesting. Orange cells are S phase MCM^{DNA} positive, blue cells are G1 phase MCM^{DNA} positive, grey cells are MCM^{DNA} negative.
f. Loaded MCM in early S phase determined by flow cytometric analysis of early S phase Wi38 from Fig. 4.2E. Orange line is first cell cycle, grey line is second cell cycle.
g. Flow cytometry of chromatin-bound protein on NHF1-htert cells synchronized in G0 by contact inhibition in 0.1% FBS for 72 hours and released from G0 into the cell cycle, harvesting 24 hours after release (first cell cycle) and 48 hours after release (second cell cycle). Flow cytometry measured DNA Content (DAPI), Loaded MCM (anti-Mcm2) and DNA Synthesis (EdU). Orange cells are S phase MCM^{DNA} positive, blue cells are G1 phase MCM^{DNA} positive, grey cells are MCM^{DNA} negative.
h. Loaded MCM in early S phase determined by flow cytometric analysis of NHF1 from Fig. 4.2G. Orange line is first cell cycle, grey line is second cell cycle.
i. Flow cytometry of chromatin-bound protein on RPE1 cells synchronized in G0 by starvation in 0% FBS for 72 hours and released from G0 into the cell cycle, harvesting 24 hours after release (first cell cycle) and 48 hours after release (second cell cycle). Flow cytometry measured DNA Content (DAPI), Loaded MCM (anti-Mcm2) and DNA Synthesis (EdU). Orange cells are S phase MCM^{DNA} positive, blue cells are G1 phase MCM^{DNA} positive, grey cells are MCM^{DNA} negative.
j. Loaded MCM in early S phase determined by flow cytometric analysis of RPE1 from Fig. 4.2I. Orange line is first cell cycle, grey line is second cell cycle.

Fig. 4.2A shows the flow cytometry gating scheme. We marked cells blue for 2C DNA content (G1) that are negative for DNA synthesis but positive for DNA-loaded MCM (G1- MCM^{DNA} pos.). MCM loading is unidirectional in G1 phase, increasing in G1 until the maximum amount of loaded MCM at the G1/S transition (Kuipers et al., 2011). The column of blue cells with 2C DNA on the flow cytometry plot reflects cells at different G1 stages, cells in early G1 have less loaded MCM and cells in late G1 have more loaded MCM (Fig. 4.1). Loaded MCMs are very stable and are only unloaded in S phase as replication terminates (Moreno et al., 2014; Maric et al., 2014). We marked cells orange for S phase based on EdU incorporation and DNA-loaded MCM (S-MCM^{DNA} pos.). In actively proliferating populations with robust licensing prior to S phase entry, we consistently observe that the majority of cells reach a similar maximum loaded MCM per cell in G1 (blue) before becoming EdU positive (orange) in very early S phase. In this way, we accurately measured loaded MCM in very early S phase even in fully asynchronous populations. (Fig. 4.1A "G1/S" marked by the arrow).

Our goal was to apply this method to measure how much MCM had been loaded by the time of the G1/S transition in the first cell cycle compared to the amount loaded at G1/S in the second cell cycle (Fig. 4.1B). We arrested RPE1-hTert cells in G0 by contact inhibition (in the presence of growth serum) for 48 hours. Contact-inhibited G0 cells showed a robust cell cycle exit to G0 with very little loaded MCM; 94% of cells were G0/G1 but only 1% were still in S phase (Fig. 4.1C and Fig. 4.2B). We then released cells to re-enter the cell cycle by plating at sub-confluent cell density. G0 cells also expressed the expected high levels of p27 and low Cyclin D1 compared to cells in the first cycle (Fig. 4.2C). We pulse-labeled cells with EdU and harvested some cells in G0 and some at 24 hrs when they were a mix of first G1 and ~50-70% first S phase cells. In a separate continuous EdU labeling experiment in which EdU was added at the time of release, we determined that nearly 100% of cells had entered S phase by 28 hours (Fig. 4.2D), and almost no cells remained in G0/G1. Thus, we concluded that additional

cells harvested 48 hours after release had completed their first S phase and were into their second cell cycle.

Strikingly, the amount of loaded MCM at the G1/S transition was markedly different between the first and second cell cycles after G0. Cells in the first cell cycle progressed into S phase (orange cells) with substantially less MCM loaded than cells in the second cell cycle. By the second cell cycle, G1 cells progressed into S phase as a tight group with relatively high amounts of loaded MCM (transition from blue to orange). In contrast, many cells in the first cell cycle entered S phase with low amounts of loaded MCM. This behavior creates the filled orange triangle on flow cytometry plots of the first S phase instead of the normally clear region under a high arc characteristic of the second S phase. We also observed decreased loaded MCM in the first cycle using biochemical chromatin fractionation and immunoblotting (Fig. 4.1D).

To quantify the amount of loaded MCM at the G1/S transition, we analyzed the S phase cells from Fig. 4.1C, and defined very early S phase cells as EdU-positive with ~2C DNA content (Fig. 4.1E black rectangles). Early S phase cells in the first cycle had a broad range of loaded MCM levels that included many cells with low MCM, whereas early S phase cells in the second cycle primarily had high loaded MCM levels. The second cell cycle was nearly indistinguishable from asynchronously proliferating cells that had not been arrested. We thus used the second cell cycle to define the normal licensing levels, and classified cells with less MCM loaded in early S as “underlicensed cells” (Fig. 4.1E dashed line). To more readily visualize and compare the different populations, we generated histograms of loaded MCM levels in early S phase cells (Fig. 4.1F). On this plot the differences between the first and second S phases were readily apparent (compare orange and grey lines). We quantified the differences as fold change between the mean MCM loaded in the first and second S phases. Cells in the first cycle after re-entry from G0 loaded only half as much MCM as cells in the second cell cycle (Fig. 4.1G). We then used this same comparison to test if this underlicensed first cell cycle is common among different untransformed cell lines or methods of quiescence

induction. We observed similar underlicensing after quiescence induction in RPE1-hTert by serum starvation and re-stimulation and in two fibroblast cell lines arrested by contact inhibition and release (Fig. 4.1G and Fig. 4.2E-J). We observed that not only was the mean MCM loaded of the first S phase half that of subsequence S phases, but also that the majority of first S phase cells were underlicensed (Fig. 4.1H). Thus, re-entry from G0 is characterized by substantial underlicensing in the first cell cycle.

Cells re-entering S phase from G0 are hypersensitive to replication stress.

Cells typically load extra MCM in G1 to license dormant origins that protect against replication stress in S phase (Woodward et al., 2006; Ge et al., 2007; Ibarra et al., 2008). Given our observations that the first S phase is underlicensed relative to the subsequent S phase, we hypothesized that cells re-entering the cell cycle from G0 would be hypersensitive to replication stress in the first S phase. To test that idea directly, we treated cells in the first or second cell cycle after G0 with low-dose gemcitabine, a drug that depletes nucleotides to cause replication stress (Ewald et al., 2007). We used flow cytometry to measure the expression of γH2AX, a common replication stress marker (Ewald et al., 2007)(Fig. 4.3A, B, and Fig. 4.4A). We specifically analyzed mid-S phase cells to control for differences in cell cycle distribution, and we counted the number of γH2AX-positive S phase cells with expression equal to or greater than the top 5% of untreated cells (Fig. 4.3C, dashed line). By this measurement, cells in the first S phase after G0 are significantly more sensitive to replication stress than cells in the second S phase (Fig. 4.3D). Moreover, gemcitabine-treated first S phase cells expressed double the amount of γH2AX per cell than cells in the second S phase, suggesting that not only were more total cells exhibiting a replication stress response but also that there was more replication stress per cell (Fig. 4.3E, F). This hypersensitivity to replication stress in the underlicensed first cell cycle suggests that cell cycle re-entry is an inherently risky cycle with respect to genome stability compared to subsequent cell cycles.

Figure 4.3

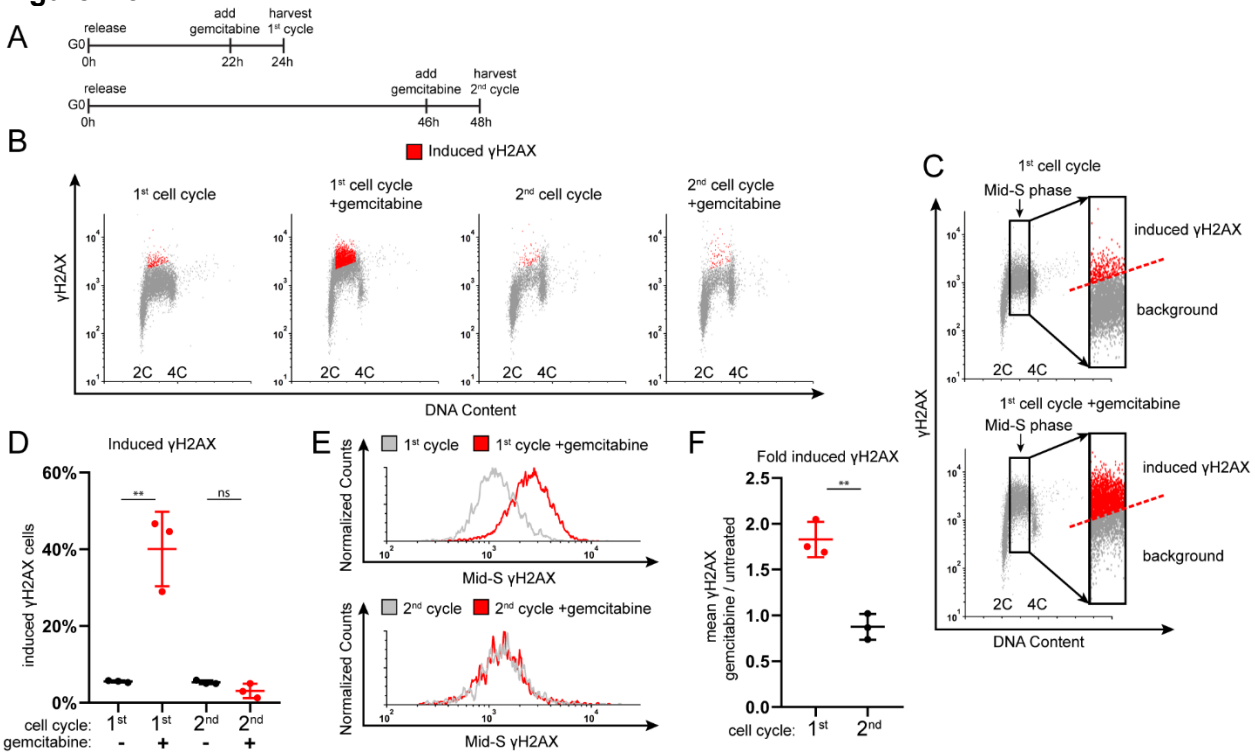

Figure 4.3. The first S phase after G0 is hypersensitive to replication stress.

a. Diagram of gemcitabine treatment. RPE1 cells synchronized in G0 by contact inhibition and released into the first (harvest 24 hrs later) or second cell cycle (harvest 48 hrs later) were treated with 50 nM gemcitabine for the last 2 hours before harvesting for flow cytometry.

b. Chromatin flow cytometry of cells treated as Fig. 4.3A and stained for DNA content (DAPI), DNA Loaded MCM (anti-Mcm2, Fig. 4.4) and γH2AX (anti-H2AX phospho S139). Red cells are replication stress (gemcitabine) induced γH2AX positive, as indicated in Fig. 4.3C.

c. Gating of cells from Fig. 4.3B isolate γH2AX induced by gemcitabine. Rectangle gate isolates Mid S phase cells, between 2C and 4C DNA Content. Inset: Shows only Mid S phase cells, replication stress (gemcitabine) induced γH2AX (red cells in gate) are defined as cells equal to or above the top 5% of untreated cells, also plotted red in Fig. 4.3B.

d. Percentage of replication stress (gemcitabine) induced γH2AX in first and second cell cycles from cells in Fig. 4.3B. n=3 biological replicates, center line is mean with SD error bars. Untreated and gemcitabine treated compared by unpaired, two tailed t test. First cell p=0.0035**. Second cell cycle p=0.1174 (ns).

e. Histograms of mid S phase γH2AX intensity from cells in Fig. 4.3B, upper panel is first cell cycle and lower panel is second cell cycle. Grey lines are untreated cells, red lines are gemcitabine treated cells. Y axis counts are normalized to peak value of untreated cells.

f. Fold induced γH2AX. Y axis ratio is mean Mid S γH2AX intensity of gemcitabine treated cells divided by mean Mid S γH2AX intensity of untreated cells from cells in Fig. 4.3E, n=3 biological replicates. Plotted center line is mean, error bars are SD. Samples compared by unpaired, two tailed t test, p=0.0023**.

Figure 4.4

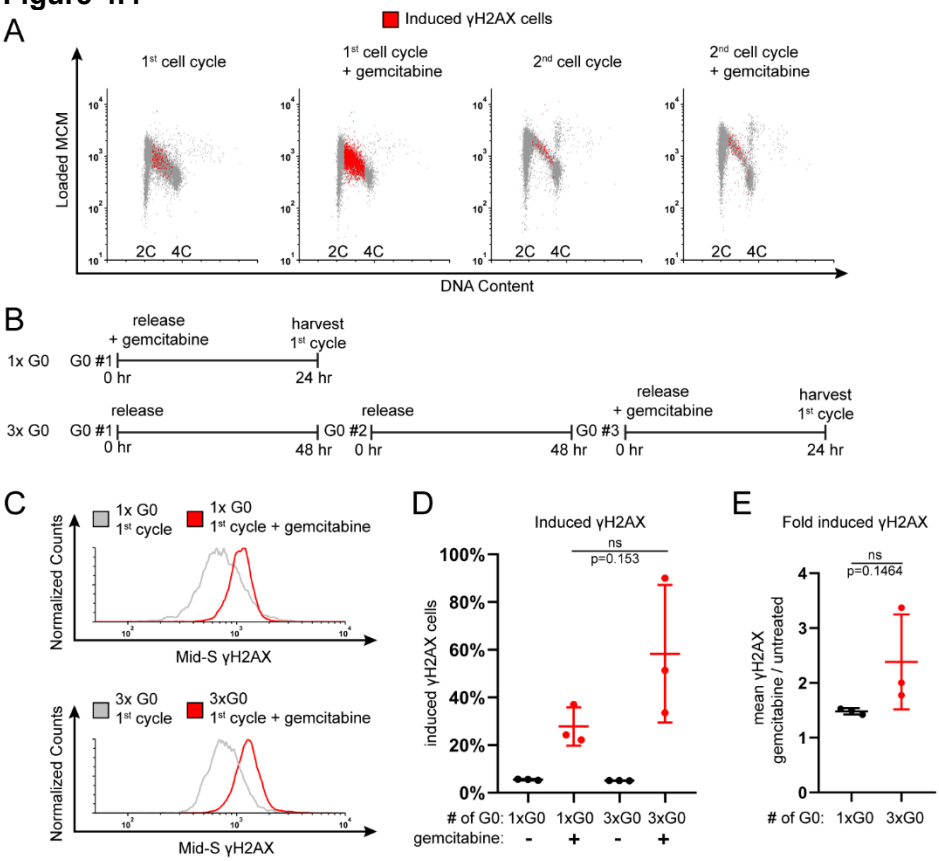

Figure 4.4. Repeated transitions between G0 and proliferation trend towards an increased replication stress sensitivity

a. Flow cytometry of chromatin-bound protein from cells in Fig. 4.3B, showing DNA loaded MCM (anti-MCM2). Red cells are gemcitabine (replication stress) induced γH2AX positive, as indicated in Fig. 4.3C.

b. Diagram of experiment. For 1xG0: RPE1 cells were synchronized in G0 by contact inhibition for 48 hours, then released into the cell cycle with 5 nM gemcitabine, harvesting cells 24 hours after release. For 3xG0: RPE1 cells were synchronized in G0 by contact inhibition for 48 hours, released into the cell cycle without gemcitabine and grown to confluency to repeat the G0 by contact inhibition a second time, then repeating once again for a 3rd G0. Then cells were released into the cell cycle with 5 nM gemcitabine, harvesting cells 24 hours after release.

c. Flow cytometry of chromatin-bound protein from cells treated as in Fig. 4.4B, measuring DNA Content (DAPI) and γH2AX (anti H2AX phospho S139). Histograms plot γH2AX of Mid-S phase cells as described in Fig 4.3C. Upper panel is 1xG0, lower panel is 3xG0. Grey lines are first cell cycle untreated, red lines are first cell cycle treated with 5 nM gemcitabine.

d. Percentage of replication stress-induced γH2AX in 1xG0 and 3xG0 release into the first cycle from Fig. 4.4C. Horizontal bars indicate means, error bars mark standard deviation (SD), n=3 biological replicates. 1xG0 and 3xG0 compared by unpaired, two tailed t test. p=0.153 (ns).

e. Comparison of γH2AX intensity per cell presented as fold-change between gemcitabine-treated and untreated cells from Fig. 4.4C. Horizontal bars indicate means, error bars mark standard deviation (SD), n=3 biological replicates. Samples compared by unpaired, two tailed t test. p=0.1464 (ns).

Many cells *in vivo* switch between periods of active proliferation and periods of G0, repeatedly re-entering the cell cycle to proceed through this presumably underlicensed first cell cycle. We considered the possibility that repeated cell cycle exit and re-entry would lead to additional replication stress sensitivity over time. To measure accumulation of replication stress during repeated cell cycle re-entry, we synchronized RPE1 cells in G0 by contact inhibition for 48 hours and released them into the cell cycle for about 48 hours (~2-3 cycles) and then they became contact inhibited again. We reiterated this procedure for a total of 3 rounds of G0 arrest and re-entry. In the third release, we treated with gemcitabine and measured the induction of γH2AX as before (Fig. 4.4B, C). Cells re-entering S phase from three repeated arrests in G0 ("3xG0") were more likely to induce γH2AX cells than cells that been arrested only once ("1xG0"), and these cells were also more intensely γH2AX positive per cell (Fig. 4.4D, E). The increased replication stress sensitivity after three rounds of G0 was variable due to inherent variations in the G0 synchronization over multiple rounds (Kwon et al., 2017; Wang et al., 2017). This variability was reflected by unpaired t test p values of ~p=0.15 for both the number of γH2AX positive cells and the γH2AX intensity Fig. 4.4D, E. Nevertheless, we observed a clear trend that repeated cell cycle re-entry from G0 increased sensitivity to replication stress.

Proliferating epithelial cells have a robust p53-dependent origin licensing checkpoint.

Our findings raised a larger question about the relationship between origin licensing and S phase entry. The consistently high amount of loaded MCM we observed prior to G1/S in the second and subsequent cell cycles is consistent with an active origin licensing checkpoint (e.g. Fig. 1A arrow). The origin licensing checkpoint delays S phase entry when the amount of loaded MCM is still low in untransformed cells by delaying the activation of G1 Cyclin Dependent Kinases (CDK) (McIntosh and Blow, 2012). Evidence for this checkpoint is low CDK activity and lengthening of G1 in proliferating cells treated to reduce MCM loading by siRNA-mediated depletion of MCM loading factors or by overproduction of the MCM loading inhibitor, Geminin (Shreeram et al., 2002; Liu et al., 2009; Nevis et al., 2009). The origin licensing

checkpoint ensures that S phase begins with abundant licensed dormant origins that protect against replication stress. Because we observed routinely underlicensed cells in the first S phase after G0 and consistently higher licensing in the second cell cycle, we hypothesized that the origin licensing checkpoint is mostly active in the second and subsequent cell cycles.

Origin licensing checkpoint activity is cell type-dependent however (Shreeram et al., 2002). We therefore sought first to assess checkpoint status in proliferating untransformed epithelial cells (RPE1-hTert). We decreased origin licensing with siRNA targeting Cdc10 dependent transcript 1 (Cdt1), an essential MCM loading protein (Pozo and Cook, 2016). We used either a pool of four siCdt1 sequences (siCdt1 A) or a single independent siCdt1 (siCdt1 B) and analyzed Cdt1 protein by immunoblotting (Fig. 4.5B). We then tested both MCM loading and the length of G1 phase. Cdt1 depletion induced both a reduction in the rate of G1 phase MCM loading (Fig. 4.6A, B) and also a striking G1 lengthening. G1 length dramatically increased by several-fold (12 to 42 hrs for siCdt1B), and the more profound Cdt1 depletion by siCdt1 B caused a greater G1 delay (Fig. 4.5F). Importantly, Cdt1 depletion changed neither the amount of early S loaded MCM (compare black and grey lines in Fig. 4.5C, and fold change in Fig. 4.5D) nor the percentage of underlicensed early S phase cells (Fig. 4.5E). By the time cells finally entered S phase, they had achieved normal amounts of loaded MCM. These observations indicate that actively proliferating RPE1 cells wait for the normal amount of loaded MCM in G1 phase before entering S phase.

A cell cycle checkpoint that delays progression to the next phase is distinct from a simple incapacity to proceed to the next phase because it is possible for genetic alterations to bypass a checkpoint and induce premature cell cycle progression (Hartwell and Weinert, 1989). The origin licensing checkpoint delays the activation of Cyclin E/CDK2 (Fig. 4.5A) (Nevis et al., 2009). To test if the G1 phase delay can be bypassed in Cdt1-depleted RPE1-hTert cells, we overproduced Cyclin E1 to prematurely activate CDK2. We used flow cytometry to measure DNA loaded MCM, plotting a histogram of early S phase loaded MCM (Fig. 4.5C and Fig. 4.6A).

Figure 4.5

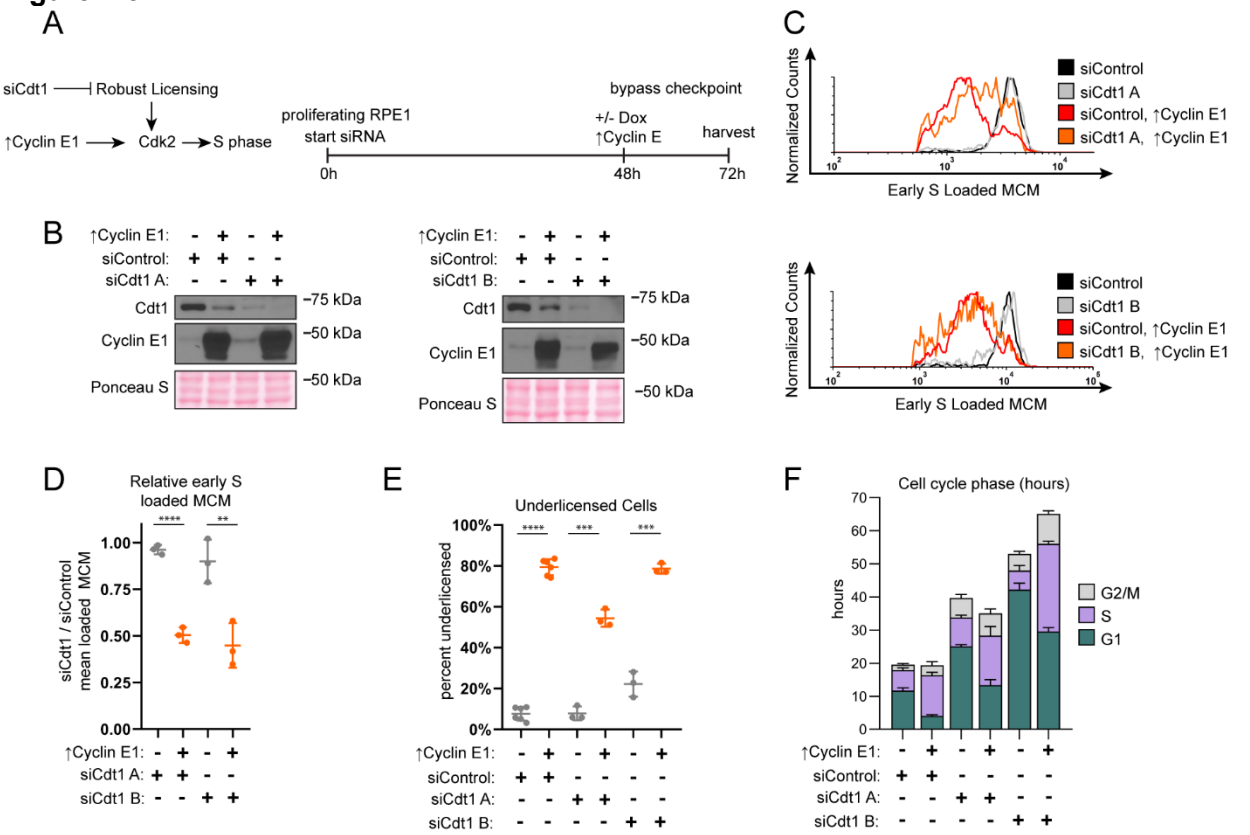

Figure 4.5. Cyclin E1 overproduction bypasses the licensing checkpoint-induced G1 arrest in proliferating cells

a. Left: Model. Robust licensing promotes CDK2 activation and S phase entry. Cdt1 depletion by RNAi prevents robust licensing, CDK2 activation, and S phase entry. Cyclin E1 overproduction in Cdt1-depleted cells directly activates CDK2 independently of licensing and induces S phase entry. Right: Diagram of the experimental workflow. Proliferating RPE1-hTert cells containing integrated doxycycline inducible exogenous Cyclin E1 were treated with siControl, or independent siRNAs targeting Cdt1 (siCdt1 A, or siCdt1 B) for 72 hours. 100 ng/mL doxycycline to overproduce Cyclin E1 were added at 48 hours.

b. Immunoblots of the indicated proteins in total protein lysates of cells treated as in Fig. 4.5A. ↑Cyclin E1 indicates addition of 100 ng/mL doxycycline at 48 hours to overproduce Cyclin E1.

c. Loaded MCM in early S phase determined by flow cytometric analysis of cells treated as in Fig. 4.5A, measuring DNA content (DAPI), DNA-Loaded MCM (anti-Mcm2) and DNA synthesis (EdU). Black lines are siControl treated cells, grey lines are siCdt1 A (upper) or siCdt1 B (lower), red lines are siControl plus overproduced Cyclin E1. Orange lines are siCdt1 A (upper) or siCdt1 B (lower) plus overproduced Cyclin E1. See Fig. 4.6A for complete flow cytometry plots.

d. Comparison of early S phase DNA-loaded MCM per cell from Fig. 4.5C. Values plotted are the ratio of mean loaded MCM in cells treated with siCdt1 and cells treated with siControl. Horizontal bars indicate means, error bars mark standard deviation (SD), n=3 biological replicates. Control and Cyclin E-overproducing cells were compared by unpaired, two tailed t test, siCdt1 A p<0.001****. siCdt1 B p=0.0096**.

e. Percentage of underlicensed cells from cells treated as Fig. 4.5A. Horizontal bars indicate means, error bars mark standard deviation (SD), n=3 biological replicates. Control and Cyclin E-overproducing cells were compared by unpaired, two tailed t test. SiControl p<0.001****, siCdt1 A p=0.001***, siCdt1 B p=0.001***.

f. Mean lengths of G1 (green), S (purple), and G2/M (grey) phases in hours for cells treated as Fig. 4.5A. G1 lengths: siControl = 11.7 hrs, siControl + ↑Cyclin E1 = 4.1 hours, siCdt1 A = 25.1 hrs, siCdt1 A + ↑Cyclin E1= 13.4 hrs, siCdt1 B = 42.3 hrs, siCdt1 B + ↑Cyclin E1 = 29.6 hours. Error bars are SD, n=minimum 3 biological replicates. Cell cycle phase percentages from DNA Content vs DNA synthesis plots (see Fig. 4.2) were multiplied by the doubling time in hours to calculate hours for each phase. Doubling time is the mean of 3 biological replicates.

Figure 4.6

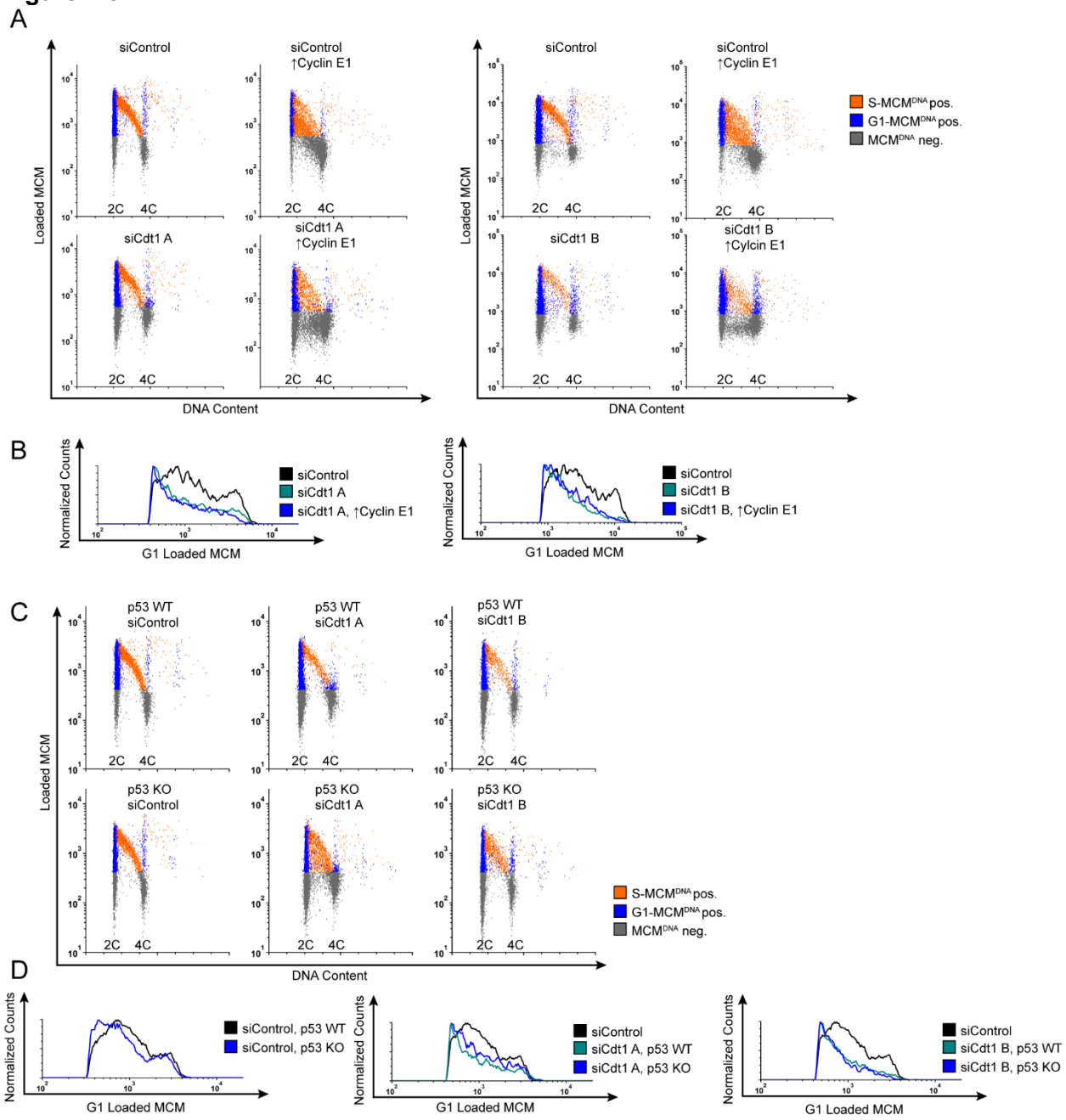

Figure 4.6. Flow cytometry plots of siRNA in proliferating cells.

a. Flow cytometry of chromatin-bound protein of cells shown in Fig. 4.5C, measuring DNA Content (DAPI), Loaded MCM (anti-Mcm2) and DNA Synthesis (EdU). Orange cells are S phase MCM^{DNA} positive, blue cells are G1 phase MCM^{DNA} positive, grey cells are MCM^{DNA} negative.

b. Loaded MCM in G1 cells from Fig 4.5C. Black lines are siControl treated cells. Green lines are siCdt1 A (left) or siCdt1 B (right). Blue lines are siCdt1 A, ↑Cyclin E1 (left) or siCdt1 B, ↑Cyclin E1 (right).

c. Flow cytometry of chromatin-bound protein of cells shown in Fig. 4.7C, measuring DNA Content (DAPI), Loaded MCM (anti-Mcm2) and DNA Synthesis (EdU). Orange cells are S

phase MCM^{DNA} positive, blue cells are G1 phase MCM^{DNA} positive, grey cells are MCM^{DNA} negative.
d. Loaded MCM in G1 cells from Fig. 4.7C. Left histogram: Black line is siControl, p53 WT, blue line is siControl p53 KO. Middle and right histograms: Black lines are siControl, p53 WT, green lines are siCdt1A, p53 WT (left) or siCdt1 B, p53 WT (right), blue lines are siCdt1 A p53 KO (left) or siCdt1 B p53 KO (right). Note the black siControl p53 WT are the same sample on all three histograms.

As expected from prior reports, Cyclin E1 overproduction in control cells shortened G1 phase nearly three-fold (siControl vs ↑Cyclin E1, Fig. 4.5F) (Matson et al., 2017; Resnitzky et al., 1994). In addition Cyclin E1 overproduction alone induced underlicensing as measured by the amount of early S loaded MCM (compare black and red lines, Fig. 4.5C, and the percentage of underlicensed cells, Fig. 4.5E) (Ekholm-Reed et al., 2004; Matson et al., 2017). Strikingly, when we overproduced Cyclin E1 after Cdt1 depletion (Fig. 4.5A), early S phase cells became severely underlicensed, quantified by both MCM loaded per cell (compare grey and orange lines, Fig. 4.5C and fold change in Fig. 4.5D), and the percentage of underlicensed cells (Fig. 4.5E). Moreover, G1 length decreased even in the Cdt1-depleted cells (Fig. 4.5F). We previously determined that the apparent decease in Cdt1 protein upon Cyclin E1 overproduction is an indirect effect of cell cycle phase distribution because Cdt1 is stable in G1 and unstable in S phase (Matson et al., 2017). Since Cyclin E1 overproduction bypassed the strong G1 delay in control Cdt1-depleted cells and induced S phase entry with low amounts of loaded MCM, the G1 delay is caused by a *bona fide* origin licensing checkpoint.

Full origin licensing checkpoint activity in normal human fibroblasts requires the p53 tumor suppressor (Fig. 4.7A)(Nevis et al., 2009). To test if p53-deficient epithelial cells are more likely to enter S phase underlicensed, we compared isogenic WT and p53 homozygous null RPE1-hTert cells (Rodriguez-Rodriguez et al., 2018). We analyzed the effects of reduced origin licensing from Cdt1 depletion on both G1 length and early S phase licensing status. We first noted by immunoblotting that Cdt1 depletion induced accumulation of both p53 and the CDK2 inhibitor p21, the product of a p53-inducible gene, whereas p53 null cells lacked both p53 and detectable levels of p21 (Fig. 4.7B). The absence of p53 had little effect on either G1 phase MCM loading (Fig. 4.6C) or the amount of MCM loaded by early S phase in otherwise unperturbed cells (compare black and grey lines in Fig 4.7C, fold change in Fig. 4.7D, and percentage of underlicensed cells in Fig 4.7E). As before, Cdt1 depletion slowed MCM loading in WT cells increased G1 length by several-fold (Fig. 4.7F, Fig. S3D). In contrast, Cdt1-depleted

Figure 4.7

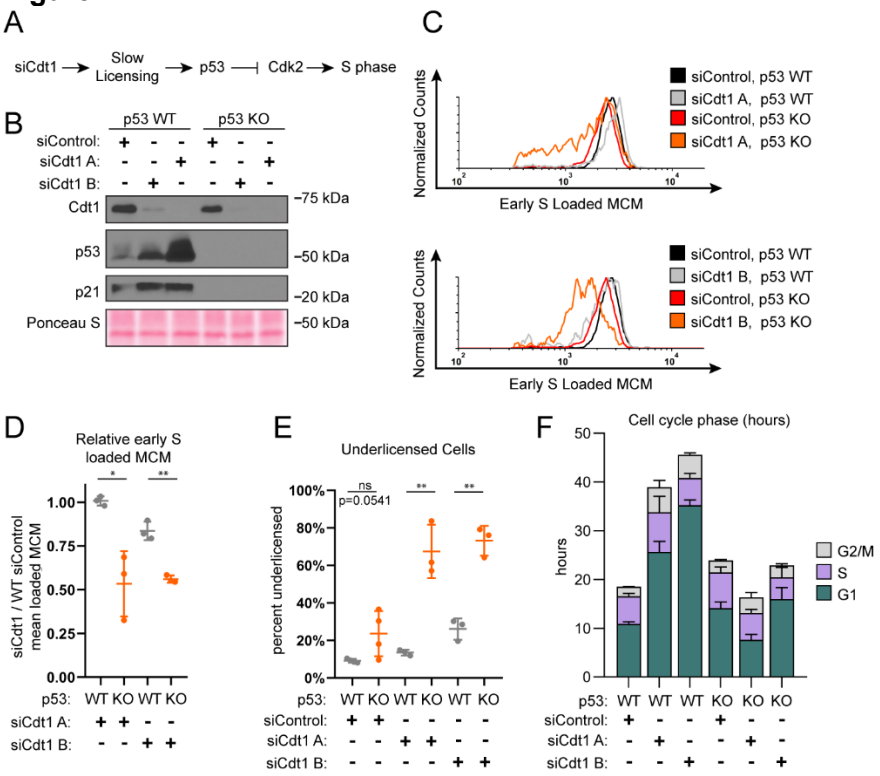

Figure 4.7 p53 knockout cripples the licensing checkpoint, causing underlicensing

a. Model. Cdt1 depletion causes slow origin licensing leading to p53-dependent inhibition of CDK2 which delays S phase entry.

b. Immunoblot of the indicated endogenous proteins in total protein lysates of RPE1-hTert p53 WT or p53 null, (knockout "KO") cells treated with siControl, siCdt1 A, or siCdt1 B for 72 hours.

c. Loaded MCM in early S phase determined by flow cytometric analysis of cells treated as in Fig. 4.7B, measuring DNA Content (DAPI), loaded MCM (anti-Mcm2), and DNA synthesis (EdU). Histograms plot early S phase loaded MCM. Black lines are siControl + p53 WT, grey lines are siCdt1A + p53 WT (top) or siCdt1 B + p53 WT (bottom), red lines are siControl + p53 KO, orange lines are siCdt1 A + p53 KO (top) or siCdt1 B + p53 KO (bottom). The black siControl + p53 WT and red siControl + p53 KO are the same data on both histograms. Counts for all lines were normalized to siControl + p53 WT.

d. Comparison of early S phase DNA-loaded MCM per cell from Fig. 4.7C. Values plotted are the ratio of mean loaded MCM in cells treated with siCdt1 and cells treated with siControl as indicated. Horizontal bars indicate means, error bars mark standard deviation (SD), n=3 biological replicates. WT and p53 KO cells were compared by unpaired, two tailed t test. SiCdt1 A p=0.0122*, siCdt1 B p=0.0011**.

e. Percentage of underlicensed cells from Fig. 4.7C. Horizontal bars indicate means, error bars mark standard deviation (SD), n=3 biological replicates. WT and p53 KO cells were compared by unpaired, two tailed t test. SiControl p=0.0541 (ns), siCdt1 A p=0.0028**, siCdt1 B p=0.0011**

f. Mean length of G1 (green), S (purple), and G2/M (grey) phases in hours for cells treated as Fig. 4.7C. G1 length: WT + siControl=10.9 hrs, WT + siCdt1 A = 25.7 hrs, WT + siCdt1 B= 35.5 hrs, p53 KO + siControl=14.1 hrs, p53 KO + siCdt1 A=7.6 hrs, p53 KO + siCdt1 B=16 hrs. Error bars are SD, n= minimum 3 biological replicates. Cell cycle phase percentages from DNA Content vs DNA synthesis plots (see Fig. 4.2) were multiplied by the doubling time in hours to calculate hours for each phase. Doubling time is the mean of 3 biological replicates.

cells lacking p53 entered S phase with significantly less MCM loaded (compare red and orange lines in Fig. 4.7C, fold change in Fig. 4.7D, and percentage of underlicensed cells in Fig. 4.7E). Moreover, unlike p53 WT cells, Cdt1 depletion in p53 null cells did not cause G1 lengthening (Fig. 4.7F). Thus, loss of p53 cripples the origin licensing checkpoint in proliferating cells, allowing premature S phase entry of underlicensed cells. We note that even in control cells that had not been depleted of Cdt1, the p53 null cells entered S phase at a slightly lower amount of loaded MCM on average compared to p53 WT cells (compare black and red lines in Fig. 4.7C). We also detected a modest increase in the percentage of underlicensed p53 null siControl cells (Fig. 4.7E). Overall we conclude that these untransformed epithelial cells utilize a p53-dependent checkpoint to couple the timing of S phase entry to the status of origin licensing.

The first G1 phase after G0 has an impaired origin licensing checkpoint.

We had established in Figures 1 and 2 that cells re-entering the first cell cycle after G0 are routinely underlicensed relative to subsequent cycles. We hypothesized that the first cell cycle has an impaired origin licensing checkpoint that poorly couples the length of G1 phase to the status of MCM loading. To test that hypothesis, we compared actively proliferating cells treated with siCdt1 to G0 cells re-entering the first cycle also treated with siCdt1 (Fig. 4.8A). We measured cell cycle phase distribution by DNA Content (DAPI) and DNA Synthesis (EdU) (Fig. 4.8B). The actively proliferating cells treated with siCdt1 increased the percentage of G1 cells as before, but there was little effect on G1 distribution in Cdt1-depleted cells re-entering the first cell cycle from G0 (Fig. 4.8B). These data indicated that cells re-entering the cell cycle from G0 failed to extend G1 when licensing was reduced, consistent with a weak origin licensing checkpoint. We also tested if the loss of p53 enhanced this apparent checkpoint deficiency (Fig. 4.8C). First cell cycle p53 null cells were no worse than first cell cycle WT cells with respect to cell cycle phase distribution (Fig. 4.8D). In contrast, p53 loss had affected the checkpoint behavior of actively proliferating cells. We note that siControl p53 null cells re-entering the first cycle also started S phase sooner than their corresponding p53 WT cells based on cell cycle

Figure 4.8

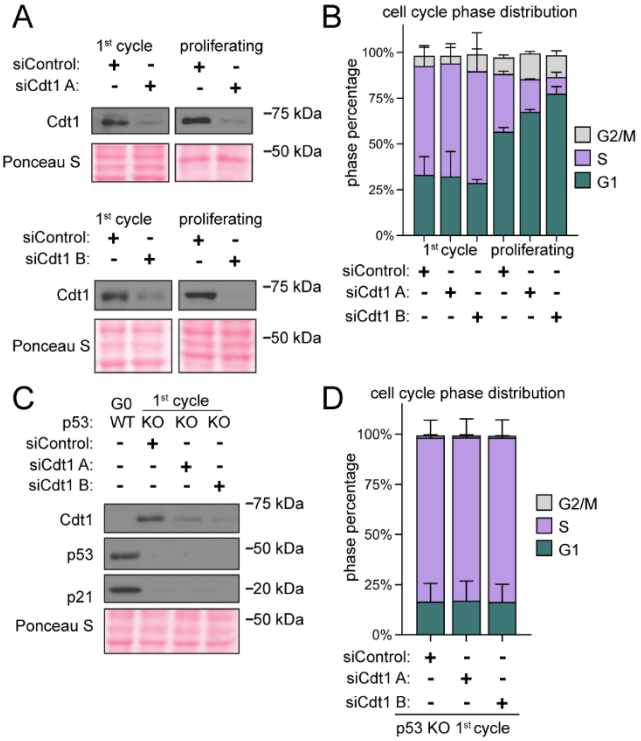

Figure 4.8. Cells re-entering the first G1 after G0 lack a checkpoint-induced G1 arrest

a. Immunoblot of total protein lysates of cells released from G0 into the first cell cycle with siControl or siCdt1 (24 hours after release) and of proliferating cells treated with siControl or siCdt1 for 72 hours.

b. Cell cycle phase distribution of cells treated as Fig. 4.8A defined by DNA synthesis (EdU) and DNA Content (DAPI) using flow cytometry. Data plotted are mean percentage of G1 (green), S (purple), and G2/M (grey) phases. G1 percentage: 1st cycle siControl = 33%, 1st cycle siCdt1 A = 32.2%, 1st cycle siCdt1 B = 28.7%, proliferating siControl = 56.7%, proliferating siCdt1 A = 67.5%, proliferating siCdt1 B = 77.5%. Error bars are SD, n= minimum 3 biological replicates. Cell cycle phase percentages from DNA Content vs DNA Synthesis plots (see Fig. 4.2).

c. Immunoblot of total protein lysate of RPE1-hTert WT and p53 KO cells synchronized in G0 or released into the first cell cycle with siControl or siCdt1 (24 hours after release) as indicated.

d. Cell cycle phase distribution of cells treated as Fig. 4.8C defined by DNA synthesis (EdU) and DNA Content (DAPI) using flow cytometry. Data plotted are mean percentage of G1 (green), S (purple), and G2/M (grey) phases. Error bars are SD, n= minimum 3 biological replicates. G1 percentage 16.6% (siControl) 17.0% (siCdt1 A) 16.4% (siCdt1B). Cell cycle phase percentages from DNA Content vs DNA Synthesis plots (see Fig. 4.2).

distributions at the same time after G0 release (Fig. 4.8B 33% G1 vs, 16.6% G1 in Fig. 4.8D). The faster S phase entry by the p53 null cells could be due to both the impaired licensing checkpoint and the general loss of basal p21 protein (Fig. 4.8C) (Overton et al., 2014), among other possible p53-dependent effects), and each could promote faster CDK2 activation in the first cell cycle. The ability of actively proliferating cells to activate the licensing checkpoint to extend G1 during siCdt1 treatment combined with the observation that G0 cells do not extend G1 during the same treatment and enter S phase underlicensed strongly suggests cells in the first cell cycle after G0 have an impaired origin licensing checkpoint.

G0 cells re-entering the first cell cycle load MCM to license origins slowly.

We considered two explanations for underlicensing in the first S phase after G0: Cells may start loading MCM much later in the first G1 and, despite their longer G1, actually have less time to load than cells in the second cycle. Alternatively, cells in the first cycle may begin loading at the same time as in other cycles but they load MCM more slowly than cells in the second cycle. In both cases, the compromised origin licensing checkpoint is unable to extend G1 in response to the low MCM loading status resulting in an underlicensed first S phase. To distinguish between those explanations, we measured the nuclear accumulation of the Cell Division Cycle 6 (Cdc6) protein, an essential MCM loading protein. Cdc6 is degraded by the Anaphase promoting complex-Cdh1 (APC^{Cdh1}) in G1 phase, both in cells re-entering the cell cycle and in proliferating cells (Petersen et al., 2000; Mailand and Diffley, 2005). CDK2/Cyclin E1 phosphorylates Cdc6 in late G1 to protect it from APC^{Cdh1}, allowing Cdc6 protein to accumulate (Mailand and Diffley, 2005). Because Cdc6 is essential for MCM loading, Cdc6 accumulation is one of the rate-limiting steps for MCM loading in G1. The time for MCM loading ends when S phase starts and Cdc6 is exported from the nucleus to the cytoplasm (Petersen et al., 1999b). Therefore, the time Cdc6 is detectable in nuclei is one proxy for the length of available MCM loading time in G1 phase and is a marker for the functional border between

G0/early G1 when MCM is not loaded (or loaded very slowly) and late G1 when MCM can be loaded.

We used live cell imaging of fluorescently tagged protein biosensors to compare the length of available MCM loading time between the first and second cell cycles after G0. We imaged an RPE1 cell line stably expressing three fluorescent fusion proteins: 1) full length Cdc6 fused to mVenus (Segev et al., 2016), 2) Proliferating Cell Nuclear Antigen (PCNA) fused to mTurq2 to track cell nuclei and the borders of S phase (Burgess et al., 2012; Grant, Kedziora et al., 2018), and 3) a CDK kinase activity sensor fused to mCherry (Hahn et al., 2009). This kinase sensor was previously established to report CDK2 activity in G1 and early S phase and both CDK2 and Cdk1 activity in S and G2 phase; it is not a direct reporter of CDK4/6 activity (Spencer et al., 2013; Schwarz et al., 2018). CDK2 phosphorylates the reporter beginning in late G1 phase to induce export from the nucleus to the cytoplasm. The higher the ratio of cytoplasmic/nuclear signal, the higher the kinase activity. We imaged RPE1 cells expressing all three biosensors synchronized in G0 and released into the cell cycle for 72 hours, capturing an image every 10 minutes, starting 6.5 hours after release. PCNA-mTurq2 is present throughout the cell cycle and is punctate during S phase (Fig. 4.9A). Cdc6-mVenus is not present in G0 due to APC^{Cdh1}-mediated degradation. Nuclear Cdc6 first appeared in G1 and increased until S phase at which point it was lost from the nuclei and accumulated in the cytoplasm instead. After mitosis, Cdc6 was degraded in early G1 phase, then nuclear Cdc6 increased again later in G1 (Fig. 4.9A). The CDK reporter (mCherry) was nuclear in G0 (low CDK activity) and gradually became cytoplasmic beginning in late G1 (high CDK activity)(Fig. 4.9A). We tracked 50 cells through the first and second cell cycles after G0 release. Fig. 4.9B shows an individual cell trace for nuclear Cdc6 in which the first full cell cycle took nearly 35 hrs whereas the second cycle took only 20 hrs mostly from the difference in G1 length. The time Cdc6 first appeared in G1 is marked rise, and the time of maximum nuclear Cdc6 in G1 is marked peak (Fig. 4.9B). Cells began S phase as measured by the first appearance of PCNA foci about 20-30 minutes after

Figure 4.9

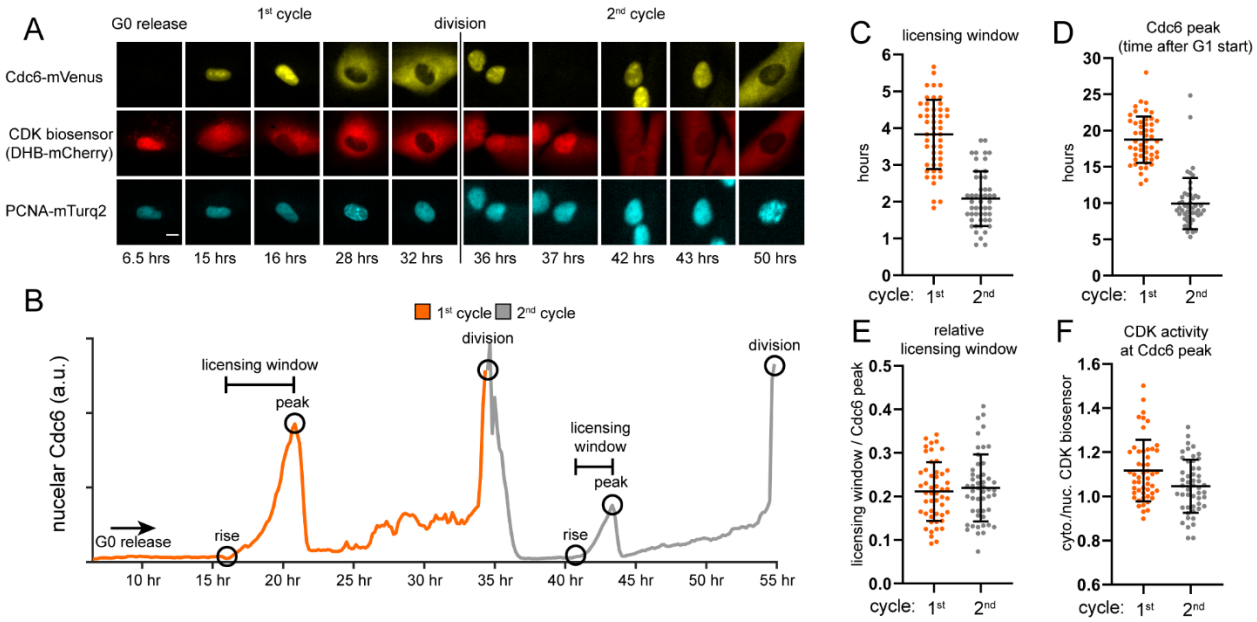

Figure 4.9. Live cell imaging of Cdc6 in first and second cycles after G0.
a. Micrograph of RPE1 cells expressing Cdc6-mVenus, DHB-mCherry, and PCNA mTurq2 synchronized in G0 by contact inhibition and released, imaging for 72 hours, images every 10 minutes, with representative time points shown, rounded to whole hours. Images were background subtracted and brightness/contrast adjusted. Representative cell shown out of n=50 cells, with two cell cycles for each cell. Scale bar is 10 um, applies to all images.
b. An individual cell trace of mean nuclear Cdc6 intensity imaged from Fig 4.9A. Orange part is first cell cycle, grey line is a daughter cell second cell cycle. Hours on X axis indicate hours from G0 release, trace starts at 6.5 hours after release. Images were every 10 minutes. Circles indicate relevant features. Rise is first appearance of nuclear Cdc6. Peak is maximum nuclear Cdc6 before cytoplasmic translocation. Licensing window is difference between peak and rise. Division is last image before cytokinesis.
c. Quantification of licensing window time (value of Cdc6 peak time minus Cdc6 rise time) for the 50 cells imaged in Fig. 4.9A, two cell cycles for each cell.
d. Values of Cdc6 peak time for the 50 cells imaged in Fig. 4.9A, two cell cycles for each cell.
e. Ratio of licensing window time divided by Cdc6 peak time for each cell imaged as in Fig. 4.9A, 50 cells total with both first and second cell cycle
f. Ratio of mean cytoplasmic DHB-mCherry divided by mean nuclear DHB-mCherry at the time of Cdc6 peak for the 50 cells imaged in Fig. 4.9A, two cell cycles for each cell.

peak (data not shown). The length of time Cdc6 was present in G1 is the time between nuclear Cdc6 rise and peak, and represents the licensing window for robust MCM loading in G1 (Fig. 4.9B). Cells re-entering the first cell cycle after G0 had about twice as long licensing window than cells in the second cell cycle, and about twice as much time in G1 overall (Cdc6 peak time) than cells in the second cell cycle (Fig. 4.9C, D).

We calculated the licensing window to the total G1 length by dividing the licensing window time by the Cdc6 peak time and found that the licensing window is the same proportion of G1 in both the first and second cell cycles (Fig. 4.9E). These data suggest that G1 during cell cycle re-entry is a stretched rather than delayed G1 compared to actively proliferating cells in the second cycle, and cells in the first cycle have a longer amount of available time with high Cdc6 than cells in the second cycle. Cells in the second G1 have more potential time to load MCM and yet enter S phase with less loaded MCM than cells in the second cycle. Taken together, these data suggest that cells in the first G1 after G0 load MCM slowly

Cells in both the first and second cell cycles also reached a similar CDK activity (cytoplasmic/nuclear ratio greater than 1) at the time of peak nuclear Cdc6 and S phase entry (Fig. 4.9F) close to previously-reported values of 0.84-1.0 in other untransformed cell lines (Spencer et al., 2013; Schwarz et al., 2018). In other words, the underlicensed first G1 cells achieved the same level of CDK activity in late G1 as normally-licensed second G1 cells. These equivalent CDK activity indicators further supports the notion that the licensing checkpoint does not delay CDK2 activation in the first G1.

Extending the first G1 after G0 substitutes for the impaired licensing checkpoint.

Cells re-entering the cell cycle from G0 license origins slowly and begin S phase before they are fully licensed. We hypothesized that artificially extending the first G1 phase could rescue the underlicensing of the first S phase by extending time for MCM loading. If successful, then cells would enter S phase with the high amount of loaded MCM typical of proliferating cells. We chose to extend G1 phase using nutlin-3a, a p53 stabilizing drug previously shown to

Figure 4.10

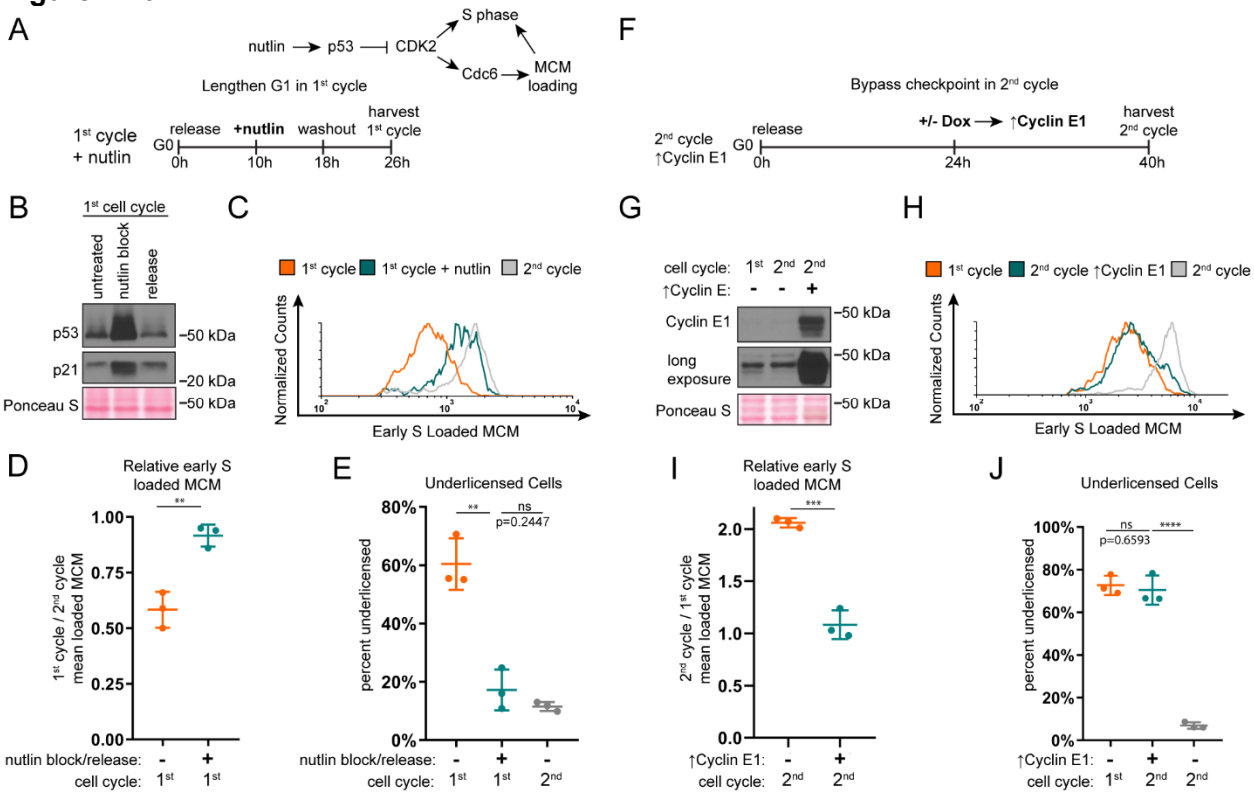

Figure 4.10. G1 length of first and second cell cycle effects amount of loaded MCM at S phase entry.

a. Model of experiment. RPE1 cells constitutively producing 5myc-Cdc6-mut (R56A, L59A, K81A, E82A, N83A, not targeted for degradation by APC^{CDH1}) were synchronized in G0 by contact inhibition, then released back into the first cell cycle. Cells were treated with 10 uM nutlin-3a 10 hours after release and then nutlin was washed out at 18 hours after release, harvesting cells 26 hours after release from G0. Untreated cells were harvested at 24 hours (first cell cycle) and 48 hours (second cell cycle) after release from G0.

b. Immunoblot of total protein lysate from cells treated as Fig. 4.10A. Untreated lane is cells at 18 hours after G0 without nutlin-3a. Nutlin block lane is cells with 10 uM nutlin-3a added at 10 hours and harvested at 18 hours after G0. Release lane is nutlin block, then washed to fresh media and harvested at 26 hours after G0.

c. Loaded MCM in early S phase determined by flow cytometric analysis from cells treated as Fig. 4.10A, measuring DNA Content (DAPI), Loaded MCM (anti-Mcm2), and DNA Synthesis (EdU). Histograms show early S loaded MCM. Orange line is first cell cycle, green line is first cell cycle with nutlin block and release, grey line is second cell cycle. See Fig. 4.11A for complete flow cytometry plots.

d. Comparison of early S phase DNA-loaded MCM from cells in Fig. 4.10C. Values plotted are the ratio of mean loaded MCM of first cell cycle with or without nutlin block and release divided by mean loaded MCM of second cell cycle. Horizontal bars indicate means, error bars mark standard deviation (SD), n=3 biological replicates. Samples were compared by unpaired, two tailed t test. p=0.0036**.

e. Percentage of underlicensed cells from Fig. 4.10C. Horizontal bars indicate means, error bars mark standard deviation (SD), n=3 biological replicates. Untreated and nutlin treated cells were compared by unpaired, two tailed t test. First cell cycle and nutlin block p=0.0027**, Nutlin block and second cell cycle p=0.2447 (ns).

f. Diagram of experiment. RPE1 cells containing integrated doxycycline inducible exogenous Cyclin E1 were synchronized in G0 by contact inhibition, then released into the cell cycle, adding 100 ng/mL of doxycycline at 24 hours after release to overproduce Cyclin E1 and shorten G1 of the second cell cycle, harvesting cells at 40 hours after release from G0. Untreated cells were harvested at 24 hours (first cell cycle) and 40 hours (second cell cycle) after release from G0.
g. Immunoblot for Cyclin E1 on total protein lysate from cells treated as Fig. 4.10F.
h. Loaded MCM in early S phase determined by flow cytometric analysis of cells treated as Fig. 4.10F, measuring DNA Content (DAPI), Loaded MCM (anti-Mcm2), and DNA Synthesis (EdU). Orange line is first cell cycle, green line is second cell cycle with ↑Cyclin E1 starting at 24 hours after G0 release, and grey line is second cell cycle. See Fig. 4.11G.
i. Comparison of early S phase loaded MCM per cell from Fig. 4.10F. Values plotted are the ratio mean loaded MCM of second cell cycle divided by mean loaded MCM of first cell cycle. Horizontal bars indicate means, error bars mark standard deviation (SD), n=3 biological replicates. Samples were compared by unpaired, two tailed t test. p=0.0036**
j. Percentage of underlicensed cells from Fig. 4.10F. Horizontal bars indicate means, error bars mark standard deviation (SD), n=3 biological replicates. Samples were compared by unpaired, two tailed t test. first cell cycle vs second cell cycle with ↑Cyclin E1 p=0.6593 (ns), second cell cycle with ↑Cyclin E1 vs second cell cycle untreated p<0.001****.

lengthen G1 (Tovar et al., 2006). We treated cells re-entering the first G1 phase with nutlin-3a beginning in mid-G1 for 8 hrs, then washed off the drug to permit passage into S phase and measured the amount of loaded MCM at S phase entry (Fig. 4.10A, B). Nutlin-3a stabilized p53, causing p21 protein accumulation. This effect is known to inhibit CDK2 kinase activity and delay S phase entry (Giono and Manfredi, 2007). An unwanted secondary effect of low CDK2 activity for our purposes is failure to protect Cdc6 in late G1 phase, which would prevent the accumulation of that essential MCM loading protein (Petersen et al., 2000; Mailand and Diffley, 2005). To allow MCM loading during the nutlin-induced G1 arrest, we constitutively expressed a mutant form of Cdc6 that does not require CDK2 activity for stability (Matson et al., 2017). We then compared licensing in these treated cells to untreated cells from the first and second cell cycles (Fig. 4.10C, Fig. 4.11A). RPE1 released from G0 typically begin to enter S phase about 16 hours after G0 release, while the nutlin 3a block and release cells begin to enter S phase about 24 hours after G0 release. Strikingly, transiently extending the first G1 phase by several hours almost fully rescued licensing in the first cell cycle to the same high level as in the second cell cycle (compare green and grey lines, Fig. 4.10C, and fold change Fig. 4.10D) and decreased the percentage of underlicensed cells to the same low level as the second cell cycle (Fig. 4.10E). Unlike the effects of stable Cdc6 on the rate of MCM loading in proliferating cells (Matson et al., 2017), neither stable Cdc6 alone or in combination with Cdt1 overproduction increased the rate of MCM loading in the first G1 phase (Fig. 4.11B and 4.11C). These genetic changes also had little-to-no effect on underlicensing in the first S phase (Fig. 4.11D-F). Therefore, the improved licensing by early S phase from nutlin-induced G1 extension is due to the increased time for MCM loading, rather than improving MCM loading itself.

Finally, we predicted that since the second cell cycle has a robust origin licensing checkpoint, bypassing the checkpoint and artificially shortening the second G1 would induce a phenotype similar to the underlicensed first cell cycle. To test this prediction, we overproduced Cyclin E1 as cells approached the second cell cycle to shorten the second G1 phase and

Figure 4.11

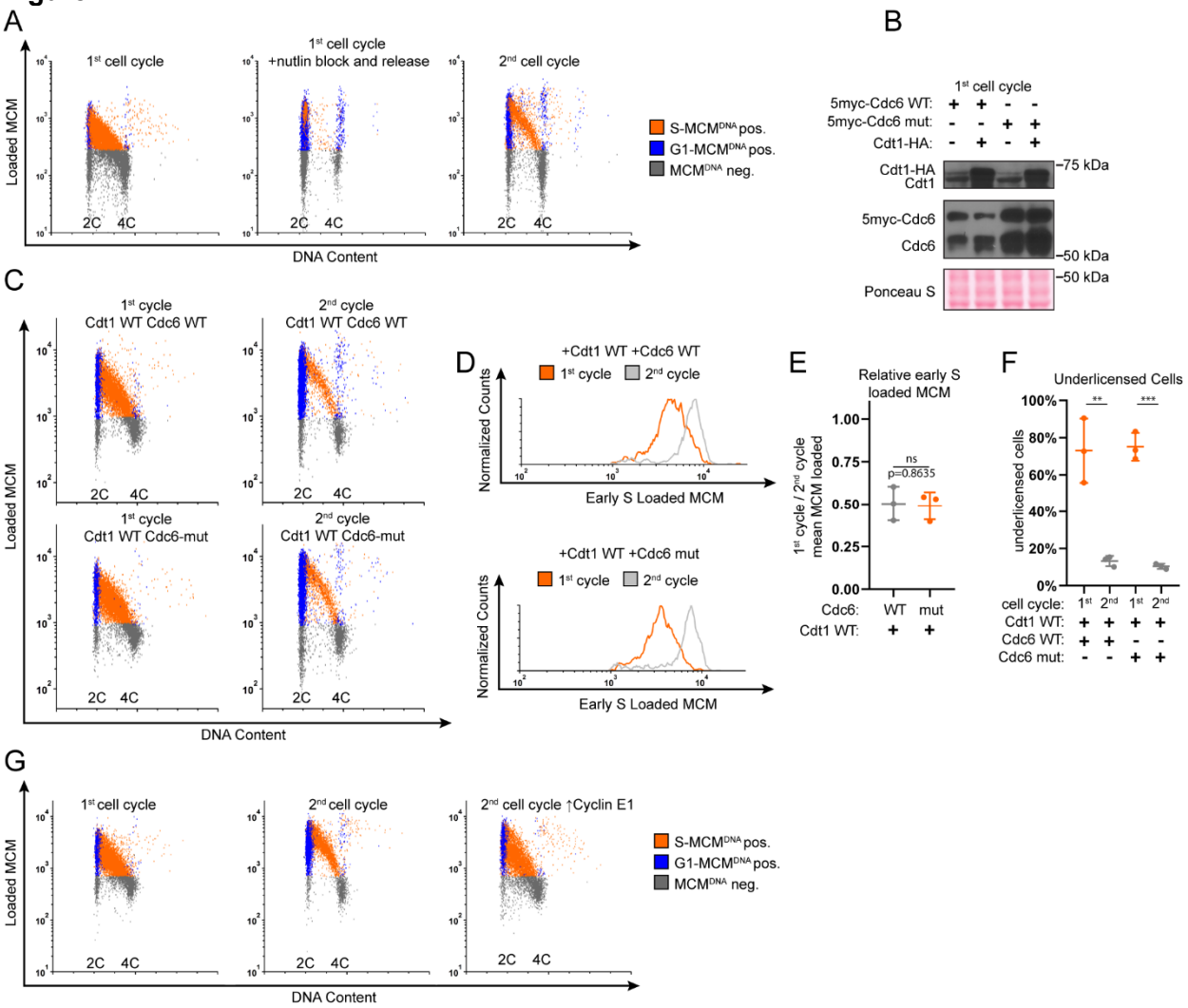

Figure 4.11 Overproduction of Cdt1 and a stable Cdc6 mutant do not rescue underlicensing in the first cell cycle after G0.

a. Flow cytometry of chromatin-bound protein from cells shown in Fig. 7C, measuring DNA Content (DAPI), Loaded MCM (anti-Mcm2) and DNA Synthesis (EdU). 1st cell cycle is 24 hrs after G0 release, 1st cycle with nutlin block and release are cells treated with 10 μM nutlin-3a from 10-18 hours and released to 26 hours after G0. 2nd cell cycle is 48 hours release from G0. Orange cells are S phase MCM^{DNA} positive, blue cells are G1 phase MCM^{DNA} positive, grey cells are MCM^{DNA} negative.

b. Immunoblot for Cdc6 and Cdt1 on total protein lysate from RPE1 cells constitutively producing either 5myc-Cdc6 WT or 5myc-Cdc6-mut (a mutant of Cdc6 that is not targeted for degradation by APC^{Cdh1}: R56A, L59A, K81A, E82A, N83A) and a doxycycline inducible Cdt1-HA. RPE1 cells were synchronized in G0 by contact inhibition, treated with 100 ng/mL doxycycline for 4 hours before re-plating cells to release into the first cell cycle, harvesting cells 24 hours after release.

c. Flow cytometry of chromatin-bound protein on cells treated as Fig. S4B, harvested 24 hours (first cell cycle) and 48 hours (second cell cycle) after G0 release, measuring DNA Content (DAPI), Loaded MCM (anti-Mcm2), and DNA Synthesis (EdU). Orange cells are S phase MCM^{DNA} positive, blue cells are G1 phase MCM^{DNA} positive, grey cells are MCM^{DNA} negative.

d. Loaded MCM of early S phase from Fig. S4C. Orange lines are cells from first cell cycle, grey lines are cells from second cell cyclist. Top panel is RPE1 cells producing Cdt1-HA WT and 5myc-Cdc6 WT, bottom panel is RPE1 cells producing Cdt1-HA WT, 5myc-Cdc6-mut.
e. Comparison of early S phase DNA-loaded MCM per cell from Fig. S4D. Values plotted are the ratio of mean loaded MCM of first cell cycle divided by mean loaded MCM of second cell cycle. Horizontal bars indicate means, error bars mark standard deviation (SD), n=3 biological replicates. First and second cell cycles compared by unpaired, two tailed t test. p=0.8635 (ns).
f. Percentage of underlicensed cells from early S phase cells in Fig. S4D. Horizontal bars indicate means, error bars mark standard deviation (SD), n=3 biological replicates. First and second cell cycles compared by unpaired, two tailed t test. Cdc6 WT p=0.0041** Cdc6 mut p=0.0001***.
g. Flow cytometry of chromatin-bound protein from cells shown in Fig. 7H, measuring DNA Content (DAPI), Loaded MCM (anti-Mcm2) and DNA Synthesis (EdU). Orange cells are S phase MCM^{DNA} positive, blue cells are G1 phase MCM^{DNA} positive, grey cells are MCM^{DNA} negative.

bypass the checkpoint. We then compared licensing in the second S phase in these Cyclin E1-overproducing cells to both control second S phase and first S phase cells (Fig. 4.10F, 4.10G, and Fig. 4.11G). The second cell cycle with a bypassed licensing checkpoint strongly resembled the first cell cycle (compare green and orange lines, Fig. 4.10H, fold change in Fig. 4.10I, and percentage of underlicensed cells in Fig. 4.10J). Taken together, we conclude that cells re-entering the cell cycle from G0 are routinely underlicensed, but that the second and subsequent cell cycles are fully licensed because of a robust p53-dependent checkpoint that ultimately controls the timing of Cyclin E/CDK2-mediated S phase entry.

Discussion

The origin licensing checkpoint protects cells from premature S phase entry that could lead to genome instability (Fig. 4.12). This checkpoint couples the activity of CDK to the status of MCM loading such that the G1 CDKs are not activated while MCM loading is still low. Cyclin E1 overproduction can bypass the checkpoint-induced delay and induce premature S phase entry while cells are still underlicensed (Fig. 4.5) (Ekholm-Reed et al., 2004; Matson et al., 2017). Moreover, p53 loss clearly impairs the normal coupling of MCM loading and S phase entry whereas p53 activation lengthens G1 to give enough time to complete licensing (Fig. 4.7, 4.8, and 4.10). These observations fit Hartwell and Weinert's classic definition for a cell cycle checkpoint (Hartwell and Weinert, 1989). A checkpoint enforces the dependence of one event on a previous event, but the dependency can be bypassed by mutation to occur out of order. The ability of mutations to induce inappropriate cell cycle progression indicates that in wild-type cells, progression could have occurred but was instead restrained by the checkpoint. This relationship is in contrast to a simple inability to progress. Of relevance to the origin licensing checkpoint, we induced S phase entry when the amount of loaded MCM was low, but not completely absent, since RNAi-mediated depletion of MCM loading factors does not prevent all MCM loading. If we could have entirely prevented MCM loading, then of course, there would

Figure 4.12

A

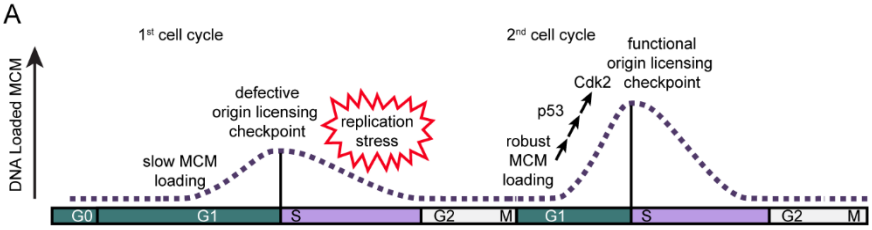

Figure 4.12 Model of MCM loading in first and second cycles after G0

a. Cells in the first cell cycle have slow MCM loading and a defective origin licensing checkpoint, and enter S phase underlicensed. The first S phase is hypersensitive to replication stress. Cells in the second cycle have a functional origin licensing checkpoint and load MCM normally. The checkpoint is p53-dependent and robust MCM loading allows CDK2 activation.

have been no DNA synthesis even in p53 null or Cyclin E-overproducing cells because MCM is an essential component of the replicative helicase.

Many questions remain about the origin licensing checkpoint itself. How do cells monitor the status of origin licensing, what conditions satisfy the checkpoint, and how is licensing status coupled to the activation of CDKs? The mere existence of the checkpoint was an unresolved question until relatively recently in large part because it appears to be restricted to untransformed metazoan cells. This restriction poses technical challenges for probing the molecular nature of the coupling because untransformed cells are more difficult to synchronize and manipulate than tumor-derived cells or yeast cells. Our results indicate that a 50% reduction in the amount of loaded MCM by the time of S phase entry sensitizes human cells to exogenous replication stress; this level is similar to that reported for checkpoint-deficient U2OS cells (Ge et al., 2007). Some stem cell types have a greater amount of loaded MCM at S phase entry than their differentiated counterparts, suggesting that the licensing threshold may vary by cell type (Ge et al., 2015; Carroll et al., 2018). The fact that p53 status correlates with licensing checkpoint proficiency gives clues that a p53-dependent process, perhaps one or more p53-regulated genes, are involved in efficient coupling. The discovery here that cell cycle re-entry induces natural underlicensing also suggests future screens for checkpoint mediators. Our analysis of origin licensing status at the G1/S transition using analytical flow cytometry provides a promising opportunity to dissect this pathway in the future.

We note that licensing checkpoint activity is only readily detected in cells with particularly slow MCM loading. In previous studies, MCM loading was artificially slowed to test for checkpoint proficiency in various genetic backgrounds (Shreeram et al., 2002; Liu et al., 2009; Nevis et al., 2009). Under normal growth conditions however both checkpoint-proficient and checkpoint-impaired cell lines enter S phase with normal high levels of MCM loading. This behavior suggests that MCM loading is usually fast enough to achieve high levels of loaded MCM in advance of the other rate-limiting molecular events necessary to trigger CDK2

activation and S phase entry. It is only slow-loading cells that are visibly affected by the checkpoint. In that sense, the origin licensing checkpoint resembles other cell cycle checkpoints that operate in all cell cycles. For example, the contribution of the mitotic spindle assembly checkpoint is most obvious when attachments are severely compromised (Lara-Gonzalez et al., 2012). The effect of the spindle assembly checkpoint on the rate of unperturbed mitotic progression is relatively minor except in individual cells that fail to form kinetochore-microtubule attachments on time (Lara-Gonzalez et al., 2012). Similarly, we did detect a modest increase in the number of underlicensed S phase cells in otherwise unperturbed proliferating p53 null cells compared to p53 WT cells (Fig. 4.7). We infer that these individual cells loaded MCM slowly, but could not effectively delay S phase entry.

We were surprised to find that the first G1 phase after cell cycle re-entry from quiescence (G0) is routinely followed by an underlicensed S phase in multiple cell lines. To our knowledge, cell cycle re-entry from G0 is the first known naturally-occurring normal underlicensed cell cycle; previous investigations required siRNA or mutations to artificially force underlicensing (McIntosh and Blow, 2012). Clearly the extra time in G1 after G0 was not enough to lead to full licensing. Our investigation leads us to conclude that the routine underlicensing in cells re-entering the cycle is the consequence of a combination of slow MCM loading plus an ineffective licensing checkpoint. If MCM loading were fast enough in the first cell cycle, then their checkpoint deficiency wouldn't matter and they would not be underlicensed in the first S phase. Although it is not yet technically possible to monitor MCM loading in real time in individual cells, we used the transition from Cdc6-negative to Cdc6-positive as a proxy for the maximum amount of time available for MCM loading (Fig. 4.9). Since cells in the first G1 phase had more time with abundant nuclear Cdc6 than cells in the second G1 phase, yet began S phase with less MCM loaded, we are confident in our assertion that MCM loading is particularly slow in the first G1 phase. If we presume that the nuclear Cdc6 levels correlate with Cdc6 activity, then some other aspect of the MCM loading process must be slower in the first G1.

It is unclear why cells re-entering G0 load MCM slowly. The difference may be caused by one or more of the fundamental differences in G1 regulation between cell cycle re-entry and active proliferation. These differences include the status of Rb phosphorylation which is monophosphorylated in proliferating G1 cells, but unphosphorylated in G0 (Narasimha, Kaulich, Shapiro et al., 2014). Rb-dependent genes include those whose products are directly involved in MCM loading, and these genes are subject to unique transcriptional repression by the DREAM complex in G0 that must be reversed at cell cycle re-entry (Litovchick et al., 2007). Proliferating cells also load MCM both before and after Rb is removed from chromatin, but cells re-entering G1 from G0 only load MCM after Rb is removed from chromatin (Håland et al., 2015). CDK2 is constitutively nuclear in proliferating cells, but is cytoplasmic in G0 (Brown et al., 2004; Dietrich et al., 1997; Nevis et al., 2009). Of additional particular relevance is the indication of a kinase-independent function of Cyclin E1 to promote loading that is only required in cells re-entering the cycle form G0 (Geng et al., 2003, 2007). These differences illustrate that cell cycle re-entry into G1 from G0 poses additional challenges and requirements not encountered during G1 in actively proliferating cells. It is striking however that both the checkpoint defect and slow MCM loading are normal just one cell cycle later after mitosis.

Previous analysis by Daigh et al. indicated that cells released from G0 had increased endogenous replication stress in the first S phase compared to actively proliferating cells. This stress was detected as mid-S phase fluctuations in CDK activity and γH2AX staining that depended on the status of the replication stress response signaling pathway (Daigh et al., 2018). Our findings here suggests a molecular mechanism by which that replication stress was generated. We propose that the underlicensed S phase after the first G1 has higher endogenous replication stress because fewer dormant origins are available. While we did not detect frank DNA damage markers in the absence of exogenous replication stress by our methods, we presume that endogenous stress was generated because these cells were uniquely sensitive to low dose gemcitabine. This hypersensitivity is a hallmark of cells that enter

S phase while underlicensed (Woodward et al., 2006; Zimmerman et al., 2013). The increased endogenous replication stress from too few licensed origins promotes genome instability from a higher frequency of stalled and un-rescued replication forks

How frequently do cells experience this naturally-underlicensed cell cycle *in vivo*? Cell cycle re-entry from quiescence is common in tissues that naturally turn over cell populations (Sosa et al., 2014; Sagot and Laporte, 2019; Wells et al., 2013). One might imagine however, that one risky cell cycle is a small contributor to overall genome instability. On the other hand, even in actively proliferating cultures, recent studies have detected populations of cells that appear to spontaneously and transiently exit to a quiescence-like state (Spencer et al., 2013; Overton et al., 2014; Arora et al., 2017; Barr et al., 2017). Such transient cell cycle exit may be even more common in tissues compared than in cell culture conditions that have been optimized for maximal uninterrupted growth. Whether or not that transient quiescence also causes underlicensing is not yet known.

Quiescent hematopoietic stem cells re-enter the cell cycle in response to stresses such as viral infection and then return to quiescence (Cheung and Rando, 2013). Interestingly, hematopoietic stem cells acquire DNA damage in the first cycle after G0, accumulate DNA damage over time in older stem cells, and become depleted as they age from repeated cell cycle re-entry (Beerman et al., 2014; Walter et al., 2015). Additionally, quiescent human T cells re-enter the first S phase even when treated with siRNA to substantially reduce the amount of loaded MCM to ~5-10% of their normal loaded amount (Orr et al., 2010). Taken together, these data suggest that at least some quiescent cells *in vivo* lack a licensing checkpoint in the first cycle, although it is unknown if the first cell cycle is naturally underlicensed compared to the second cycle *in vivo*. Old hematopoietic stem cells experience more replication stress in the first S phase after G0 compared to young stem cells, possibly because they express less MCM protein. In that regard, a defective licensing checkpoint would be particularly toxic to old quiescent cells re-entering G1 because they may enter S phase with even less loaded MCM

than young cells (Flach et al., 2014). These *in vivo* studies are consistent with our observation that artificially inducing repeated rounds of quiescence and cell cycle re-entry enhanced replication stress sensitivity (Fig. 4.4). We suggest that over many rounds of quiescence and re-entry, incremental DNA damage accrues from unresolved replication stress or incomplete replication that may pass through mitosis into the next cell generation. The ability of unresolved replication stress to carry forward into subsequent cell cycles was recently established both by artificially inducing underlicensing and by monitoring spontaneous replication stress passing from mother to daughter cells (Moreno et al., 2016; Yang et al., 2017; Arora et al., 2017; Ahuja et al., 2016). Repeated rounds of underlicensed cell cycle re-entry could contribute to the genome damage that drives both aging and oncogenesis. Thus, the most important consequences of entering a high-risk underlicensed cell cycle may primarily appear over an organism's lifetime.

Materials and Methods

Cell culture and synchronization

RPE1-hTERT cells, 293T and NHF1-hTERT cells (ATCC) were grown in Dulbecco's modified Eagle's medium (DMEM) (Sigma Aldrich) with 10% Fetal Bovine Serum (FBS) (Seradigm) and 2 mM L-glutamine (Gibco) at 37°C with 5% CO_2. Wi38 cells (ATCC) were grown in Minimum Essential Medium (MEM) with 10% FBS (Seradigm), 2 mM L-glutamine (Gibco) and Minimum Essential Medium non-essential amino acids (NEAA) (Gibco) at 37°C with 5% CO_2. Cells were passaged every three days with trypsin (Sigma Aldrich) and not allowed to reach confluency.

To synchronize RPE1 cells in G0 by contact inhibition, cells were grown to 100% confluency, washed with PBS, and incubated in DMEM with 10% FBS and 2 mM L-glutamine for 48 hours. To release cells into the first or second cell cycles, G0 cells were re-stimulated by passaging 1:10 for the first cycle, harvesting 24 hours later or 1:20 for the second cycle, harvesting 48 hours later, in DMEM with 10% FBS and 2 mM L-glutamine. To synchronize

RPE1 cells in G0 by serum starvation, cells were plated sub-confluent, washed 3 times with PBS, and starved in DMEM with 0% FBS and 2 mM L-glutamine for 72 hours. To release cells into the first or second cell cycles, cells were washed with PBS and re-stimulated by washing once with PBS and adding DMEM with 10% FBS and 2mM L-glutamine for 24 hours (first cycle) or 48 hours (second cycle). To synchronize NHF1-hTERT cells in G0, cells were grown to 100% confluency, washed with PBS, and incubated in DMEM with 0.1% FBS and 2 mM L-glutamine for 72 hours. To release cells into the first or second cell cycles, G0 cells were re-stimulated by passaging 1:4 for first cycle, harvesting 24 hours later or 1:8 for second cycle, harvesting 48 hours later, in DMEM with 10% FBS and 2 mM L-glutamine. To synchronize Wi38 cells in G0, cells were grown to 100% confluency, washed with PBS, and incubated in MEM with 0.1% FBS, 2 mM L-glutamine, and NEAA for 72 hours. To release cells into the first or second cell cycles, G0 cells were re-stimulated by passaging 1:4 for first cycle, harvesting 24 hours later or 1:8 for second cycle, harvesting 48 hours later, in in MEM with 10% FBS, 2 mM L-glutamine, and NEAA.

To synchronize RPE1 in 3 repeated G0s, cells were synchronized in G0 by contact inhibition (above), re-stimulated into the cell cycle by passaging 1:6 in DMEM with 10% FBS and 2 mM L-glutamine, and grown to 100% confluency within 48-72 hours to start the second G0 by contact inhibition for 48 hours. Cells were re-stimulated as before and grown to 100% confluency to start the 3rd G0 for 48 hours. To release cells for the experiment, G0 cells were re-stimulated by passaging 1:10 in DMEM with 10% FBS and 2 mM L-glutamine, harvesting the first cell cycle at 24 hours after re-stimulation.

DNA Cloning and cell lines

The RPE1 CRISPR p53 KO was a gift of Dr. Prasad Jallepalli and described previously (Rodriguez-Rodriguez et al., 2018). The RPE1 cells with doxycycline inducible Cyclin E1 and the RPE1 cells with doxycycline inducible Cdt1 and stable Cdc6 WT or Cdc6-mut were described previously (Matson et al., 2017). The pLenti-PGK hygro PCNA-mTurq2 was

described previously (Grant et al., 2018). The CSII-EF zeo DHB-mCherry CDK activity reporter was a gift Dr. Sabrina Spencer. The CSII-EF zeo Cdc6-mVenus was a gift from Dr. Michael Brandeis. Each reporter is under control of a constitutive heterologous promoter.

To make the RPE1 line containing PCNA-mTurq2, Cdc6-mVenus, and DHB-mCherry, the plasmids were transfected into 293T with pCI-GPZ or ΔNRF and VSVG virus packaging plasmids with 50 ug/mL Polyethylenimine (Aldrich Chemistry). Viral supernatants were transduced onto RPE1 cells with 8 ug/mL Polybrene (Millipore).

A clonal cell line was picked based on fluorescence of all 3 biosensors.

siRNA transfections and drug treatment

siRNA concentration and sequences:

siControl, (siLuciferase) 100 nM (synthesized by Life Technologies)

5′-CUUACGCUGAGUACUUCGA-3′

siCdt1 A, mixture of 4 sequences, 25 nM each. (siGENOME CDT1 siRNA, Dharmacon)

5’-CCAAGGAGGCACAGAAGCA-3’

5’-GCUUCAACGUGGAUGAAGU-3’

5’-UCUCCGGGCCAGAAGAUAA-3’

5’-GGACAUGAUGCGUAGGCGU-3’

siCdt1 B, 50 nM (synthesized by Life Technologies)

5'-CCUACGUCAAGCUGGACAATT-3'

For siRNA transfections, siRNA was spotted into plates with DharmaFECT 4 transfection reagent (Dharmacon) and Opti-MEM (Gibco), incubating for 20 minutes before adding cells in DMEM with 10% FBS and 2 mM L-glutamine (final concentrations), harvesting cells 72 hours later for proliferating experiments, and 24 hours later for G0 release, as described above. To overproduce Cyclin E1 or Cdt1-HA, 100 ng/mL of doxycycline (CalBiochem) was added at times indicated in the figure legend. To block and release cells with nutlin-3a (Sigma Aldrich), RPE1 were synchronized in G0 by contact inhibition, released into the first cell cycle, adding 10 uM

nutlin-3a 10 hours after release, washing off nutlin-3a 18 hours after release by washing 3 times with PBS and adding back DMEM with 10% FBS and 2 mM L-glutamine. To treat cells with gemcitabine (Sigma Aldrich) in Fig. 4.3, cells were synchronized in G0 by contact inhibition, released into the first cycle and treated with 50 nM gemcitabine from 22-24 hours or released into the second cycle and treated with 50 nM gemcitabine from 44-46 hours. To treat cells with gemcitabine in Fig. 4.4, cells were synchronized in one or three G0 (above), adding 5 nM gemcitabine at time of re-stimulation from 0-24 hours.

Total protein lysate and chromatin fractionation

To prepare total protein lysate for immunoblot, cells were harvested with trypsin and frozen in dry ice, then lysed in cold cytoskeletal buffer (CSK) (10 mM Pipes pH 7.0, 300 mM sucrose, 100 mM NaCl, 3 mM $MgCl_2$ hexahydrate) with 0.5% triton x-100 (Sigma Aldrich) and protease and phosphatase inhibitors (0.1 mM Pefabloc, 1 µg/mL pepstatin A, 1 µg/mL leupeptin, 1 µg/mL aprotinin, 10 µg/mL phosvitin, 1 mM β-glycerol phosphate, 1 mM sodium orthovanadate) on ice for 15 minutes. Lysate was centrifuged at 13,000 x g at 4°C for 10 minutes, and a Bradford Assay (Biorad) was done on the supernatant to load equal amounts of protein per sample.

To prepare chromatin fractions for immunoblot, cells were harvested with trypsin and frozen in dry ice, then lysed in cold CSK with 0.5% triton x-100, 1 mM ATP, 5 mM $CaCl_2$ and protease and phosphatase inhibitors (complete CSK) on ice for 20 minutes. Then a Bradford assay for equal loading was done on the lysate, a small aliquot removed from each sample as total lysate, and complete CSK was added to each sample, mixed, and centrifuged for 5 min, 1,000 x g. The supernatant was removed, pellet was washed again with complete CSK, incubated for 10 minutes on ice, and then centrifuged for 5 min, 1,000 x g. The supernatant was removed, and DNA loaded proteins were released by incubation with S7 nuclease (Sigma Aldrich) in complete CSK at room temperature (RT) for 10 minutes. Samples were centrifuged again, keeping the supernatant as the chromatin fraction.

Immunoblotting

Samples were diluted with loading buffer to final concentration: 1% SDS, 2.5% 2-mercaptoethanol, 0.1% bromophenol blue, 50 mM Tris pH 6.8, 10% glycerol then boiled. Samples were run on SDS-PAGE gels, then transferred to nitrocellulose (GE Healthcare) or polyvinylidene difluoride membranes (Thermo Fisher). After transferring, samples were blocked in 5% milk in tris buffered saline with 0.1% tween 20 (TBST), then incubated overnight at 4°C in primary antibody with 2.5% milk in TBST. Then membranes were washed with TBST, incubated in horseradish peroxidase conjugated (HRP) secondary antibody for 1 hour at RT, washed with TBST, and imaged with ECL Prime (Amersham) on autoradiography film (Denville). Antibodies were: Mcm2 (BD Biosciences Cat#610700, 1:10,000), Cyclin E1 (Cell Signaling Technology #4129S, 1:2,000), p53 (Santa Cruz Biotechnology, sc-126, 1:2,000), p21 (Cell Signaling Technology, #2947S, 1:6,000) Cdc6 (Santa Cruz Biotechnology, sc-9964, 1:2,000), Cdt1 (Santa Cruz Biotechnology, sc-365305, 1:3,000), Donkey-anti-Mouse-HRP (Jackson ImmunoResearch, 1:10,000) Donkey-anti-Rabbit-HRP (Jackson ImmunoResearch, 1:10,000). Membranes were stained with Ponceau S (Sigma Aldrich) to determine equal protein loading.

Flow cytometry

Cells stained with EdU were incubated with 10 uM EdU for 30 minutes before harvesting, except in Fig 4.2D, when cells were incubated with 1 uM EdU from re-stimulation to harvesting. Cells were harvested with trypsin to measure DNA loaded proteins by flow cytometry. Cells were washed once with PBS, centrifuged at 2,000 x g for 3 minutes, then supernatant was aspirated and pellets lysed on ice in cold CSK with 0.5% triton X-100 and protease and phosphatase inhibitors for 5 minutes. After incubation, 1% Bovine serum albumin (Fisher) in PBS (B-PBS) was added to each sample, mixed, and centrifuged at 2,000 x g for 3 minutes. Supernatant was aspirated, pellets were fixed with 4% paraformaldehyde (Electron Microscopy Sciences) in PBS for 15 minutes at RT. Then B-PBS was added, mixed, and

samples centrifuged (2,000 x g for 7 minutes, all following steps). Supernatant was aspirated, B-PBS was added, and samples stored at 4°C before labeling.

EdU labeling was done before antibody staining. Cells were centrifuged, supernatant aspirated, and incubated in PBS with 1 mM $CuSO_4$, 100 mM ascorbic acid (fresh), 1 uM Alexa Flour-647-azide (Life Technologies) for 30 minutes, RT in the dark. Then B-PBS with 0.5% NP-40 (United States Biochemical) was added, mixed, and centrifuged. For antibody staining, supernatant was aspirated, cells incubated in primary antibody: anti-Mcm2 (1:200, BD Biosciences, Cat#610700), anti-γH2AX (1:200, Cell Signaling Technologies, #9718S) in B-PBS with 0.5% NP-40 for 1 hour at 37°C in the dark. Next, B-PBS with 0.5% NP-40 was added, mixed, and samples centrifuged. Supernatant was aspirated, cells incubated in secondary antibody: Donkey-anti-Mouse-Alexa Flour 488 (1:1,000, Jackson ImmunoResearch, for Mcm2), Donkey-anti-Rabbit-Alexa Flour 647 (1:1,000, Jackson ImmunoResearch, for γH2AX) in B-PBS with 0.5% NP-40 for 1 hour at 37°C in the dark. Then B-PBS with 0.5% NP-40 was added, mixed, and samples centrifuged. Finally, supernatant was aspirated, cells were incubated in 1 ug/mL DAPI (Sigma Aldrich) and 100 ng/mL RNAse A (Sigma Aldrich) in B-PBS with 0.5% NP-40 overnight at 4°C in the dark. For negative control samples used to draw positive/negative gates, cells were not incubated with EdU but were labeled with Alexa Flour-647-azide, and were not incubated with primary antibody but were labeled with secondary antibody and DAPI.

Data were acquired primarily on an Attune NxT flow cytometer (Thermo Fisher), with some data acquired on a CyAn ADP flow cytometer (Beckman Coulter). Data was analyzed using FCS Express 6 (De Novo Software). Gates are shown in Fig. 4.2. Gate to isolate cells from debris was from Forward Scatter-Area vs Side Scatter Area. Gate to isolate singlets from doublets was from DAPI Area vs DAPI height (Parent gate: cells). Gate to isolate cell cycle phases was from DAPI Area (DNA Content) vs 647-Area (DNA Synthesis, EdU) (Parent gate: singlets). Color gates to isolate S-MCM^{DNA} positive, G1-MCM^{DNA} positive and MCM^{DNA} negative were on 647 Area (DNA Synthesis, EdU) vs 488 Area (Loaded MCM), using a negative control

sample to mark positive cells (Parent gate: singlets). Early S phase gate was on DAPI Area (DNA Content) vs 488-Area (Loaded MCM), gating cells with 2C DNA content, S-MCM^{DNA} positive in early S phase (Parent gate: S-MCM^{DNA} positive). Mid S phase gate was on DAPI Area (DNA Content) vs 647-Area (γH2AX), cells between 2C and 4C DNA Content (Parent gate: singlets). Replication stress induced γH2AX was gated as cells equal to or greater than the top 5%-6% of γH2AX signal from untreated cells (Parent gate: Mid S). Each flow cytometry plot typically has 9,000-11,000 total single cells.

Y axis is cell counts, normalized to peak value of second cell cycle.

Doubling time

Cells were plated with siRNA and counted 48 hours or 72 hours later after dissociating with trypsin using a Luna II automated cell counter (Logos Biosystems). Each treatment was done with 3 biological replicates and each dish in the replicate was counted twice as technical replicates. Doubling time was calculated using Prism 8 (GraphPad) regression analysis: exponential growth equation. Doubling times from the 3 biological replicates were averaged, and then the average doubling time was multiplied by the cell cycle phase percentages to obtain cell cycle phase hours.

Live cell imaging

Cells were plated for live cell imaging with G0 by contact inhibition and re-stimulation in Flourobrite DMEM (Gibco) with 10% FBS and 2 mM L-glutamine in #1.5 glass bottom plates (Cellvis) in a humidified enclosure at 37° C with 5% CO_2. Movie started 6.5 hours after plating, cells were imaged for 72 hours with images every 10 minutes. Cells were imaged on a Nikon Ti Eclipse inverted microscope with a 20x (NA 0.75) Apochromat dry objective lens with the Nikon Perfect Focus System. The camera was an Ando Zyla 4.2 sCMOS detector with 12 bit resolution, filters were from Chroma: (excitation; beam splitter; emission filter) CFP - 436/20 nm; 455 nm; 480/40 nm, YFP - 500/20 nm; 515 nm; 535/30 nm; and mCherry - 560/40 nm; 585 nm; 630/75 nm. Images were collected with Nikon NIS-Elements AR software.

Images were analyzed with Fiji version 1.51n, ImageJ. Briefly, images were background subtracted and tracked with custom ImageJ scrips based on the PCNA signal, and nuclear signal quantified in a region of interest as described previously (Grant, Kedziora et al., 2018). Cdc6 traces of mean nuclear intensity were scored as follows: Cdc6 peak time: frame with highest nuclear Cdc6 intensity before the sharp drop in intensity indicating export to the cytoplasm. Cdc6 rise time: frame with Cdc6 nuclear intensity 2 standard deviations greater than the lowest Cdc6 nuclear intensity before Cdc6 peak time. Licensing window time: Cdc6 peak time minus Cdc6 rise time. Relative licensing window time: Licensing window time divided by Cdc6 peak time.

For DHB cytoplasmic measurement, fluorescence signal of the cytoplasm was approximated by measuring signal within a ring-shaped region (5 px wide) around the nucleus. The ratio between the cytoplasm and the nucleus was calculated using mean signals of the ring-shaped cytoplasmic region and the full nuclear region.

CHAPTER 5: CONCLUSIONS AND FUTURE DIRECTIONS

In this work, we demonstrated the significance of both the rate of MCM loading and the amount of loaded MCM at S phase entry. Pluripotent stem cells use a fast MCM loading rate during their short G1 phase, while differentiated cells use a slow MCM loading rate during their long G1 phase. A higher amount of Cdt1 protein contributes to the fast loading of the MCM complex in stem cells. Both Cdt1 protein levels and MCM loading rate decrease during early stem cell differentiation to all lineages. The fast MCM loading rate maintains the pluripotency of stem cells, as prematurely decreasing the MCM loading rate in stem cells promotes their differentiation. The stem cells and differentiated cells have different loading rates but reach the same amount of loaded MCM at S phase entry. We showed that the origin licensing checkpoint enforces the amount of loaded MCM at S phase entry in actively proliferating cells. The licensing checkpoint is a true cell cycle checkpoint and not a requirement for S phase entry, because it can be bypassed by Cyclin E1 overproduction or p53 knockout to force premature S phase entry with underlicensing. Surprisingly, cells re-entering the cell cycle from G0 are underlicensed due to a defective origin licensing checkpoint. The underlicensing causes hypersensitivity to replication stress during the 1st S phase after re-entry. The hypersensitivity accumulates over multiple rounds of quiescence and re-entry, demonstrating that repeated cell cycle re-entry is toxic over long periods. Thus, controlling both the amount of loaded MCM and the rate of MCM loading is important for proper cell cycle progression, genome stability and cell fate outcomes.

While we made significant progress in understanding MCM loading in diverse cellular contexts, many questions remain unanswered for future work. The remainder of this chapter will address two questions for future directions of study.

Does chromatin influence the rapid MCM loading in stem cells?

We demonstrated that stem cells have higher amounts of the MCM loading protein Cdt1 than differentiated cells. The increased Cdt1 promotes faster MCM loading, but it may not be the only rate limiting factor in the fast loading stem cells. There is only a twofold difference in the amount of Cdt1 but a six fold difference in the rate of MCM loading between stem cells and differentiated cells. It is not clear if the amount of Cdt1 is sufficient to produce the larger increase in MCM loading rate. Other factors may also be rate limiting for MCM loading in stem cells.

One interesting factor that might contribute to MCM loading rate is the epigenetic chromatin structure of the cell. Stem cells have more euchromatin across their genome and less heterochromatin than differentiated cells. DNA in euchromatin is called “open chromatin” because it is accessible to other factors such as RNA polymerases or transcription factors. DNA in heterochromatin is called “closed chromatin” because it is compacted and less accessible to external factors. The open chromatin in stem cells may facilitate rapid MCM loading. MCM loading onto DNA replication origins in metazoans is not sequence specific. Instead, origins seem to be located in regions of open chromatin that are more accessible to MCM and its loading proteins. Closed heterochromatin may require additional chromatin remodeling factors to allow MCM loading, such as the origin recognition complex-associated protein ORCA. Therefore, it may be easier and faster to load MCM into regions of open euchromatin than closed heterochromatin. The greater amounts of open euchromatin in stem cells may facilitate rapid MCM loading, while differentiated cells may require extensive heterochromatin remodeling before MCM loading takes place.

Our lab is actively investigating the role of epigenetic marks in regulating MCM loading rate. I have worked with two rotating graduate students, Rachel Cherney and Jackson Peterson, to measure how epigenetic markers for euchromatin and heterochromatin change during

differentiation. Their goal was to correlate changes in histone marks that control open or closed chromatin with changes in MCM loading during differentiation. They both measured specific histone modifications at the same time points that the MCM loading rate decreased during early differentiation. Rachel found that H3K4me3, a marker of open chromatin, was higher in pluripotent cells than their isogenic differentiated counterparts. She also found that differentiated cells have more H3K27me3, a marker of repressed heterochromatin, than pluripotent cells. Jackson found that pluripotent stem cells have high levels of H4 acetylation, a marker of open chromatin, and that the acetylation rapidly decreases at the same time as the MCM loading rate decreases during differentiation towards mesoderm. He also found that the transcription factor Myc decreases during differentiation towards mesoderm. Myc promotes global open chromatin and is also one of the four genes used to reprogram differentiated cells into induced pluripotent stem cells. Taken together, these data suggest that changes in epigenetics and chromatin structure correlate with changes in MCM loading rate. Future work should artificially manipulate chromatin structure to determine if changing chromatin structure can also change loading rate.

How does the origin licensing checkpoint measure the amount of loaded MCM?

We demonstrated that actively proliferating cells have a functional origin licensing checkpoint. The checkpoint ensures cells have a threshold amount of loaded MCM before entering S phase. If a cell lacks the threshold amount of loaded MCM, the origin licensing checkpoint decreases CDK2 activity to prevent S phase entry. However, the molecular sensor for the amount of loaded MCM or the exact number of MCM to pass the threshold is unknown. Cells load about 100,000 to 250,000 MCM double hexamers onto replication origins every cell cycle (Rodriguez-Martinez and Mechali, 2014). It seems unlikely a sensor protein could monitor MCM and tell the difference between 100,000 MCM and 99,999 MCM to activate the origin licensing checkpoint or that the threshold for S phase is a precise number of loaded MCM. Instead a more generalized signal might activate the checkpoint.

One option could be that the lack of loaded MCM at some genomic region generates a signal. This signal would be analogous to how the spindle assembly checkpoint works, which occurs not by counting the number of attached kinetochores, but by the detection of just one unattached kinetochore to activate the spindle assembly checkpoint (Lara-Gonzalez et al., 2012). Perhaps a certain histone modification is sensed by the checkpoint. MCM loading involves some changes in histone modification by Cdt1 that recruits HBO1 to genomic loci. Additionally, ORC also participates in nucleosome remodeling (Miotto and Struhl, 2008, 2010; Azmi et al., 2017). MCM loading onto regions of DNA that actively generate a signal could remodel the nucleosomes and turn off the signal. Alternatively, loaded MCM double hexamers themselves could recruit or activate an inhibitor of the licensing checkpoint, similar to how double hexamers specifically recruit Dbf4-dependent kinase (Abid Ali et al., 2017). As the amount of loaded MCM double hexamers increases, the amount of activated/recruited licensing checkpoint inhibitor would increase, eventually saturating the checkpoint to allow Cdk2 activity and S phase entry. A model of gradual inhibition would fit with the observation that the amount of loaded MCM dictates the strength of the licensing checkpoint response, i.e. the less loaded MCM, the stronger the checkpoint response. Discovering more pieces of the pathway from the sensor to the effector will facilitate greater understanding of the licensing checkpoint.

Future work to discover the molecular players in the origin licensing checkpoint could take a candidate gene approach. We know the pathway is p53-dependent. Therefore, we could screen genes upstream or downstream of p53 as candidates for additional components of the licensing checkpoint. First, we could identify if the checkpoint depends on p53-dependent transcription by adding back WT p53 or mutants that are defective for DNA binding to RPE1 CRISPR p53 null cells, and measuring underlicensing by flow cytometry. Knowing whether the licensing checkpoint requires p53-dependent transcription will guide selection of candidate genes to screen. Then, a medium throughput approach would use previously established CRISPR knockout lines from published screens, treat cells with siCdt1, and measure

underlicensing by flow cytometry (Zimmermann et al., 2018; McKinley and Cheeseman, 2017). The readout would be an underlicensing phenotype that matches the RPE1 p53 KO cells. Candidates could be furthered tested for epistasis with the p53 KO to determine if they function in the same pathway. An alternative approach is an unbiased mass spectrometry screen to identify potential licensing checkpoint proteins. We could compare cells re-entering the cell cycle from G0 (a defective licensing checkpoint) with cells synchronized in the following G1 (a functional licensing checkpoint), measuring total protein and phosphorylation levels under the two conditions. Alternatively, we could perform MCM chromatin immunoprecipitation and total chromatin fraction with the idea that a sensor for the licensing checkpoint either senses something with MCM directly on DNA, or the lack of MCM on DNA. Potential candidates would be proteins that are regulated differently between the two G1 phases. Potential candidates could be screened further for underlicensing by the same flow cytometry assay. In summary, we can use p53, to search for related proteins in the checkpoint, or we can use two unique cell cycles with and without the checkpoint to screen for potential checkpoint proteins.

Future work on origin licensing clearly has more impact than just allowing cells to replicate their DNA in S phase. Discovering how MCM loading rate changes during stem cell differentiation by epigenetics or otherwise would improve therapies to build new tissues from induced pluripotent stem cells. Understanding the origin licensing checkpoint would improve understanding of how quiescence contributes to aging by repeated cell cycle re-entry without a functional licensing checkpoint. Discoveries for both MCM loading rate in stem cells and the licensing checkpoint may converge in cancer. Cancer cells often revert to a stem cell like state with rapid cell cycles and rapid MCM loading rate, in addition to loss of p53 and the origin licensing checkpoint. Understanding what contributes to MCM loading rate and the origin licensing checkpoint could provide new avenues for cancer therapy by decreasing origin licensing in cancer cells without the licensing checkpoint. In conclusion, uncovering regulation of MCM loading rate and the licensing checkpoint would be new advances for the cell cycle field.

REFERENCES

Abid Ali, F., M.E. Douglas, J. Locke, V.E. Pye, A. Nans, J.F.X. Diffley, and A. Costa. 2017. Cryo-EM structure of a licensed DNA replication origin. *Nat. Commun.* 8:2241. doi:10.1038/s41467-017-02389-0.

Ahuja, A.K., K. Jodkowska, F. Teloni, A.H. Bizard, R. Zellweger, R. Herrador, S. Ortega, I.D. Hickson, M. Altmeyer, J. Mendez, and M. Lopes. 2016. A short G1 phase imposes constitutive replication stress and extensive fork remodeling in mouse embryonic stem cells. *Nat. Commun.* 15:10660. doi:10.1038/ncomms10660.

Alvarez, S., M. Díaz, J. Flach, S. Rodriguez-Acebes, A.J. López-Contreras, D. Martínez, M. Cañamero, O. Fernández-Capetillo, J. Isern, E. Passegué, and J. Méndez. 2015. Replication stress caused by low MCM expression limits fetal erythropoiesis and hematopoietic stem cell functionality. *Nat. Commun.* 6:8548. doi:10.1038/ncomms9548.

Alver, R.C., G.S. Chadha, and J.J. Blow. 2014. The contribution of dormant origins to genome stability: From cell biology to human genetics. *DNA Repair (Amst).* 19:182–189. doi:10.1016/j.dnarep.2014.03.012.

Aparicio, O.M. 2013. Location, location, location: it's all in the timing for replication origins. *Genes Dev.* 27:117–28. doi:10.1101/gad.209999.112.

Arias, E.E., and J.C. Walter. 2005. Replication-dependent destruction of Cdt1 limits DNA replication to a single round per cell cycle in Xenopus egg extracts. *Genes Dev.* 19:114–126. doi:10.1101/gad.1255805.

Arias, E.E., and J.C. Walter. 2007. Strength in numbers: preventing rereplication via multiple mechanisms in eukaryotic cells. *Genes Dev.* 21:497–518. doi:10.1101/gad.1508907.

Arora, M., J. Moser, H. Phadke, A.A. Basha, and S.L. Spencer. 2017. Endogenous Replication Stress in Mother Cells Leads to Quiescence of Daughter Cells. *Cell Rep.* 19:1351–1364. doi:10.1016/j.celrep.2017.04.055.

Azmi, I.F., S. Watanabe, M.F. Maloney, S. Kang, J.A. Belsky, D.M. MacAlpine, C.L. Peterson, and S.P. Bell. 2017. Nucleosomes influence multiple steps during replication initiation. *Elife*. 6:e22512. doi:10.7554/eLife.22512.

Bach, S., M. Knockaert, J. Reinhardt, O. Lozach, S. Schmitt, B. Baratte, M. Koken, S.P. Coburn, L. Tang, T. Jiang, D.C. Liang, H. Galons, J.F. Dierick, L.A. Pinna, F. Meggio, F. Totzke, C. Schachtele, A.S. Lerman, A. Carnero, Y. Wan, N. Gray, and L. Meijer. 2005. Roscovitine targets, protein kinases and pyridoxal kinase. *J. Biol. Chem.* 280:31208–31219. doi:10.1074/jbc.M500806200.

Balazsi, G., A. Van Oudenaarden, and J.J. Collins. 2011. Cellular decision making and biological noise: From microbes to mammals. *Cell*. 144:910–925. doi:10.1016/j.cell.2011.01.030.

Ballabeni, A., M. Melixetian, R. Zamponi, L. Masiero, F. Marinoni, and K. Helin. 2004. Human Geminin promotes pre-RC formation and DNA replication by stabilizing CDT1 in mitosis. *EMBO J.* 23:3122–3132. doi:10.1038/sj.emboj.7600314.

Ballabeni, A., I.-H. Park, R. Zhao, W. Wang, P.H. Lerou, G.Q. Daley, and M.W. Kirschner. 2011. Cell cycle adaptations of embryonic stem cells. *Proc. Natl. Acad. Sci.* 108:19252–19257.

doi:10.1073/pnas.1116794108.

Bar-On, O., M. Shapira, K. Skorecki, A. Hershko, and D.D. Hershko. 2010. Regulation of APC/C (Cdh1) ubiquitin ligase in differentiation of human embryonic stem cells. *Cell Cycle*. 9:1986–9. doi:10.4161/cc.9.10.11727.

Barr, A.R., S. Cooper, F.S. Heldt, F. Butera, and H. Stoy. 2017. DNA damage during S-phase mediates the proliferation-quiescence decision in the subsequent G1 via p21 expression ¨. *Nat. Commun. Commun*. March:14728. doi:10.1038/ncomms14728.

Barr, A.R., F.S. Heldt, T. Zhang, C. Bakal, and B. Novak. 2016. A Dynamical Framework for the All-or-None G1/S Transition. *Cell Syst.* 2:27–37. doi:10.1016/j.cels.2016.01.001.

Beerman, I., J. Seita, M.A. Inlay, I.L. Weissman, and D.J. Rossi. 2014. Quiescent hematopoietic stem cells accumulate DNA damage during aging that is repaired upon entry into cell cycle. *Cell Stem Cell*. 15:37–50. doi:10.1016/j.stem.2014.04.016.

Bendall, S.C., E.F. Simonds, P. Qiu, E.D. Amir, P.O. Krutzik, R. Finck, R. V Bruggner, R. Melamed, A. Trejo, O.I. Ornatsky, R.S. Balderas, S.K. Plevritis, K. Sachs, D. Pe, S.D. Tanner, and G.P. Nolan. 2011. Single-Cell Mass Cytometry of Differential Immune and Drug Responses Across a Human Hematopoietic Continuum. *Science*. 332:687–697. doi:10.1126/science.1198704.

Bernardo, A.S., T. Faial, L. Gardner, K.K. Niakan, D. Ortmann, C.E. Senner, E.M. Callery, M.W. Trotter, M. Hemberger, J.C. Smith, L. Bardwell, A. Moffett, and R.A. Pedersen. 2011. BRACHYURY and CDX2 mediate BMP-induced differentiation of human and mouse pluripotent stem cells into embryonic and extraembryonic lineages. *Cell Stem Cell*. 9:144–155. doi:10.1016/j.stem.2011.06.015.

Bhattacharya, S., J. Garriga, J. Calbó, T. Yong, D.S. Haines, and X. Graña. 2003. SKP2 associates with p130 and accelerates p130 ubiquitylation and degradation in human cells. *Oncogene*. 22:2443–2451. doi:10.1038/sj.onc.1206339.

Blagosklonny, M. V., and A.B. Pardee. 2002. The restriction point of the cell cycle. *Cell Cycle*. 1:103–110. doi:10.4161/cc.1.2.108.

Blow, J.J., X.Q. Ge, and D.A. Jackson. 2011. How dormant origins promote complete genome replication. *Trends Biochem. Sci.* 36:405–14. doi:10.1016/j.tibs.2011.05.002.

Boward, B., T. Wu, and S. Dalton. 2016. Control of cell fate through cell cycle and pluripotency networks. *Stem Cells*. n/a-n/a. doi:10.1002/stem.2345.

Bowers, J.L., J.C.W. Randell, S. Chen, and S.P. Bell. 2004. ATP hydrolysis by ORC catalyzes reiterative Mcm2-7 assembly at a defined origin of replication. *Mol. Cell*. 16:967–978. doi:10.1016/j.molcel.2004.11.038.

Brown, K.A., R.L. Roberts, C.L. Arteaga, and B.K. Law. 2004. Transforming growth factor-beta induces Cdk2 relocalization to the cytoplasm coincident with dephosphorylation of retinoblastoma tumor suppressor protein. *Breast Cancer Res*. 6:R130-9. doi:10.1186/bcr762.

Burgess, A., T. Lorca, and A. Castro. 2012. Quantitative Live Imaging of Endogenous DNA

Replication in Mammalian Cells. *PLoS One*. 7. doi:10.1371/journal.pone.0045726.

Calder, A., I. Roth-Albin, S. Bhatia, C. Pilquil, J.H. Lee, M. Bhatia, M. Levadoux-Martin, J. McNicol, J. Russell, T. Collins, and J.S. Draper. 2013. Lengthened G1 Phase Indicates Differentiation Status in Human Embryonic Stem Cells. *Stem Cells Dev.* 22:279–295. doi:10.1089/scd.2012.0168.

Cappell, S.D., M. Chung, A. Jaimovich, and S.L. Spencer. 2016. Irreversible APC Cdh1 Inactivation Underlies the Point of No Return for Cell-Cycle Entry. *Cell*. 166:167–180. doi:10.1016/j.cell.2016.05.077.

Carpenter, A.E., T.R. Jones, M.R. Lamprecht, C. Clarke, I.H. Kang, O. Friman, D.A. Guertin, J.H. Chang, R.A. Lindquist, J. Moffat, P. Golland, and D.M. Sabatini. 2006. CellProfiler: image analysis software for identifying and quantifying cell phenotypes. *Genome Biol.* 7:R100. doi:10.1186/gb-2006-7-10-r100.

Carroll, T.D., I.P. Newton, Y. Chen, J.J. Blow, and I. Näthke. 2018. Lgr5+intestinal stem cells reside in an unlicensed G1 phase. *J. Cell Biol.* jcb.201708023. doi:10.1083/jcb.201708023.

Champy, C. 1922. L'action de l'extrait thyroïdien. *Arch. Morph. Gén. exp.* 4:1–56.

Chandrasekaran, S., T.X. Tan, J.R. Hall, and J.G. Cook. 2011. Stress-stimulated mitogen-activated protein kinases control the stability and activity of the Cdt1 DNA replication licensing factor. *Mol. Cell. Biol.* 31:4405–16. doi:10.1128/MCB.06163-11.

Chen, J.Y., J.R. Lin, F.C. Tsai, and T. Meyer. 2013. Dosage of Dyrk1a shifts cells within a p21-Cyclin D1 signaling map to control the decision to enter the cell cycle. *Mol. Cell*. 52:87–100. doi:10.1016/j.molcel.2013.09.009.

Chen, T., and S.Y.R. Dent. 2013. Chromatin modifiers and remodellers: regulators of cellular differentiation. *Nat. Rev. Genet.* 15:93–106. doi:10.1038/nrg3607.

Chen, Y., S. Keegan, M. Kahli, P. Tonzi, D. Fenyö, T.T. Huang, and D.J. Smith. 2019. Transcription shapes DNA replication initiation and termination in human cells. *Nat. Struct. Mol. Biol.* 26:67–77. doi:10.1038/s41594-018-0171-0.

Cheung, T.H., and T. a Rando. 2013. Molecular regulation of stem cell quiescence. *Nat. Rev. Mol. Cell Biol.* 14:329–40. doi:10.1038/nrm3591.

Chiorino, G., J.A. Metz, D. Tomasoni, and P. Ubezio. 2001. Desynchronization rate in cell populations: mathematical modeling and experimental data. *J Theor Biol*. 208:185–199. doi:10.1006/jtbi.2000.2213.

Choi, S.C., J.H. Choi, C.Y. Park, C.M. Ahn, S.J. Hong, and D.S. Lim. 2012. Nanog regulates molecules involved in stemness and cell cycle-signaling pathway for maintenance of pluripotency of P19 embryonal carcinoma stem cells. *J. Cell. Physiol.* 227:3678–3692. doi:10.1002/jcp.24076.

Clijsters, L., J. Ogink, and R. Wolthuis. 2013. The spindle checkpoint, APC/CCdc20, and APC/CCdh1 play distinct roles in connecting mitosis to S phase. *J. Cell Biol.* 201:1013–1026. doi:10.1083/jcb.201211019.

Cocker, J.H., S. Piatti, C. Santocanale, K. Nasmyth, and J.F. Diffley. 1996. An essential role for the Cdc6 protein in forming the pre-replicative complexes of budding yeast. *Nature*. 379:180–2. doi:10.1038/379180a0.

Coleman, K.E., G.D. Grant, R.A. Haggerty, K. Brantley, E. Shibata, B.D. Workman, A. Dutta, D. Varma, J.E. Purvis, and J.G. Cook. 2015. Sequential replication-coupled destruction at G1 / S ensures genome stability. *Genes Dev.* 29:1734–1746. doi:10.1101/gad.263731.115.Selectivity.

Coller, H.A. 2007. What's taking so long? S-phase entry from quiescence versus proliferation. *Nat. Rev. Mol. Cell Biol.* 8:667–670.

Coller, H.A. 2011. The essence of quiescence. *Science*. 334:1074–5. doi:10.1126/science.1216242.

Coller, H.A., L. Sang, and J.M. Roberts. 2006. A New Description of Cellular Quiescence. *PLoS Biol*. 4:e83. doi:10.1371/journal.pbio.0040083.

Cook, J.G., C.-H. Park, T.W. Burke, G. Leone, J. DeGregori, A. Engel, and J.R. Nevins. 2002. Analysis of Cdc6 function in the assembly of mammalian prereplication complexes. *Proc. Natl. Acad. Sci.* 99:1347–1352.

Coronado, D., M. Godet, P.Y. Bourillot, Y. Tapponnier, A. Bernat, M. Petit, M. Afanassieff, S. Markossian, A. Malashicheva, R. Iacone, K. Anastassiadis, and P. Savatier. 2013. A short G1 phase is an intrinsic determinant of naïve embryonic stem cell pluripotency. *Stem Cell Res.* 10:118–131. doi:10.1016/j.scr.2012.10.004.

Costa, A., I. Ilves, N. Tamberg, T. Petojevic, E. Nogales, M.R. Botchan, and J.M. Berger. 2011. The structural basis for MCM2-7 helicase activation by GINS and Cdc45. *Nat. Struct. Mol. Biol.* 18:471–7. doi:10.1038/nsmb.2004.

Coster, G., and J.F.X. Diffley. 2017. Bidirectional eukaryotic DNA replication is established by quasi-symmetrical helicase loading. *Science (80-.).* 318:314–318. doi:10.1126/science.aan0063.

Czerniak, B., F. Herz, R.P. Wersto, and L.G. Koss. 1992. Asymmetric distribution of oncogene products at mitosis. *Proc. Natl. Acad. Sci. U. S. A.* 89:4860–4863.

Daigh, L.H., C. Liu, M. Chung, K.A. Cimprich, and T. Meyer. 2018. Stochastic Endogenous Replication Stress Causes ATR-Triggered Fluctuations in CDK2 Activity that Dynamically Adjust Global DNA Synthesis Rates. *Cell Syst.* 7:17–27.e3. doi:10.1016/j.cels.2018.05.011.

Darzynkiewicz, Z., H. Crissman, and J.W. Jacobberger. 2004. Cytometry of the cell cycle: Cycling through history. *Cytometry*. 58A:21–32. doi:10.1002/cyto.a.20003.

Darzynkiewicz, Z., H. Crissman, F. Traganos, and J. Steinkamp. 1982. Cell Heterogeneity During the Cell Cycle. *J. Cell. Physiol.* 474:465–474.

Deegan, T.D., and J.F. Diffley. 2016. MCM: one ring to rule them all. *Curr. Opin. Struct. Biol.* 37:145–151. doi:10.1016/j.sbi.2016.01.014.

DePamphilis, M.L. 2003. The 'ORC cycle': a novel pathway for regulating eukaryotic DNA replication. *Gene*. 310:1–15. doi:10.1016/S0378-1119(03)00546-8.

DePamphilis, M.L., J.J. Blow, S. Ghosh, T. Saha, K. Noguchi, and A. Vassilev. 2006. Regulating the licensing of DNA replication origins in metazoa. *Curr. Opin. Cell Biol.* 18:231–9. doi:10.1016/j.ceb.2006.04.001.

Dietrich, C., K. Wallenfang, F. Oesch, and R. Wieser. 1997. Translocation of cdk2 to the nucleus during G1-phase in PDGF-stimulated human fibroblasts. *Exp. Cell Res.* 232:72–78. doi:10.1006/excr.1997.3507.

Dimitrova, D.S., T.A. Prokhorova, J.J. Blow, I.T. Todorov, and D.M. Gilbert. 2002. Mammalian nuclei become licensed for DNA replication during late telophase. *J. Cell Sci.* 115:51–59.

Dobrowolski, S., M. Harter, and D.W. Stacey. 1994. Cellular ras activity is required for passage through multiple points of the G0/G1 phase in BALB/c 3T3 cells. *Mol. Cell. Biol.* 14:5441–5449. doi:10.1128/MCB.14.8.5441.Updated.

Dong, P., M. V Maddali, J.K. Srimani, F. Thélot, J.R. Nevins, B. Mathey-Prevot, and L. You. 2014. Division of labour between Myc and G1 cyclins in cell cycle commitment and pace control. *Nat. Commun.* 5:4750. doi:10.1038/ncomms5750.

Dueck, H., J. Eberwine, and J. Kim. 2015. Variation is function: Are single cell differences functionally important? *BioEssays*. 38:172–180. doi:10.1002/bies.201500124.

Edgar, B.A., and T.L. Orr-Weaver. 2001. Endoreplication cell cycles: More for less. *Cell*. 105:297–306. doi:10.1016/S0092-8674(01)00334-8.

Egozi, D., M. Shapira, G. Paor, O. Ben-Izhak, K. Skorecki, and D.D. Hershko. 2007. Regulation of the cell cycle inhibitor p27 and its ubiquitin ligase Skp2 in differentiation of human embryonic stem cells. *FASEB J.* 21:2807–2817. doi:10.1096/fj.06-7758com.

Ekholm-Reed, S., J. Méndez, D. Tedesco, A. Zetterberg, B. Stillman, and S.I. Reed. 2004. Deregulation of cyclin E in human cells interferes with prereplication complex assembly. *J. Cell Biol.* 165:789–800. doi:10.1083/jcb.200404092.

Ekholm, S., P. Zickert, S. Reed, and A. Zetterberg. 2001. Accumulation of cyclin E is not a prerequisite for passage through the restriction point. *Mol. Cell. Biol.* 21:3256–3265. doi:10.1128/MCB.21.9.3256-3265.2001.

Evertts, A.G., A.L. Manning, X. Wang, N.J. Dyson, B. a Garcia, and H. a Coller. 2013. H4K20 methylation regulates quiescence and chromatin compaction. *Mol. Biol. Cell*. 24:3025–37. doi:10.1091/mbc.E12-07-0529.

Evrin, C., P. Clarke, J. Zech, R. Lurz, J. Sun, S. Uhle, H. Li, B. Stillman, and C. Speck. 2009. A double-hexameric MCM2-7 complex is loaded onto origin DNA during licensing of eukaryotic DNA replication. *Proc. Natl. Acad. Sci. U. S. A.* 106:20240–5. doi:10.1073/pnas.0911500106.

Ewald, B., D. Sampath, and W. Plunkett. 2007. H2AX phosphorylation marks gemcitabine-

induced stalled replication forks and their collapse upon S-phase checkpoint abrogation. *Mol. Cancer Ther.* 6:1239–1249. doi:10.1158/1535-7163.MCT-06-0633.

Farrell, J.A., and P.H. O'Farrell. 2014. From Egg to Gastrula: How the Cell Cycle Is Remodeled During the *Drosophila* Mid-Blastula Transition. *Annu. Rev. Genet.* 48:269–294. doi:10.1146/annurev-genet-111212-133531.

Feng, D., Z. Tu, W. Wu, and C. Liang. 2003. Inhibiting the Expression of DNA Replication-Initiation Proteins Induces Apoptosis in Human Cancer Cells 1. 7356–7364.

Ferrell, J.E., T.Y.-C. Tsai, and Q. Yang. 2011. Modeling the cell cycle: why do certain circuits oscillate? *Cell*. 144:874–885. doi:10.1016/j.cell.2011.03.006.

Filipczyk, A.A., A.L. Laslett, C. Mummery, and M.F. Pera. 2007. Differentiation is coupled to changes in the cell cycle regulatory apparatus of human embryonic stem cells. *Stem Cell Res.* 1:45–60. doi:10.1016/j.scr.2007.09.002.

Flach, J., S.T. Bakker, M. Mohrin, P.C. Conroy, E.M. Pietras, D. Reynaud, S. Alvarez, M.E. Diolaiti, F. Ugarte, E.C. Forsberg, M.M. Le Beau, B.A. Stohr, J. Méndez, C.G. Morrison, and E. Passegué. 2014. Replication stress is a potent driver of functional decline in ageing haematopoietic stem cells. *Nature*. 512:198–202. doi:10.1038/nature13619.

Foijer, F., M. Simonis, M. van Vliet, L. Wessels, R. Kerkhoven, P.K. Sorger, and H. Te Riele. 2008. Oncogenic pathways impinging on the G2-restriction point. *Oncogene*. 27:1142–1154. doi:10.1038/sj.onc.1210724.

Foijer, F., R.M.F. Wolthuis, V. Doodeman, R.H. Medema, and H. Te Riele. 2005. Mitogen requirement for cell cycle progression in the absence of pocket protein activity. *Cancer Cell*. 8:455–466. doi:10.1016/j.ccr.2005.10.021.

Foster, D. a, P. Yellen, L. Xu, and M. Saqcena. 2010. Regulation of G1 Cell Cycle Progression: Distinguishing the Restriction Point from a Nutrient-Sensing Cell Growth Checkpoint(s). *Genes Cancer*. 1:1124–31. doi:10.1177/1947601910392989.

Fragkos, M., O. Ganier, P. Coulombe, and M. Méchali. 2015. DNA replication origin activation in space and time. *Nat. Rev. Mol. Cell Biol.* 16:360–374. doi:10.1038/nrm4002.

Frigola, J., J. He, K. Kinkelin, V.E. Pye, L. Renault, M.E. Douglas, D. Remus, P. Cherepanov, A. Costa, and J.F.X. Diffley. 2017. Cdt1 stabilizes an open MCM ring for helicase loading. *Nat. Commun.* 8:15720. doi:10.1038/ncomms15720.

Gardner, N.J., P.J. Gillespie, J.T. Carrington, E.J. Shanks, S.P. McElroy, E.J. Haagensen, J.A. Frearson, A. Woodland, and J.J. Blow. 2017. The High-Affinity Interaction between ORC and DNA that Is Required for Replication Licensing Is Inhibited by 2-Arylquinolin-4-Amines. *Cell Chem. Biol.* 1–12. doi:10.1016/j.chembiol.2017.06.019.

Ge, X.Q., and J.J. Blow. 2009. The Licensing Checkpoint Opens Up. 8:2320–2322.

Ge, X.Q., J. Han, E.-C. Cheng, S. Yamaguchi, N. Shima, J.-L. Thomas, and H. Lin. 2015. Embryonic Stem Cells License a High Level of Dormant Origins to Protect the Genome against Replication Stress. *Stem Cell Reports*. 5:185–94.

doi:10.1016/j.stemcr.2015.06.002.

Ge, X.Q., D.A. Jackson, and J.J. Blow. 2007. Dormant origins licensed by excess Mcm2-7 are required for human cells to survive replicative stress. *Genes Dev.* 21:3331–41. doi:10.1101/gad.457807.

Gerdes, J., U. Schwab, H. Lemke, and H. Stein. 1983. Production of a mouse monoclonal antibody reactive with a human nuclear antigen associated with cell proliferation. *Int. J. Cancer*. 31:13–20. doi:10.1002/ijc.2910310104.

Giacinti, C., and a Giordano. 2006. RB and cell cycle progression. *Oncogene*. 25:5220–7. doi:10.1038/sj.onc.1209615.

Gillespie, P.J., G.A. Khoudoli, G. Stewart, J.R. Swedlow, and J. Blow. 2007. ELYS/MEL-28 Chromatin Association Coordinates Nuclear Pore Complex Assembly and Replication Licensing. *Curr. Biol.* 17:1657–1662. doi:10.1016/j.cub.2007.08.041.

Giono, L.E., and J.J. Manfredi. 2007. Mdm2 Is Required for Inhibition of Cdk2 Activity by p21 , Thereby Contributing to p53-Dependent Cell Cycle Arrest. *Mol. Cell. Biol. Biol.* 27:4166–4178. doi:10.1128/MCB.01967-06.

Giri, S., V. Aggarwal, J. Pontis, Z. Shen, A. Chakraborty, A. Khan, C. Mizzen, K. V Prasanth, S. Ait-Si-Ali, T. Ha, and S.G. Prasanth. 2015. The preRC protein ORCA organizes heterochromatin by assembling histone H3 lysine 9 methyltransferases on chromatin. *Elife*. 4:1–30. doi:10.7554/eLife.06496.

Gonzales, K.A.U., H. Liang, Y. Lim, Y.-S. Chan, J.-C. Yeo, C.-P. Tan, B. Gao, B. Le, Z.-Y. Tan, K.-Y. Low, Y. Liou, F. Bard, and H. Ng. 2015. Deterministic Restriction on Pluripotent State Dissolution by Cell-Cycle Pathways. *Cell*. 162:564–579. doi:10.1016/j.cell.2015.07.001.

Grant, G.D., K.M. Kedziora, J.C. Limas, J.G. Cook, and J.E. Purvis. 2018. Accurate delineation of cell cycle phase transitions in living cells with PIP-FUCCI. *Cell Cycle*. 17:2496–2516. doi:10.1080/15384101.2018.1547001.

Gray, L., and D. Griffeath. 2001. The ergodic theory of traffic jams. *J. Stat. Phys.* 105:413–452. doi:10.1023/A:1012202706850.

Gros, J., C. Kumar, G. Lynch, T. Yadav, I. Whitehouse, and D. Remus. 2015. Post-licensing Specification of Eukaryotic Replication Origins by Facilitated Mcm2-7 Sliding along DNA. *Mol. Cell*. 60:797–807. doi:10.1016/j.molcel.2015.10.022.

Hahn, A.T., J.T. Jones, and T. Meyer. 2009. Quantitative analysis of cell cycle phase durations and PC12 differentiation using fluorescent biosensors. *Cell Cycle*. 8:1044–1052. doi:10.4161/cc.8.7.8042.

Håland, T.W., E. Boye, T. Stokke, B. Grallert, and R.G. Syljuåsen. 2015. Simultaneous measurement of passage through the restriction point and MCM loading in single cells. *Nucleic Acids Res.* 43:e150. doi:10.1093/nar/gkv744.

Hartwell, L.H., and T.A. Weinert. 1989. Checkpoints : Controls that Ensure the Order of Cell Cycle Events. *Science (80-.).* 246:629–634.

Hinds, P.W., S. Mittnacht, V. Dulic, A. Arnold, S.I. Reed, and R.A. Weinberg. 1992. Regulation of retinoblastoma protein functions by ectopic expression of human cyclins. *Cell*. 70:993–1006. doi:10.1016/0092-8674(92)90249-C.

Hiraga, S., T. Ly, J. Garzón, Z. Hořejší, Y. Ohkubo, A. Endo, C. Obuse, S.J. Boulton, A.I. Lamond, and D. Anne. 2017. Human RIF1 and Protein Phosphatase 1 stimulate DNA replication origin licensing but suppress origin activation. *EMBO Rep.* 1–17. doi:10.15252/embr.201641983.

Hitomi, M., and D.W. Stacey. 1999. Cellular ras and cyclin D1 are required during different cell cycle periods in cycling NIH 3T3 cells. *Mol. Cell. Biol.* 19:4623–4632.

Hitomi, M., and D.W. Stacey. 2001. Ras-dependent cell cycle commitment during G2 phase. *FEBS Lett.* 490:123–131. doi:10.1016/S0014-5793(01)02115-9.

Hölzel, M., F. Kohlhuber, I. Schlosser, D. Hölzel, B. Lüscher, and D. Eick. 2001. Myc/Max/Mad regulate the frequency but not the duration of productive cell cycles. *EMBO Rep.* 2:1125–1132. doi:10.1093/embo-reports/kve251.

Howard, A., and S. Pelc. 1953. Synthesis of deoxyribonucleic acid in normal and irradiated cells and its relation to chromosome breakage. *Heredity (Edinb).* 6(Suppl):261–273.

Huard, J., S. Mueller, E.D. Gilles, U. Klingmuller, and S. Klamt. 2012. An integrative model links multiple inputs and signaling pathways to the onset of DNA synthesis in hepatocytes. *FEBS J.* 279:3290–3313. doi:10.1111/j.1742-4658.2012.08572.x.

Ibarra, A., E. Schwob, and J. Méndez. 2008. Excess MCM proteins protect human cells from replicative stress by licensing backup origins of replication. *Proc. Natl. Acad. Sci. U. S. A.* 105:8956–61. doi:10.1073/pnas.0803978105.

Imai, Y., A. Takahashi, A. Hanyu, S. Hori, S. Sato, K. Naka, A. Hirao, N. Ohtani, and E. Hara. 2014. Crosstalk between the Rb pathway and AKT signaling forms a quiescence-senescence switch. *Cell Rep.* 7:194–207. doi:10.1016/j.celrep.2014.03.006.

Izawa, D., and J. Pines. 2011. How APC/C-Cdc20 changes its substrate specificity in mitosis. *Nat Cell Biol*. 13:223–233. doi:10.1038/ncb2165.

Jaqaman, K., D. Loerke, M. Mettlen, H. Kuwata, S. Grinstein, S.L. Schmid, and G. Danuser. 2008. Robust single-particle tracking in live-cell time-lapse sequences. *Nat. Methods*. 5:695–702. doi:10.1038/nmeth.1237.

Johnson, A., and J.M. Skotheim. 2013. Start and the restriction point. *Curr. Opin. Cell Biol.* 25:717–723. doi:10.1016/j.ceb.2013.07.010.

Kafri, R., J. Levy, M.B. Ginzberg, S. Oh, G. Lahav, and M.W. Kirschner. 2013. Dynamics extracted from fixed cells reveal feedback linking cell growth to cell cycle. *Nature*. 494:480–483. doi:10.1038/nature11897.

Kamura, T., T. Hara, M. Matsumoto, N. Ishida, F. Okumura, S. Hatakeyama, M. Yoshida, K. Nakayama, and K.I. Nakayama. 2004. Cytoplasmic ubiquitin ligase KPC regulates

proteolysis of p27(Kip1) at G1 phase. *Nat. Cell Biol.* 6:1229–1235. doi:10.1038/ncb1194.
Kanai, D., A. Ueda, T. Akagi, T. Yokota, and H. Koide. 2015. Oct3/4 directly regulates expression of E2F3a in mouse embryonic stem cells. *Biochem. Biophys. Res. Commun.* 459:374–378. doi:10.1016/j.bbrc.2015.02.105.

Kapinas, K., R. Grandy, P. Ghule, R. Medina, K. Becker, A. Pardee, S.K. Zaidi, J. Lian, J. Stein, A. van Wijnen, and G. Stein. 2013. The abbreviated pluripotent cell cycle. *J. Cell. Physiol.* 228:9–20. doi:10.1002/jcp.24104.

Kareta, M.S., L.L. Gorges, S. Hafeez, B.A. Benayoun, S. Marro, A.F. Zmoos, M.J. Cecchini, D. Spacek, L.F.Z. Batista, M. O'Brien, Y.H. Ng, C.E. Ang, D. Vaka, S.E. Artandi, F.A. Dick, A. Brunet, J. Sage, and M. Wernig. 2015a. Inhibition of pluripotency networks by the Rb tumor suppressor restricts reprogramming and tumorigenesis. *Cell Stem Cell*. 16:39–50. doi:10.1016/j.stem.2014.10.019.

Kareta, M.S., J. Sage, and M. Wernig. 2015b. Crosstalk between stem cell and cell cycle machineries. *Curr. Opin. Cell Biol.* 37:68–74. doi:10.1016/j.ceb.2015.10.001.

Kermi, C., E. Lo Furno, and D. Maiorano. 2017. Regulation of DNA replication in early embryonic cleavages. *Genes (Basel).* 8:42. doi:10.3390/genes801004.
Kimura, H., N. Nozaki, and K. Sugimoto. 1994. DNA polymerase alpha associated protein P1, a murine homolog of yeast MCM3, changes its intranuclear distribution during the DNA synthetic period. *EMBO J.* 13:4311–20.

Kinjyo, I., J. Qin, S.-Y. Tan, C.J. Wellard, P. Mrass, W. Ritchie, A. Doi, L.L. Cavanagh, M. Tomura, A. Sakaue-Sawano, O. Kanagawa, A. Miyawaki, P.D. Hodgkin, and W. Weninger. 2015. Real-time tracking of cell cycle progression during CD8+ effector and memory T-cell differentiation. *Nat. Commun.* 6:6301. doi:10.1038/ncomms7301.

Klein, A.M., and B.D. Simons. 2011. Universal patterns of stem cell fate in cycling adult tissues. *Development*. 138:3103–3111. doi:10.1242/dev.060103.

Kuipers, M.A., T.J. Stasevich, T. Sasaki, K.A. Wilson, K.L. Hazelwood, J.G. McNally, M.W. Davidson, and D.M. Gilbert. 2011. Highly stable loading of Mcm proteins onto chromatin in living cells requires replication to unload. *J. Cell Biol.* 192:29–41. doi:10.1083/jcb.201007111.

Kunnev, D., M.E. Rusiniak, A. Kudla, A. Freeland, G.K. Cady, and S.C. Pruitt. 2010. DNA damage response and tumorigenesis in Mcm2-deficient mice. *Oncogene*. 29:3630–3638. doi:10.1038/onc.2010.125.

Kuo, A.J., J. Song, P. Cheung, S. Ishibe-Murakami, S. Yamazoe, J.K. Chen, D.J. Patel, and O. Gozani. 2012. The BAH domain of ORC1 links H4K20me2 to DNA replication licensing and Meier-Gorlin syndrome. *Nature*. 484:115–9. doi:10.1038/nature10956.

Kurose, A., T. Tanaka, X. Huang, F. Traganos, and Z. Darzynkiewicz. 2006. Synchronization in the cell cycle by inhibitors of DNA replication induces histone H2AX phosphorylation: An indication of DNA damage. *Cell Prolif.* 39:231–240. doi:10.1111/j.1365-2184.2006.00380.x.

Kwon, J.S., N.J. Everetts, X. Wang, W. Wang, K. Della Croce, J. Xing, and G. Yao. 2017. Controlling Depth of Cellular Quiescence by an Rb-E2F Network Switch. *Cell Rep.*

20:3223–3235. doi:10.1016/j.celrep.2017.09.007.
L'Italien, L., M. Tanudji, L. Russell, and X.M. Schebye. 2006. Unmasking the redundancy between Cdk1 and Cdk2 at G2 phase in human cancer cell lines. *Cell Cycle*. 5:984–993. doi:10.4161/cc.5.9.2721.

Labib, K. 2010. How do Cdc7 and cyclin-dependent kinases trigger the initiation of chromosome replication in eukaryotic cells? *Genes Dev.* 24:1208–19. doi:10.1101/gad.1933010.

Lajtha, L.G., R. Oliver, and F. Ellis. 1954. Incorporation of P32 and adenine C14 into DNA by human bone marrow cells in vitro. *Br. J. Cancer*. 8:367–379. doi:10.1038/bjc.1954.38.

Lanni, J.S., and T. Jacks. 1998. Characterization of the p53-dependent postmitotic checkpoint following spindle disruption. *Mol. Cell. Biol.* 18:1055–1064.

Lara-Gonzalez, P., F.G. Westhorpe, and S.S. Taylor. 2012. The spindle assembly checkpoint. *Curr. Biol.* 22:R966–R980. doi:10.1016/j.cub.2012.10.006.

Lau, E., T. Tsuji, L. Guo, S. Lu, and W. Jiang. 2007. The role of pre-replicative complex (pre-RC) components in oncogenesis. *FASEB J.* 21:3786–3794. doi:10.1096/fj.07-8900rev.

Lee, J., Y. Go, I. Kang, Y.-M. Han, and J. Kim. 2010. Oct-4 controls cell-cycle progression of embryonic stem cells. *Biochem. J*. 426:171–181. doi:10.1042/BJ20091439.

Legesse-Miller, A., I. Raitman, E.M. Haley, A. Liao, L.L. Sun, D.J. Wang, N. Krishnan, J.M. Lemons, E.J. Suh, E.L. Johnson, B.A. Lund, and H.A. Coller. 2012. Quiescent fibroblasts are protected from proteasome inhibition-mediated toxicity. *Mol. Biol. Cell*. 23:3566–3581. doi:10.1091/mbc.E12-03-0192.

Leonard, A.C., and M. Méchali. 2013. DNA replication origins. *Cold Spring Harb. Perspect. Biol.* 5:a010116. doi:10.1101/cshperspect.a010116.

Leung, J.Y., G.L. Ehmann, P.H. Giangrande, and J.R. Nevins. 2008. A role for Myc in facilitating transcription activation by E2F1. *Oncogene*. 27:4172–4179. doi:10.1038/onc.2008.55.

Li, H., M. Collado, A. Villasante, A. Matheu, C.J. Lynch, M. Canamero, K. Rizzoti, C. Carneiro, G. Martinez, A. Vidal, R. Lovell-Badge, and M. Serrano. 2012. P27Kip1 directly represses Sox2 during embryonic stem cell differentiation. *Cell Stem Cell*. 11:845–852. doi:10.1016/j.stem.2012.09.014.

Litovchick, L., L. a Florens, S.K. Swanson, M.P. Washburn, and J. a DeCaprio. 2011. DYRK1A protein kinase promotes quiescence and senescence through DREAM complex assembly. *Genes Dev.* 25:801–13. doi:10.1101/gad.2034211.

Litovchick, L., S. Sadasivam, L. Florens, X. Zhu, S.K. Swanson, S. Velmurugan, R. Chen, M.P. Washburn, X.S. Liu, and J. a. DeCaprio. 2007. Evolutionarily Conserved Multisubunit RBL2/p130 and E2F4 Protein Complex Represses Human Cell Cycle-Dependent Genes in Quiescence. *Mol. Cell*. 26:539–551. doi:10.1016/j.molcel.2007.04.015.

Liu, L., W. Michowski, H. Inuzuka, K. Shimizu, N.T. Nihira, J.M. Chick, N. Li, Y. Geng, A.Y. Meng, A. Ordureau, A. Kołodziejczyk, K.L. Ligon, R.T. Bronson, K. Polyak, J.W. Harper, S.P. Gygi, W. Wei, and P. Sicinski. 2017. G1 cyclins link proliferation, pluripotency and

differentiation of embryonic stem cells. *Nat. Cell Biol.* 19:177–188. doi:10.1038/ncb3474.

Liu, P., D.M. Slater, M. Lenburg, K. Nevis, J.G. Cook, and C. Vaziri. 2009. Replication licensing promotes cyclin D1 expression and G1 progression in untransformed human cells. *Cell Cycle*. 8:125–136. doi:10.4161/cc.8.1.7528.

Liu, Q., Y. Tang, L. Chen, N. Liu, F. Lang, H. Liu, P. Wang, and X. Sun. 2016. E3 ligase SCFβTrCP induced DYRK1A degradation is essential for cell cycle progression in HEK293 cells. *J. Biol. Chem.* 291:jbc.M116.717553. doi:10.1074/jbc.M116.717553.

Lu, D., J.Y. Hsiao, N.E. Davey, V. a. Van Voorhis, S. a. Foster, C. Tang, and D.O. Morgan. 2014. Multiple mechanisms determine the order of APC/C substrate degradation in mitosis. *J. Cell Biol.* 207:23–29. doi:10.1083/jcb.201402041.

Lunn, C.L., J.C. Chrivia, and J.J. Baldassare. 2010. Activation of Cdk2/Cyclin E complexes is dependent on the origin of replication licensing factor Cdc6 in mammalian cells. *Cell Cycle*. 9:4533–4541. doi:10.4161/cc.9.22.13790.

Macheret, M., and T.D. Halazonetis. 2018. Intragenic origins due to short G1 phases underlie oncogene-induced DNA replication stress. *Nature*. doi:10.1038/nature25507.

Machida, Y.J., J.K. Teer, and A. Dutta. 2005. Acute reduction of an origin recognition complex (ORC) subunit in human cells reveals a requirement of ORC for Cdk2 activation. *J. Biol. Chem.* 280:27624–27630. doi:10.1074/jbc.M502615200.

Mailand, N., and J.F.X. Diffley. 2005. CDKs promote DNA replication origin licensing in human cells by protecting Cdc6 from APC/C-dependent proteolysis. *Cell*. 122:915–26. doi:10.1016/j.cell.2005.08.013.

Malumbres, M., and M. Barbacid. 2001. To cycle or not to cycle: a critical decision in cancer. *Nat. Rev. Cancer*. 1:222–231. doi:10.1038/35106065.

Maric, M., T. Maculins, G. De Piccoli, and K. Labib. 2014. Cdc48 and a ubiquitin ligase drive disassembly of the CMG helicase at the end of DNA replication. *Science*. 346:1253596–1253596. doi:10.1126/science.1253596.

Martinsson, H.S., M. Starborg, F. Erlandsson, and A. Zetterberg. 2005. Single cell analysis of G1 check points - The relationship between the restriction point and phosphorylation of pRb. *Exp. Cell Res.* 305:383–391. doi:10.1016/j.yexcr.2005.01.023.

Massagué, J. 2004. G1 cell-cycle control and cancer. *Nature*. 432:298–306. doi:10.1038/nature03094.

Matson, J.P., R. Dumitru, P. Coryell, R.M. Baxley, W. Chen, K. Twaroski, B.R. Webber, J. Tolar, A.-K. Bielinsky, J.E. Purvis, and J.G. Cook. 2017. Rapid DNA replication origin licensing protects stem cell pluripotency. *Elife*. 6:e30473. doi:10.7554/eLife.30473.

McAdams, H.H., and A. Arkin. 1997. Stochastic mechanisms in gene expression. *Proc. Natl. Acad. Sci. U. S. A.* 94:814–819. doi:10.1073/pnas.94.3.814.

McGarry, T.J., and M.W. Kirschner. 1998. Geminin, an inhibitor of DNA replication, is degraded during mitosis. *Cell*. 93:1043–1053. doi:10.1016/S0092-8674(00)81209-X.

McIntosh, D., and J.J. Blow. 2012. Dormant origins, the licensing checkpoint, and the response to replicative stresses. *Cold Spring Harb. Perspect. Biol.* 4:1–10. doi:10.1101/cshperspect.a012955.

McKinley, K.L., and I.M. Cheeseman. 2017. Large-Scale Analysis of CRISPR/Cas9 Cell-Cycle Knockouts Reveals the Diversity of p53-Dependent Responses to Cell-Cycle Defects. *Dev. Cell*. 40:405–420.e2. doi:10.1016/j.devcel.2017.01.012.

Mendez, J., and B. Stillman. 2000. Chromatin Association of Human Origin Recognition Complex, Cdc6, and Minichromosome Maintenance Proteins during the Cell Cycle: Assembly of Prereplication Complexes in Late Mitosis. *Mol. Cell. Biol.* 20:8602–8612. doi:10.1128/MCB.20.22.8602-8612.2000.

Méndez, J., X.H. Zou-Yang, S.-Y. Kim, M. Hidaka, W.P. Tansey, and B. Stillman. 2002. Human Origin Recognition Complex Large Subunit Is Degraded by Ubiquitin-Mediated Proteolysis after Initiation of DNA Replication. *Mol. Cell*. 9:481–491. doi:10.1016/S1097-2765(02)00467-7.

Merrick, K.A., L. Wohlbold, C. Zhang, J.J. Allen, D. Horiuchi, N.E. Huskey, A. Goga, K.M. Shokat, and R.P. Fisher. 2011. Switching Cdk2 On or Off with Small Molecules to Reveal Requirements in Human Cell Proliferation. *Mol. Cell*. 42:624–636. doi:10.1016/j.molcel.2011.03.031.

Minn, A.J., L.H. Boise, and C.B. Thompson. 1996. Expression of Bcl-x(L) and loss of p53 can cooperate to overcome a cell cycle checkpoint induced by mitotic spindle damage. *Genes Dev.* 10:2621–2631. doi:10.1101/gad.10.20.2621.

Miotto, B., and K. Struhl. 2008. HBO1 histone acetylase is a coactivator of the replication licensing factor Cdt1. *Genes Dev.* 22:2633–2638. doi:10.1101/gad.1674108.

Miotto, B., and K. Struhl. 2010. HBO1 Histone Acetylase Activity Is Essential for DNA Replication Licensing and Inhibited by Geminin. *Mol. Cell*. 37:57–66. doi:10.1016/j.molcel.2009.12.012.

Moreno, A., J.T. Carrington, L. Albergante, M. Al Mamun, E.J. Haagensen, E.-S. Komseli, V.G. Gorgoulis, T.J. Newman, and J.J. Blow. 2016. Unreplicated DNA remaining from unperturbed S phases passes through mitosis for resolution in daughter cells. *Proc. Natl. Acad. Sci.* 113:E5757-64. doi:10.1073/pnas.1603252113.

Moreno, S.P., R. Bailey, N. Campion, S. Herron, and A. Gambus. 2014. Polyubiquitylation drives replisome disassembly at the termination of DNA replication. *Science*. 346:477–481. doi:10.1126/science.1253585.

Mulcahy, L.S., M.R. Smith, and D.W. Stacey. 1985. Requirement for ras proto-oncogene function during serum- stimulated growth of NIH 3T3 cells. *Nature*. 313:241–243. doi:10.1038/313241a0.

Murray, J.I., M.L. Whitfield, N.D. Trinklein, and R.M. Myers. 2004. Diverse and Specific Gene Expression Responses to Stresses in Cultured Human Cells. *Mol. Biol. Cell*. 15:2361–2374. doi:10.1091/mbc.E03.

Muzzey, D., and A. van Oudenaarden. 2009. Quantitative time-lapse fluorescence microscopy in single cells. *Annu. Rev. Cell Dev. Bioloy*. 25:301–327. doi:10.1146/annurev.cellbio.042308.113408.

Naetar, N., V. Soundarapandian, L. Litovchick, K.L. Goguen, A. a Sablina, C. Bowman-Colin, P. Sicinski, W.C. Hahn, J. a DeCaprio, and D.M. Livingston. 2014. PP2A-mediated regulation of Ras signaling in G2 is essential for stable quiescence and normal G1 length. *Mol. Cell*. 54:932–945. doi:10.1016/j.molcel.2014.04.023.

Narasimha, A.M., M. Kaulich, G.S. Shapiro, Y.J. Choi, P. Sicinski, and S.F. Dowdy. 2014. Cyclin D activates the Rb tumor suppressor by mono-phosphorylation. *Elife*. 3:1–21. doi:10.7554/eLife.02872.

Neelsen, K.J., I.M.Y. Zanini, S. Mijic, R. Herrador, R. Zellweger, A.R. Chaudhuri, K.D. Creavin, J.J. Blow, and M. Lopes. 2013. Deregulated origin licensing leads to chromosomal breaks by rereplication of a gapped DNA template. *Genes Dev.* 27:2537–2542. doi:10.1101/gad.226373.113.have.

Neganova, I., and M. Lako. 2008. G1 to S phase cell cycle transition in somatic and embryonic stem cells. *J. Anat.* 213:30–44. doi:10.1111/j.1469-7580.2008.00931.x.

Neganova, I., X. Zhang, S. Atkinson, and M. Lako. 2009. Expression and functional analysis of G1 to S regulatory components reveals an important role for CDK2 in cell cycle regulation in human embryonic stem cells. *Oncogene*. 28:20–30. doi:10.1038/onc.2008.358.

Nevis, K.R., M. Cordeiro-Stone, and J.G. Cook. 2009. Origin licensing and p53 status regulate Cdk2 activity during G1. *Cell Cycle*. 8:1952–1963. doi:10.4161/cc.8.12.8811.

Nishitani, H., Z. Lygerou, and T. Nishimoto. 2004. Proteolysis of DNA replication licensing factor Cdt1 in S-phase is performed independently of Geminin through its N-terminal region. *J. Biol. Chem.* 279:30807–30816. doi:10.1074/jbc.M312644200.

Nishitani, H., Z. Lygerou, T. Nishimoto, and P. Nurse. 2000. The Cdt1 protein is required to license DNA for replication in fission yeast. *Nature*. 404:625–628. doi:10.1038/35007110.

Niwa, H., Y. Toyooka, D. Shimosato, D. Strumpf, K. Takahashi, R. Yagi, and J. Rossant. 2005. Interaction between Oct3/4 and Cdx2 determines trophectoderm differentiation. *Cell*. 123:917–929. doi:10.1016/j.cell.2005.08.040.

O'Farrell, P.H., J. Stumpff, and T.T. Su. 2004. Embryonic Cleavage Cycles: How Is a Mouse Like a Fly? *Curr. Biol.* 14:35–45. doi:10.1016/S0960-9822(03)00933-3.

Orr, S.J., T. Gaymes, D. Ladon, C. Chronis, B. Czepulkowski, R. Wang, G.J. Mufti, E.M. Marcotte, and N.S.B. Thomas. 2010. Reducing MCM levels in human primary T cells during the G(0)-->G(1) transition causes genomic instability during the first cell cycle. *Oncogene*. 29:3803–14. doi:10.1038/onc.2010.138.

Overton, K.W., S.L. Spencer, W.L. Noderer, T. Meyer, and C.L. Wang. 2014. Basal p21 controls population heterogeneity in cycling and quiescent cell cycle states. *Proc. Natl. Acad. Sci. U. S. A.* 2014:1–8. doi:10.1073/pnas.1409797111.

Pardee, A. 1974. A restriction point for control of normal animal cell proliferation. *Proc. Natl. Acad. Sci. U. S. A.* 71:1286–1290.

Pauklin, S., P. Madrigal, A. Bertero, and L. Vallier. 2016. Initiation of stem cell differentiation involves cell cycle-dependent regulation of developmental genes by Cyclin D. *Genes Dev.* 30:421–433. doi:10.1101/gad.271452.115.

Pauklin, S., and L. Vallier. 2013. The Cell-Cycle State of Stem Cells Determines Cell Fate Propensity. *Cell*. 155:135–147. doi:10.1016/j.cell.2013.08.031.

Peeper, D.S., T.M. Upton, M.H. Ladha, E. Neuman, J. Zalvide, R. Bernards, J.A. DeCaprio, and M.E. Ewen. 1997. Ras signalling linked to the cell-cycle machinery by the retinoblastoma protein. *Nature*. 386:177–181. doi:10.1038/386177a0.

Perucca, P., O. Cazzalini, M. Madine, M. Savio, R.A. Laskey, V. Vannini, E. Prosperi, and L.A. Stivala. 2009. Loss of p21 CDKN1A impairs entry to quiescence and activates a DNA damage response in normal fibroblasts induced to quiescence. *Cell Cycle*. 8:105–114. doi:10.4161/cc.8.1.7507.

Petersen, B.O., J. Lukas, C.S. Sørensen, J. Bartek, and K. Helin. 1999a. Phosphorylation of mammalian CDC6 by cyclin A/CDK2 regulates its subcellular localization. *EMBO J.* 18:396–410. doi:10.1093/emboj/18.2.396.

Petersen, B.O., J. Lukas, C.S. Sørensen, J. Bartek, and K. Helin. 1999b. Phosphorylation of mammalian CDC6 by cyclin A/CDK2 regulates its subcellular localization. *EMBO J.* 18:396–410. doi:10.1093/emboj/18.2.396.

Petersen, B.O., C. Wagener, F. Marinoni, E.R. Kramer, M. Melixetian, E.L. Denchi, C. Gieffers, C. Matteucci, J. Peters, and K. Helin. 2000. Cell cycle – and cell growth – regulated proteolysis of mammalian CDC6 is dependent on APC – CDH1. *Genes Dev.* 14:2330–2343. doi:10.1101/gad.832500.ORC.

Powell, S.K., H.K. Macalpine, J.A. Prinz, Y. Li, J.A. Belsky, and D.M. Macalpine. 2015. Dynamic loading and redistribution of the Mcm 2 - 7 helicase complex through the cell cycle. *EMBO J.* 34:531–543.

Pozo, P., and J. Cook. 2016. Regulation and Function of Cdt1; A Key Factor in Cell Proliferation and Genome Stability. *Genes (Basel).* 8:2. doi:10.3390/genes8010002.

Prioleau, M., and D.M. Macalpine. 2016. DNA replication origins — where do we begin ? 1683–1697. doi:10.1101/gad.285114.116.ical.

Pruitt, S.C., K.J. Bailey, and A. Freeland. 2007. Reduced Mcm2 expression results in severe stem/progenitor cell deficiency and cancer. *Stem Cells*. 25:3121–3132. doi:10.1634/stemcells.2007-0483.

Raj, A., and A. van Oudenaarden. 2008. Nature, Nurture, or Chance: Stochastic Gene Expression and Its Consequences. *Cell*. 135:216–226. doi:10.1016/j.cell.2008.09.050.

Randell, J.C.W., J.L. Bowers, H.K. Rodríguez, and S.P. Bell. 2006. Sequential ATP hydrolysis

by Cdc6 and ORC directs loading of the Mcm2-7 helicase. *Mol. Cell*. 21:29–39. doi:10.1016/j.molcel.2005.11.023.

Remus, D., F. Beuron, G. Tolun, J.D. Griffith, E.P. Morris, and J.F.X. Diffley. 2009. Concerted loading of Mcm2-7 double hexamers around DNA during DNA replication origin licensing. *Cell*. 139:719–30. doi:10.1016/j.cell.2009.10.015.

Remus, D., and J.F.X. Diffley. 2009. Eukaryotic DNA replication control: lock and load, then fire. *Curr. Opin. Cell Biol.* 21:771–777. doi:10.1016/j.ceb.2009.08.002.

Resnitzky, D., M. Gossen, H. Bujard, and S.I. Reed. 1994. Acceleration of the G1/S phase transition by expression of cyclins D1 and E with an inducible system. *Mol. Cell. Biol.* 14:1669–79. doi:10.1128/MCB.14.3.1669.

Rizzardi, L.F., K.E. Coleman, D. Varma, J.P. Matson, S. Oh, and J.G. Cook. 2015. Cyclin-dependent Kinase 1 (CDK1)-dependent Inhibition of the E3 Ubiquitin Ligase, CRL4CDT2, Ensures Robust Transition from S Phase to Mitosis. *J. Biol. Chem.* 290:556–67. doi:10.1074/jbc.M114.614701.

Rizzardi, L.F., and J.G. Cook. 2012. Flipping the Switch from G1 to S Phase with E3 Ubiquitin Ligases. *Genes Cancer*. 3:634–648. doi:10.1177/1947601912473307.

Robinson, M., P. Chapani, T. Styan, R. Vaidyanathan, and S.M. Willerth. 2016. Functionalizing Ascl1 with Novel Intracellular Protein Delivery Technology for Promoting Neuronal Differentiation of Human Induced Pluripotent Stem Cells. *Stem Cell Rev. Reports*. 12:476–483. doi:10.1007/s12015-016-9655-7.

Rodriguez-Martinez, M., and M. Mechali. 2014. DNA Replication Origins. *Cold Spring Harb. Perspect. Biol.* 5:a010116. doi:10.1002/9780470015902.a0006170.pub2.

Rodriguez-Rodriguez, J.A., C. Lewis, K.L. McKinley, V. Sikirzhytski, J. Corona, J. Maciejowski, A. Khodjakov, I.M. Cheeseman, and P. V. Jallepalli. 2018. Distinct Roles of RZZ and Bub1-KNL1 in Mitotic Checkpoint Signaling and Kinetochore Expansion. *Curr. Biol.* 28:3422–3429.e5. doi:10.1016/j.cub.2018.10.006.

Roy, S., P. Gascard, N. Dumont, J. Zhao, D. Pan, S. Petrie, M. Margeta, and T.D. Tlsty. 2013. Rare somatic cells from human breast tissue exhibit extensive lineage plasticity. *Proc. Natl. Acad. Sci. U. S. A.* 110:4598–4603. doi:10.1073/pnas.1218682110.

Sagot, I., and D. Laporte. 2019. Quiescence, an individual journey. *Curr. Genet.* 0:1–5. doi:10.1007/s00294-018-00928-w.

Sakaue-Sawano, A., H. Kurokawa, T. Morimura, A. Hanyu, H. Hama, H. Osawa, S. Kashiwagi, K. Fukami, T. Miyata, H. Miyoshi, T. Imamura, M. Ogawa, H. Masai, and A. Miyawaki. 2008. Visualizing Spatiotemporal Dynamics of Multicellular Cell-Cycle Progression. *Cell*. 132:487–498. doi:10.1016/j.cell.2007.12.033.

Samel, S.A., A. Fernández-Cid, J. Sun, A. Riera, S. Tognetti, M.C. Herrera, H. Li, and C. Speck. 2014. A unique DNA entry gate serves for regulated loading of the eukaryotic replicative helicase MCM2–7 onto DNA. *Genes Dev.* 28:1653–1666. doi:10.1101/gad.242404.114.

Sang, L., H.A. Coller, and J.M. Roberts. 2008. Control of the Reversibility of Cellular Quiescence by the Transcriptional Repressor HES1. *Science*. 321:1095–1100. doi:10.1126/science.1155998.

Schwarz, C., A. Johnson, E. Zatulovskiy, C.J. Kravitz, A. Doncic, J.M. Skotheim, E. Zatulovskiy, C.J. Kravitz, and A. Doncic. 2018. A Precise Cdk Activity Threshold Determines Passage through the Restriction Point. *Mol. Cell*. 253–264. doi:10.1016/j.molcel.2017.12.017.

Scognamiglio, R., N. Cabezas-Wallscheid, M.C. Thier, S. Altamura, A. Reyes, A.M. Prendergast, D. Baumgartner, L.S. Carnevalli, A. Atzberger, S. Haas, L. Von Paleske, T. Boroviak, P. Worsdorfer, M.A.G. Essers, U. Kloz, R.N. Eisenman, F. Edenhofer, P. Bertone, W. Huber, F. Van Der Hoeven, A. Smith, and A. Trumpp. 2016. Myc Depletion Induces a Pluripotent Dormant State Mimicking Diapause. *Cell*. 164:668–680. doi:10.1016/j.cell.2015.12.033.

Sears, R., F. Nuckolls, E. Haura, Y. Taya, K. Tamai, and J.R. Nevins. 2000. Multiple Ras-dependent phosphorylation pathways regulate Myc protein stability. *Genes Dev.* 14:2501–2514. doi:10.1101/gad.836800.

Segev, H., D. Zenvirth, K.J. Simpson-Lavy, N. Melamed-Book, and M. Brandeis. 2016. Imaging Cell Cycle Phases and Transitions of Living Cells from Yeast to Woman. *In* Cell Cycle Oscillators: Methods and Protocols. A.S. Coutts and L. Weston, editors. Springer New York, New York, NY. 321–336.

Sela, Y., N. Molotski, S. Golan, J. Itskovitz-Eldor, and Y. Soen. 2012. Human embryonic stem cells exhibit increased propensity to differentiate during the G1 phase prior to phosphorylation of retinoblastoma protein. *Stem Cells*. 30:1097–1108. doi:10.1002/stem.1078.

Shaulian, E., and M. Karin. 2002. AP-1 as a regulator of cell life and death. *Nat Cell Biol*. 4:E131-136. doi:10.1038/ncb0502-e131.

Shen, Z., K.M. Sathyan, Y. Geng, R. Zheng, A. Chakraborty, B. Freeman, F. Wang, K. V. Prasanth, and S.G. Prasanth. 2010. A WD-repeat protein stabilizes ORC binding to chromatin. *Mol. Cell*. 40:99–111. doi:10.1016/j.molcel.2010.09.021.

Shima, N., A. Alcaraz, I. Liachko, T.R. Buske, C.A. Andrews, R.J. Munroe, S.A. Hartford, B.K. Tye, and J.C. Schimenti. 2007. A viable allele of Mcm4 causes chromosome instability and mammary adenocarcinomas in mice. *Nat. Genet.* 39:93–98. doi:10.1038/ng1936.

Shreeram, S., A. Sparks, D.P. Lane, and J.J. Blow. 2002. Cell type-specific responses of human cells to inhibition of replication licensing. *Oncogene*. 21:6624–6632. doi:10.1038/sj.onc.1205910.

Siddiqui, K., K.F. On, and J.F.X. Diffley. 2013. Regulating DNA replication in Eukarya. *Cold Spring Harb. Perspect. Biol.* 5. doi:10.1101/cshperspect.a012930.

Sigal, A., R. Milo, A. Cohen, N. Geva-Zatorsky, Y. Klein, Y. Liron, N. Rosenfeld, T. Danon, N. Perzov, and U. Alon. 2006. Variability and memory of protein levels in human cells. *Nature*. 444:643–646. doi:10.1038/nature05316.

Simons, B.D., and H. Clevers. 2011. Stem cell self-renewal in intestinal crypt. *Exp. Cell Res.* 317:2719–2724. doi:10.1016/j.yexcr.2011.07.010.

Skarstad, K., and T. Katayama. 2013. Regulating DNA replication in bacteria. *Cold Spring Harb. Perspect. Biol.* 5:1–17. doi:10.1101/cshperspect.a012922.

Skinner, S.O., H. Xu, S. Nagarkar-Jaiswal, P.R. Freire, T.P. Zwaka, and I. Golding. 2016. Single-cell analysis of transcription kinetics across the cell cycle. *Elife*. 5:1–24. doi:10.1017/CBO9781107415324.004.

Snijder, B., and L. Pelkmans. 2011. Origins of regulated cell-to-cell variability. *Nat. Rev. Mol. Cell Biol.* 12:119–125. doi:10.1038/nrm3044.

Sosa, M.S., P. Bragado, and J. a. Aguirre-Ghiso. 2014. Mechanisms of disseminated cancer cell dormancy: an awakening field. *Nat. Rev. Cancer*. 14:611–622. doi:10.1038/nrc3793.

Soufi, A., and S. Dalton. 2016. Cycling through developmental decisions: how cell cycle dynamics control pluripotency, differentiation and reprogramming. *Development*. 143:4301–4311. doi:10.1242/dev.142075.

Spencer, S.L., S.D. Cappell, F.-C. Tsai, W.K. Overton, C.L. Wang, and T. Meyer. 2013. The proliferation-quiescence decision is controlled by a bifurcation in CDK2 activity at mitotic exit. *Cell*. 155:369–383. doi:10.1016/j.cell.2013.08.062.

Spiller, D.G., C.D. Wood, D.A. Rand, and M.R.H. White. 2010. Measurement of single-cell dynamics. *Nature*. 465:736–745. doi:10.1038/nature09232.

Stewart-Ornstein, J., and G. Lahav. 2016. Dynamics of CDKN1A in Single Cells Defined by an Endogenous Fluorescent Tagging Toolkit. *Cell Rep.* 14:1800–1811. doi:10.1016/j.celrep.2016.01.045.

Sugimoto, N., Y. Tatsumi, T. Tsurumi, A. Matsukage, T. Kiyono, H. Nishitani, and M. Fujita. 2004. Cdt1 Phosphorylation by Cyclin A-dependent Kinases Negatively Regulates Its Function without Affecting Geminin Binding. *J. Biol. Chem.* 279:19691–19697. doi:10.1074/jbc.M313175200.

Sugiyama, M., A. Sakaue-Sawano, T. Iimura, K. Fukami, T. Kitaguchi, K. Kawakami, H. Okamoto, S. Higashijima, and A. Miyawaki. 2009. Illuminating cell-cycle progression in the developing zebrafish embryo. *Proc. Natl. Acad. Sci. U. S. A.* 106:20812–20817. doi:10.1073/pnas.0906464106.

Sun, J., C. Evrin, S. a Samel, A. Fernández-Cid, A. Riera, H. Kawakami, B. Stillman, C. Speck, and H. Li. 2013. Cryo-EM structure of a helicase loading intermediate containing ORC-Cdc6-Cdt1-MCM2-7 bound to DNA. *Nat. Struct. Mol. Biol.* 20:944–51. doi:10.1038/nsmb.2629.

Sun, J., a. Fernandez-Cid, a. Riera, S. Tognetti, Z. Yuan, B. Stillman, C. Speck, and H. Li. 2014. Structural and mechanistic insights into Mcm2-7 double-hexamer assembly and function. *Genes Dev.* 28:2291–2303. doi:10.1101/gad.242313.114.

Susaki, E., K. Nakayama, and K.I. Nakayama. 2007. Cyclin D2 translocates p27 out of the

nucleus and promotes its degradation at the G0-G1 transition. *Mol. Cell. Biol.* 27:4626–4640. doi:10.1128/MCB.00862-06.

Symeonidou, I.-E., P. Kotsantis, V. Roukos, M.-A. Rapsomaniki, H.E. Grecco, P. Bastiaens, S. Taraviras, and Z. Lygerou. 2013. Multi-step Loading of Human Minichromosome Maintenance Proteins in Live Human Cells. *J. Biol. Chem.* 288:35852–35867. doi:10.1074/jbc.M113.474825.

Tanaka, S., and J.F.X. Diffley. 2002. Deregulated G 1 -cyclin expression induces genomic instability by preventing efficient pre-RC formation. *Genes Dev.* 16:2639–2649. doi:10.1101/gad.1011002.

Tardat, M., J. Brustel, O. Kirsh, C. Lefevbre, M. Callanan, C. Sardet, and E. Julien. 2010. The histone H4 Lys 20 methyltransferase PR-Set7 regulates replication origins in mammalian cells. *Nat. Cell Biol.* 12:1086–1093. doi:10.1038/ncb2113.

Taylor, J.H. 1960. Asynchronous duplication of chromosomes in cultured cells of Chinese hamster. *J. Biophys. Bochemical Cytol.* 7:455–464. doi:10.1083/jcb.7.3.455.

Teer, J.K., Y.J. Machida, H. Labit, O. Novac, O. Hyrien, K. Marheineke, M. Zannis-Hadjopoulos, and A. Dutta. 2006. Proliferating human cells hypomorphic for origin recognition complex 2 and pre-replicative complex formation have a defect in p53 activation and Cdk2 kinase activation. *J. Biol. Chem.* 281:6253–6260. doi:10.1074/jbc.M507150200.

Ticau, S., L.J. Friedman, N.A. Ivica, J. Gelles, and S.P. Bell. 2015. Single-Molecule Studies of Origin Licensing Reveal Mechanisms Ensuring Bidirectional Helicase Loading. *Cell*. 1–13. doi:10.1016/j.cell.2015.03.012.

Todorov, I.T., A. Attaran, and S.E. Kearsey. 1995. BM28, a Human Member of the MCM2-3-5 Family, Is Displaced from Chromatin during DNA Replication. *J. Cell Biol.* 129:1433–1445.

Toledo, L.I., M. Altmeyer, M.-B. Rask, C. Lukas, D.H. Larsen, L.K. Povlsen, S. Bekker-Jensen, N. Mailand, J. Bartek, and J. Lukas. 2013. ATR Prohibits Replication Catastrophe by Preventing Global Exhaustion of RPA. *Cell*. 155:1088–1103. doi:10.1016/j.cell.2013.10.043.

Tovar, C., J. Rosinski, Z. Filipovic, B. Higgins, K. Kolinsky, H. Hilton, X. Zhao, B.T. Vu, W. Qing, K. Packman, O. Myklebost, D.C. Heimbrook, and L.T. Vassilev. 2006. Small-molecule MDM2 antagonists reveal aberrant p53 signaling in cancer: implications for therapy. *Proc. Natl. Acad. Sci. U. S. A.* 103:1888–93. doi:10.1073/pnas.0507493103.

Truong, L.N., and X. Wu. 2011. Prevention of DNA re-replication in eukaryotic cells. *J. Mol. Cell Biol.* 3:13–22. doi:10.1093/jmcb/mjq052.

Tsunematsu, T., Y. Takihara, N. Ishimaru, M. Pagano, T. Takata, and Y. Kudo. 2013. Aurora-A controls pre-replicative complex assembly and DNA replication by stabilizing geminin in mitosis. *Nat. Commun.* 4:1–11. doi:10.1038/ncomms2859.

Tyson, J.J., and B. Novak. 2008. Temporal Organization of the Cell Cycle. *Curr. Biol.* 18:759–768. doi:10.1016/j.cub.2008.07.001.

Tyson, J.J., and B. Novák. 2015. Models in biology: lessons from modeling regulation of the eukaryotic cell cycle. *BMC Biol.* 13:46. doi:10.1186/s12915-015-0158-9.

VanOudenhove, J.J., R.A. Grandy, P.N. Ghule, J.B. Lian, J.L. Stein, S.K. Zaidi, and G.S. Stein. 2016. Unique Regulatory Mechanisms for the Human Embryonic Stem Cell Cycle. *J. Cell. Physiol.* doi:10.1002/jcp.25567.

Varma, D., S. Chandrasekaran, L.J.R. Sundin, K.T. Reidy, X. Wan, D. a D. Chasse, K.R. Nevis, J.G. DeLuca, E.D. Salmon, and J.G. Cook. 2012. Recruitment of the human Cdt1 replication licensing protein by the loop domain of Hec1 is required for stable kinetochore-microtubule attachment. *Nat. Cell Biol.* 14:593–603. doi:10.1038/ncb2489.

Walker, P.M.B. 1954. The Mitotic Index and Interphase Processes. *J. Exp. Biol.* 31:8–15.

Walter, D., A. Lier, A. Geiselhart, F.B. Thalheimer, S. Huntscha, M.C. Sobotta, B. Moehrle, D. Brocks, I. Bayindir, P. Kaschutnig, K. Muedder, C. Klein, A. Jauch, T. Schroeder, H. Geiger, T.P. Dick, T. Holland-Letz, P. Schmezer, S.W. Lane, M. a. Rieger, M. a. G. Essers, D. a. Williams, A. Trumpp, and M.D. Milsom. 2015. Exit from dormancy provokes DNA-damage-induced attrition in haematopoietic stem cells. *Nature*. 520:549–552. doi:10.1038/nature14131.

Wang, X., K. Fujimaki, G.C. Mitchell, J.S. Kwon, K. Della Croce, C. Langsdorf, H.H. Zhang, and G. Yao. 2017. Exit from quiescence displays a memory of cell growth and division. *Nat. Commun.* 8:321. doi:10.1038/s41467-017-00367-0.

Watanabe, K., M. Ueno, D. Kamiya, A. Nishiyama, M. Matsumura, T. Wataya, J.B. Takahashi, S. Nishikawa, S. Nishikawa, K. Muguruma, and Y. Sasai. 2007. A ROCK inhibitor permits survival of dissociated human embryonic stem cells. *Nat. Biotechnol.* 25:681–686. doi:10.1038/nbt1310.

Weinberg, R.A. 1995. The retinoblastoma protein and cell cycle control. *Cell*. 81:323–330. doi:10.1016/0092-8674(95)90385-2.

Weis, M.C., J. Avva, J.W. Jacobberger, and S.N. Sreenath. 2014. A data-driven, mathematical model of mammalian cell cycle regulation. *PLoS One*. 9:e97130. doi:10.1371/journal.pone.0097130.

Welch, C.M., H. Elliott, G. Danuser, and K.M. Hahn. 2011. Imaging the coordination of multiple signalling activities in living cells. *Nat. Rev. Mol. Cell Biol.* 12:749–756. doi:10.1038/nrm3212.

Wells, A., L. Griffith, J.Z. Wells, and D.P. Taylor. 2013. The dormancy dilemma: quiescence versus balanced proliferation. *Cancer Res.* 73:3811–6. doi:10.1158/0008-5472.CAN-13-0356.

Wheeler, L.W., N.H. Lents, and J.J. Baldassare. 2008. Cyclin A-CDK activity during G1 phase impairs MCM chromatin loading and inhibits DNA synthesis in mammalian cells. *Cell Cycle*. 7:2179–2188. doi:10.4161/cc.7.14.6270.

Woodward, A.M., T. Göhler, M.G. Luciani, M. Oehlmann, X. Ge, A. Gartner, D. a Jackson, and J.J. Blow. 2006. Excess Mcm2-7 license dormant origins of replication that can be used

under conditions of replicative stress. *J. Cell Biol.* 173:673–83. doi:10.1083/jcb.200602108.
Yang, W., M. Chung, T. Kudo, and T. Meyer. 2017. Competing memories of mitogen and p53 signalling control cell-cycle entry. *Nature*. 549:404–408. doi:10.1038/nature23880.

Yao, G., T.J. Lee, S. Mori, J.R. Nevins, and L. You. 2008. A bistable Rb-E2F switch underlies the restriction point. *Nat. Cell Biol.* 10:476–482. doi:10.1038/ncb1711.

Yekezare, M., B. Gómez-González, and J.F.X. Diffley. 2013. Controlling DNA replication origins in response to DNA damage - inhibit globally, activate locally. *J. Cell Sci.* 126:1297–1306. doi:10.1242/jcs.096701.

Yim, H., J.-W. Park, S.U. Woo, S.-T. Kim, L. Liu, C.-H. Lee, and S.K. Lee. 2013. Phosphorylation of Cdc6 at serine 74, but not at serine 106, drives translocation of Cdc6 to the cytoplasm. *J. Cell. Physiol.* 228:1221–1228. doi:10.1002/jcp.24275.

Yu, C.C.W., A.L. Woods, and D.A. Levison. 1992. The assessment of cellular proliferation by immunohistochemistry: A review of currently available methods and their applications. *Histochem. J.* 24:121–131. doi:10.1007/BF01047461.

Yuan, X., J. Srividhya, T. De Luca, J.-H.E. Lee, and J.R. Pomerening. 2014. Uncovering the role of APC-Cdh1 in generating the dynamics of S-phase onset. *Mol. Biol. Cell*. 25:441–456. doi:10.1091/mbc.E13-08-0480.

Zeman, M.K., and K.A. Cimprich. 2014. Causes and consequences of replication stress. *Nat. Cell Biol.* 16:2–9. doi:10.1038/ncb2897.

Zetterberg, A., and O. Larsson. 1985. Kinetic analysis of regulatory events in G1 leading to proliferation or quiescence of Swiss 3T3 cells. *Proc. Natl. Acad. Sci. U. S. A.* 82:5365–5369. doi:10.1073/pnas.82.16.5365.

Zetterberg, A., O. Larsson, and K.G. Wiman. 1995. What is the restriction point? *Curr. Opin. Cell Biol.* 7:835–842.

Zhang, C., A. Spektor, H. Cornils, J.M. Francis, E.K. Jackson, and S. Liu. 2015. Chromothripsis from DNA damage in micronuclei. *Nature*. 522:179–184. doi:10.1038/nature14493.

Zhang, C.Z., and D. Pellman. 2015. From Mutational Mechanisms in Single Cells to Mutational Patterns in Cancer Genomes. *Cold Spring Harb. Symp. Quant. Biol.* LXXX. doi:10.1101/sqb.2015.80.027623.

Zhang, Y., L. Huang, H. Fu, O.K. Smith, C.M. Lin, K. Utani, M. Rao, W.C. Reinhold, C.E. Redon, M. Ryan, R. Kim, Y. You, H. Hanna, Y. Boisclair, Q. Long, and M.I. Aladjem. 2016. A replicator-specific binding protein essential for site-specific initiation of DNA replication in mammalian cells. *Nat Commun*. 7:1–14. doi:10.1038/ncomms11748.

Zhou, Y., H.M. Stone, S. Oh, P.N. Pozo, and J.G. Cook. 2018. Phosphoregulation of Cdt1 in G2 and M phases prevents re-replication independently of Geminin . *bioRxiv*. doi:https://doi.org/10.1101/366666.

Zielke, N., J. Korzelius, M. vanStraaten, K. Bender, G.F.P. Schuhknecht, D. Dutta, J. Xiang, and B. a. Edgar. 2014. Fly-FUCCI: A Versatile Tool for Studying Cell Proliferation in Complex

Tissues. *Cell Rep.* 7:588–598. doi:10.1016/j.celrep.2014.03.020.
Zimmerman, K.M., R.M. Jones, E. Petermann, and P.A. Jeggo. 2013. Diminished Origin-Licensing Capacity Specifically Sensitizes Tumor Cells to Replication Stress. *Mol. Cancer Res.* 11:370–380. doi:10.1158/1541-7786.MCR-12-0491.

Zimmermann, M., O. Murina, M.A.M. Reijns, A. Agathanggelou, R. Challis, Ž. Tarnauskaite, M. Muir, A. Fluteau, M. Aregger, A. McEwan, W. Yuan, M. Clarke, M.B. Lambros, S. Paneesha, P. Moss, M. Chandrashekhar, S. Angers, J. Moffat, V.G. Brunton, T. Hart, J. De Bono, T. Stankovic, A.P. Jackson, and D. Durocher. 2018. CRISPR screens identify genomic ribonucleotides as a source of PARP-trapping lesions. *Nature*. 559:285–289. doi:10.1038/s41586-018-0291-z.